



Kaunas University of Technology
Faculty of Mathematics and Natural Sciences

**Development of Photospectrometric Measurement System for
the Analysis of Dosimetric Gels and Comparative Study of the
Obtained Results**

Master's Final Degree Project

Mantvydas Merkis

Project author

Lect. dr. Benas Gabrielis Urbonavičius

Supervisor

Kaunas, 2020



Kaunas University of Technology
Faculty of Mathematics and Natural Sciences

Development of Photospectrometric Measurement System for the Analysis of Dosimetric Gels and Comparative Study of the Obtained Results

Master's Final Degree Project
Medical physics (code 6213GX001)

Mantvydas Merkis

Project author

**Lect. dr. Benas Gabrielis
Urbonavičius**

Supervisor

Prof. dr. Liutauras Marcinauskas

Reviewer

Kaunas, 2020



Kaunas University of Technology
Faculty of Mathematics and Natural Sciences
Mantvydas Merkis

Development of Photospectrometric Measurement System for the Analysis of Dosimetric Gels and Comparative Study of the Obtained Results

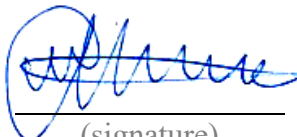
Declaration of Academic Integrity

I confirm that the final project of mine, Mantvydas Merkis, on the topic „Development of Photospectrometric Measurement System for the Analysis of Dosimetric Gels and Comparative Study of the Obtained Results“ is written completely by myself; all the provided data and research results are correct and have been obtained honestly. None of the parts of this thesis have been plagiarised from any printed, Internet-based or otherwise recorded sources. All direct and indirect quotations from external resources are indicated in the list of references. No monetary funds (unless required by Law) have been paid to anyone for any contribution to this project.

I fully and completely understand that any discovery of any manifestations/case/facts of dishonesty inevitably results in me incurring a penalty according to the procedure(s) effective at Kaunas University of Technology.

Mantvydas Merkis

(name and surname filled in by hand)



(signature)

Merkis Mantvydas. Development of Photospectrometric Measurement System for the Analysis of Dosimetric Gels and Comparative Study of the Obtained Results. Master's Final Degree Project / supervisor lect. dr. Benas Gabrielis Urbonavičius; Faculty of Mathematics and Natural Sciences, Kaunas University of Technology.

Study field and area (study field group): Medical Technology (G09), Health Sciences.

Keywords: polymer gel dosimetry, photospectrometric analysis, readout of polymer gels, 3D dosimetry, dosimetric gels.

Kaunas, 2020. 74.

Summary

Novel radiation therapy techniques offer both better tumor control and lower probability of complications. However, more sophisticated techniques require more complex procedure verification because in case of steep dose gradients even minor differences between planned and actual dose distribution can cause severe complications. Dosimetric gels are effectively the only dosimetric method that meets the increasing needs of radiotherapy procedure verification. These dosimeters are able to capture three-dimensional dose distribution with high spatial accuracy. Also, dosimetric gels are tissue-equivalent in terms of absorption of ionizing radiation. Various techniques are used for dose distribution analysis in dosimetric gels, for example, magnetic resonance imaging, computed tomography, optical imaging. Nevertheless, these methods are not optimal - most of them lack spatial resolution, equipment is expensive, complicated, non-modifiable, acquired data is redundant.

In this work specialized photospectrometric two-dimensional imaging system for dose distribution analysis in dosimetric gels was designed. The system consists of a spectrometer, data processing software, and a unique cuvette positioning device that enables to acquire spectral information from the entire sample. Designed system achieves 0.125 - 0.15 mm spatial resolution. It is significantly higher when compared to most of the existing dosimetric gel imaging methods, which typically achieve 0.5 – 1 mm spatial resolution. It enables to use the designed system for characterization of dosimetric gels, irradiated with steep dose gradients.

Created system was tested with nMAG polymer gel dosimeter, irradiated with a complex shape radiation field using a linear accelerator. For comparison, the same polymer gel was scanned with conventional imaging technique (computed tomography) and alternative scanning techniques (diagnostic ultrasound, flatbed scanning). Created system demonstrates superior performance comparing to both conventional and alternative techniques. Designed system has the highest dose sensitivity, linearity of response and sufficient spatial resolution. High sensitivity of the system was achieved by optimizing the readout wavelength, which in the case of nMAG samples was 509 nm.

Merkis Mantvydas. Fotospektrometrinės sistemos dozimetrinių gelių analizei sukūrimas ir gelių tyrimo rezultatų lyginamoji analizė. Magistro baigiamasis projektas / lekt. dr. Benas Gabrielis Urbonavičius; Kauno technologijos universitetas, matematikos ir gamtos mokslų fakultetas.

Studijų kryptis ir sritis (studijų krypčių grupė): medicinos technologijos (G09), sveikatos mokslai.

Reikšminiai žodžiai: polimerinių gelių dozimetrija, fotospektrometrinė analizė, polimerinių gelių nuskaitymas, 3D dozimetrija, dozimetriniai geliai.

Kaunas, 2020. 74 p.

Santrauka

Naujausių spindulinės terapijos technikų naudojimas leidžia efektyviau kontroliuoti ligą bei sumažinti komplikacijų riziką. Šios technikos reikalauja detalesnio procedūrų verifikavimo, kadangi esant dideliems dozės gradientams netgi maži skirtumai tarp teorinio bei praktinio dozės pasiskirstymų gali ženkliai padidinti komplikacijų riziką. Vis augančius verifikavimo poreikius gali patenkinti tik dozimetriniai geliai. Šie dozimetrai leidžia gauti trimatį dozės pasiskirstymą, kuris pasižymi didele erdvine skyra. Taip pat dozimetriniai geliai yra ekvivalentūs biologiniam audiniui jonizuojančiosios spinduliuotės sugerties prasme. Galimi įvairūs dozės pasiskirstymo dozimetriniuose geluose nustatymo metodai, pavyzdžiui, kompiuterinė tomografija, magnetinio rezonanso tomografija, ultragarsinis vaizdinimas. Deja, šie metodai nėra optimalūs – daugelio erdvinė skyra nepakankama, įranga yra brangi ir sudėtinga, o gaunami duomenys dažnai yra pertekliniai.

Šiaip problemai spręsti buvo sukurta fotospektrometrinė vaizdinimo dvimatėje erdvėje sistema, skirta dozimetrinių gelių analizei. Sukurtą sistemą sudaro fotospektrometras, duomenų apdorojimo programinė įranga bei unikalus kiuvetės pozicionavimo prietaisas, kuris leidžia gauti spektrinę informaciją iš viso bandinio tūrio. Sistema gali skenuoti bandinius su 0.125 – 0.15 mm erdvine skyra. Taigi, gauti rezultatai yra geresni lyginant su daugeliu esamų vaizdinimo sistemų, kurių erdvinė skiriamoji geba siekia 0.5 – 1 mm. Tai leidžia sukurtą fotospektrometrinę sistemą pritaikyti dozimetrinių gelių su dideliais dozės gradientais tyrimams.

Sistemos testavimas buvo atliktas skenuojant nMAG polimerinį dozimetrinį gelį, kuris su linijiniu greitintuvu buvo apšvitintas sudėtingos formos lauku. Siekiant palyginti rezultatus tie patys bandiniai buvo nuskaityti panaudojant įprastą vaizdinimo metodiką (kompiuterinė tomografija) bei alternatyvias technikas (skanavimas dokumentų skeneriu, diagnostinio ultragarso aparatu). Bandymų metu išsiaiškinta, kad fotospektrometrinė vaizdinimo sistema daugeliu atvejų lenkia kitas vaizdinimo metodikas. Sukurta sistema pasižymi geriausiu atsako tiesiškumu, jautrumu, pakankama erdvine skyra. Aukštas sistemos jautrumas buvo pasiektas optimizuojant nuskaitymo bangos ilgį, kuris nMAG polimeriniam dozimetriniam geliiui buvo 509 nm.

Table of contents

List of figures	8
List of tables	10
List of abbreviations.....	11
Introduction	12
1. Theoretical overview	13
1.1. Review of dosimetry techniques	13
1.2. Basic principles of gel dosimetry	16
1.2.1. Processes in polymer gels.....	16
1.2.2. Development of gel dosimeters and their formulations	20
1.2.3. Requirements for polymer gel dosimeters.....	21
1.3. Applications of polymer gel dosimetry	23
1.3.1. External beam radiation therapy.....	23
1.3.2. Brachytherapy.....	23
1.3.3. Measurement of particle dose distributions.....	24
1.3.4. Dosimetric investigations	24
1.4. Read-out techniques of polymer gel dosimeters	24
1.4.1. Magnetic resonance imaging	25
1.4.2. Ultrasound imaging	26
1.4.3. Computed tomography imaging	27
1.4.4. Optical imaging	28
2. Materials and methods.....	32
2.1. Design of dosimetric gel optical imaging system.....	32
2.1.1. Design of scanning mechanism	33
2.1.2. Optical scanning system electronics.....	34
2.1.3. Design of software.....	36
2.2. Dosimetric Gel.....	39
2.3. Irradiation of the dosimetric gel	39
2.4. Readout methods used for imaging comparison	40
2.4.1. Scanning using designed optical imaging system	40
2.4.2. Scanning using diagnostic ultrasound imaging device.....	40
2.4.3. Scanning using a document scanner.....	41
2.4.4. Scanning using computed tomography	41
2.5. Data processing	41
3. Results and discussion.....	44
3.1. Determination of the optimal nMAG readout wavelength.....	44
3.2. Imaging of nMAG samples using designed optical imaging system	45
3.3. Imaging of nMAG samples using diagnostic ultrasound	48
3.4. Imaging of nMAG samples using a document scanner.....	50
3.5. Imaging of nMAG samples using CT	55
3.6. Comparison of imaging techniques	58
Conclusions	62
Acknowledgement.....	63
List of references.....	64

Appendices	68
Appendix 1. Conference “Multidisciplinary Research of Physical and Technological Sciences” ...	68
Appendix 2. Created tool for data, acquired with the designed system, processing in Matlab environment.	69
Appendix 3. Created tool for data, acquired with computed tomography and document scanner, processing in Matlab environment.	72

List of figures

Fig. 1. Typical NTCP and TCP curves.....	13
Fig. 2. Structure of a linear accelerator with EPID	14
Fig. 3. Examples of various gel dosimeters: a) Fricke gel dosimeter irradiated with 12 MeV electron beams demonstrate color change; b) polymer gel dosimeter irradiated using intensity-modulated radiation therapy	15
Fig. 4. Created polymer structures with different concentrations of crosslinker: a) only linear polymer is used; b) low fraction of crosslinker is used; c) high fraction of crosslinker is used; d) polymer gel consists only of crosslinker	17
Fig. 5. Summary of processes in polymer gel dosimeters.....	19
Fig. 6. Dose overshoots due to diffusion of monomers to irradiated area	22
Fig. 7. Dose distribution around high dose rate brachytherapy source acquired by scanning polymer gel dosimeter with MRI.....	24
Fig. 8. Schematic of basic processes in MRI: a) alignment with external magnetic field; b) orientation change of net magnetization vector; c) realignment of net magnetization vector; d) longitudinal component recovery; e) transverse component recovery	25
Fig. 9. Ultrasound scanner with translational mechanism (a); acquired transmission image (b); image, acquired using TOF method (c).....	27
Fig. 10. Dose profile of unfiltered, filtered (adaptive mean filtering) and noise free images.....	28
Fig. 11. Initial CT image (a); image after 360 iterations (b) - changes in the image becomes apparent due to the CT imaging dose.....	28
Fig. 12. Schematic of first generation optical tomography system.....	29
Fig. 13. Images and profiles along dotted lines of three means acquired with MRI (a) and OCT (b)	30
Fig. 14. Designed optical scanning system	32
Fig. 15. Main frame of horizontal positioning mechanism	33
Fig. 16. Horizontal frame mounting structure to vertical frame	33
Fig. 17. Cuvette holding structure	34
Fig. 18. Fabricated parts of optical fiber holder	34
Fig. 19. Structural schematic of the electronics of the positioning system.....	35
Fig. 20. General view of the control electronics	36
Fig. 21. Simplified structure of microcontroller program	36
Fig. 22. Scanning protocol for dose transition regions	37
Fig. 23. User interface for manual control of the positioning system.....	38
Fig. 24. Structural scheme of microcontroller program for manual table control.....	38
Fig. 25. Irradiation of samples arrangement: a) samples with polymer gel on the irradiation table; b) linear accelerator before irradiation.....	40
Fig. 26. Simplified structural scheme of data processing program for designed optical imaging system	42
Fig. 27. Simplified structural scheme of polymer gel image analysis program.....	43
Fig. 28. A photo of irradiated nMAG gel samples: 1-5 cuvettes - calibration samples, 6-8 cuvettes - samples with steep dose gradients.	44
Fig. 29. Calibration curves at different wavelengths	44
Fig. 30. Dose calibration curve at optimal wavelength (designed optical scanning system).....	45

Fig. 31. Dose mapping results of the first complex irradiation field sample using designed optical imaging system: a) 2D dose map; b) 3D dose surface; c) averaged dose profile in longitudinal direction.....	46
Fig. 32. Dose mapping results of the second complex irradiation field sample using designed optical imaging system: a) 2D dose map; b) 3D dose surface; c) averaged dose profile in longitudinal direction.....	47
Fig. 33. Dose mapping results of the third complex irradiation field sample using designed optical imaging system: a) 2D dose map; b) 3D dose surface; c) averaged dose profile in longitudinal direction.....	48
Fig. 34. With 7.5 MHz linear transducer acquired ultrasound images of samples irradiated with 0.5 Gy (a) and 2 Gy (b) dose.	49
Fig. 35. With 2.5 MHz micro – convex transducer acquired ultrasound images of samples irradiated with 0.5 Gy (a) and 2 Gy (b) dose.	49
Fig. 36. With 6.5 MHz endocavity ultrasound probe acquired images of samples irradiated with 0.5 Gy (a) and 2 Gy (b) dose.	50
Fig. 37. Relative pixel intensity-dose calibration curve acquired with document scanner	51
Fig. 38. Joint dose map of calibration vials (1 - 5 vials) and samples with steep dose gradients (6 - 8 vials).	51
Fig. 39. Dose mapping results of the first complex irradiation field sample using flatbed document scanner: a) 2D dose map; b) 3D dose surface; c) averaged dose profile in longitudinal direction. ..	52
Fig. 40. Dose mapping results of the second complex irradiation field sample using flatbed document scanner: a) 2D dose map; b) 3D dose surface; c) averaged dose profile in longitudinal direction. ..	53
Fig. 41. Dose mapping results of the third complex irradiation field sample using flatbed document scanner: a) 2D dose map; b) 3D dose surface; c) averaged dose profile in longitudinal direction. ..	54
Fig. 42. Relative pixel intensity – dose calibration curve acquired with CT scanner.....	55
Fig. 43. Joint 2D dose map of irradiated nMAG samples (CT scan).....	56
Fig. 44. Dose mapping results of the first complex irradiation field sample using CT scanning: a) 2D dose map; b) 3D dose surface; c) averaged dose profile in longitudinal direction.	56
Fig. 45. Dose mapping results of the second complex irradiation field sample using CT scanning: a) 2D dose map; b) 3D dose surface; c) averaged dose profile in longitudinal direction.....	57
Fig. 46. Dose mapping results of the third complex irradiation field sample using CT scanning: a) 2D dose map; b) 3D dose surface; c) averaged dose profile in longitudinal direction.	58
Fig. 47. Comparison of averaged dose profiles in the dose transition regions for the samples with complex irradiation field, using different imaging modes: a) designed optical imaging system; b) CT; c) document scanner.	59
Fig. 48. Comparison of calibration curves obtained using different dosimetric gel imaging methods: CT, document scanner and created photospectrometric system.....	60

List of tables

Table 1. Comparison of the most common radiation dosimeters	16
Table 2. Common formulations of polymer gel dosimeters	21
Table 3. Comparison of polymer gel imaging techniques	31
Table 4. Comparison of investigated imaging techniques	60

List of abbreviations

Abbreviations:

TLD – thermoluminescent detector;

2D – two-dimensional;

3D – three-dimensional;

TCP – tumor control probability;

NTCP – normal tissue control probability;

OSL – optically stimulated luminescence;

EPID – electronic portal imaging device;

THPC – tetrakis (hydroxymethyl) phosphonium chloride;

Bis – *N,N'*-methylene-bis-acrylamide;

AAm – acrylamide;

MAA – methacrylic acid;

AA – ascorbic acid;

THPS – tetrakis (hydroxymethyl) phosphonium sulfate;

NIPAM – N-isopropylacrylamide;

VIPAR – N-vinylpyrrolidone argon;

HEA – 2-hydroxyethylacrylate;

AAm – acrylamide;

RF – radiofrequency;

TOF – time of flight;

CCD – charge-coupled device;

OCT – optical computed tomography;

CT – x-ray computed tomography;

MRI – magnetic resonance imaging;

PMMA – poly(methyl methacrylate);

FWHM – full width at half maximum;

LED – light-emitting diode.

Introduction

Accurate delivery of radiation dose to the patient is one of the most important requirements in radiation therapy. Radiation dose for healthy tissues should be minimal, while maximum prescribed dose must reach the tumor volume. Therefore, dose must be delivered precisely to the treatment area. New emerging techniques, such as adaptive radiotherapy and volumetrically modulated arc therapy, can help solving this problem more efficiently [1]. However, there are many factors, that can lead to deviations from intended radiation dose distribution. Hence, validation procedures are mandatory, which allow to estimate the differences between planned and actual dose [2].

Many different tools are dedicated for the acquisition of the dose distribution data. Point detectors, for example, thermoluminescent detectors (TLDs), silicon diodes, ionization chambers, can be positioned in the volume of interest to acquire two-dimensional (2D) dose distribution, but technical solutions are cumbersome and inefficient. Such scanning configurations have limited spatial accuracy. Radiographic or radiochromic films does not have this limitation. These films enable to acquire 2D dose distribution with high spatial accuracy. Similar concept can be applied in dosimetric gels that have unique capability to measure dose distribution in three-dimensional (3D) space. These dosimeters perfectly meet the increasing needs for radiotherapy procedure verification [2].

Polymer gel dosimeters are the most commonly used dosimetric gels. Polymer gel dosimeter typically consists of monomers in gelatin matrix. When the gel is irradiated, due to polymerization of monomers, physical properties of the gel are affected, for example, optical density. Extent of polymerization depends on the absorbed dose [3]. Polymer gels have many advantages when compared to other dosimetric methods: tissue-equivalency, good spatial resolution and ability to measure dose distribution in three dimensions [4].

In order to acquire dose distribution data from polymer gel dosimeter, various methods can be used: magnetic resonance imaging (MRI), optical imaging, computed tomography (CT), ultrasound imaging. Nevertheless, existing imaging techniques are expensive, sophisticated, non-modifiable, some of them have insufficient dose sensitivity, spatial resolution, lack of extensive studies. Therefore, current methods are not optimal for analysis of dosimetric gels [2, 4, 5].

In this work, a design of simple, high spatial resolution, compact and open source photospectrometric 2D dose mapping system for primary analysis of dosimetric gels is described. Also, performance comparison with different dose readout techniques, including ultrasound, CT, optical imaging and photospectrometric scanning is performed to determine the most optimal imaging method.

Objective of this work: to develop a photospectrometric system for polymer gel imaging and perform a comparative study of different polymer gel imaging techniques.

Tasks:

1. Design and build a unique photospectrometric system for polymer gel imaging.
2. Prepare dosimetric gel samples simulating complicated irradiation fields.
3. Perform a comparative study of different dosimetric gel readout methods.

1. Theoretical overview

1.1. Review of dosimetry techniques

Modern radiation therapy is becoming more accurate, individualized to the patient and thus more complex. Novel techniques, such as volumetrically modulated arc therapy, image-guided radiation therapy, adaptive radiation therapy allow to reduce side effects to the patient and increase probability of cure, using complex treatment plans, higher radiation doses for the tumor, smaller treatment volumes, narrower irradiation margins [1]. However, these new techniques are more risky - inaccurately delivered treatment can lead to severe negative consequences for the patient. Output accuracy highly depends on various uncertainties in treatment delivery and planning, for example, set-up uncertainties, mechanical tolerances in the equipment, tumor localization and coverage with beams. Human body is a complex structure, tumor can be located near clinical organs, for example, spinal cord, which damage can cause irreversible disablement. Moreover, dose accuracy has significant influence on treatment effectiveness. From tumor control probability (TCP) and normal tissue complication probability (NTCP) curves (Fig. 1) it is obvious that even small variation in dose level ΔD has considerable influence on tumor control ΔP_T and extent of complications ΔP_{NT} [6].

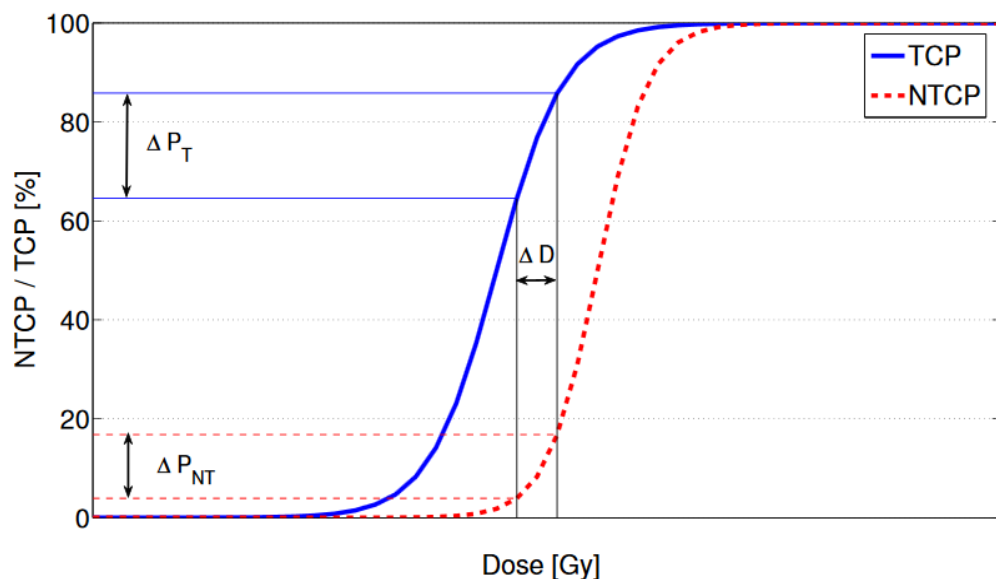


Fig. 1. Typical NTCP and TCP curves [6].

In order to avoid severe negative consequences, accuracy of treatment delivery must be validated to ensure prescribed dose to the tumor and minimal dose for normal tissues. Nonetheless, abilities to verify treatment do not progress as rapidly as the development of various treatment techniques. Nowadays, validation of treatment is implemented by measuring the dose distribution in phantoms which imitate patient. Traditional dosimeters, for example, ionization chambers and dosimetric films, are mostly used for dose distribution measurements [7]. These methods are labor-intensive and only partial dose distribution data is acquired [8].

One-dimensional (point) dosimeters are widely used in radiotherapy to validate dose delivery, calibrate output. They provide measurements in one point only, hence limited amount of dose distribution information can be acquired. Ionization chambers are popular one-dimensional dosimeters in radiotherapy. These chambers have linear response, high stability, can be used with

various beam energies, measurements can be gathered in real time. Limitation of these dosimeters is size. It can be a challenge to use them where steep dose gradients, inhomogeneous dose distributions are present [9]. Real-time measurements of small radiation fields can be acquired using silicon diodes and diamond detectors. However, these detectors demonstrate dependence from direction, sensitivity to lower energy photons (silicon diodes) or dependency on dose rate (diamond detectors). TLDs, optically stimulated luminescence (OSL) dosimeters are a popular point dosimeters choice, but they are more labor-intensive because readout of the dosimeter must be implemented separately using specialized equipment [6].

2D dosimeters allow to evaluate the dose distribution in the plane, thus providing more information comparing to point dosimeters. Most common types of 2D dosimeters are radiographic and radiochromic films, detector arrays, electronic portal imaging devices (EPIDs) [10]. Radiographic films enable to determine relative dose distribution in a plane. Nevertheless, artifacts are common in images, results can change between batches. Furthermore, this technique is labor-intensive - development of films is needed, particular developing conditions must be ensured. Radiochromic films are more convenient solution as they are self-developing. However, analysis of films is difficult, only relative dose data is acquired, energy dependence is demonstrated. Alternatively, 2D arrays of ionization chambers or semiconductor detectors can be used for the acquisition of 2D dose distribution. This technique allows to acquire absolute dose data simultaneously, measurements can be repeated. Although this method has drawbacks – spatial resolution is limited and depends on density of detectors. Interpolation of acquired results may be needed [11]. In 2D dose mapping, EPIDs are becoming popular. This device is integrated to a linear accelerator and projection images are acquired using treatment beam. EPIDs are typically used to determine patient placement, detect patients' motion. Also, EPIDs can be applied in a pretreatment verification, in-vivo dosimetry. Additionally, with this tool 3D dose distribution can be reconstructed [12].

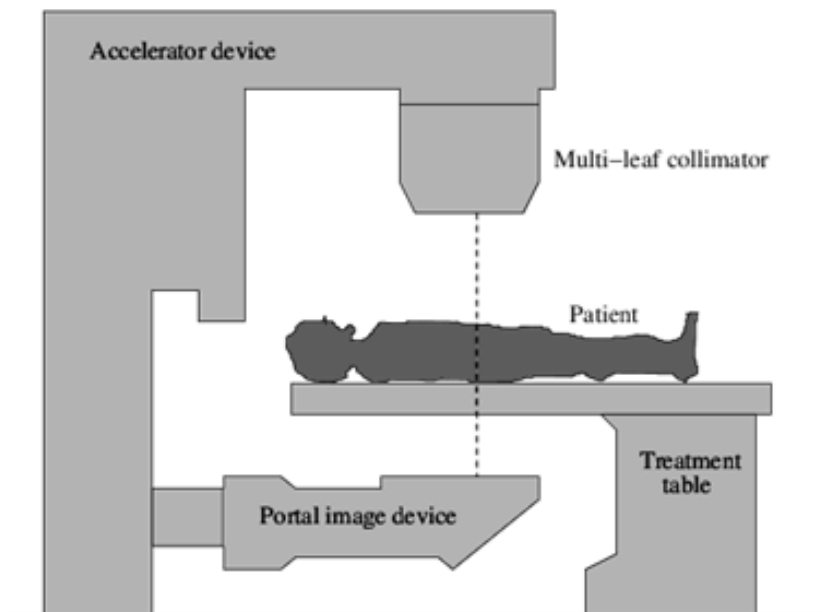


Fig. 2. Structure of a linear accelerator with EPID [13].

3D dose measurements are getting increasingly popular and important in clinical practice. In order to acquire a 3D dose distribution, point dosimeters, such as ionization chambers or semiconductor detectors, are distributed in the phantom. Detectors can be placed in a plane, ring or cross-sectioning planes [6]. Limitations are the same as in 2D dosimetric systems: sparse 3D dose distribution data is provided, accuracy depends on density of dosimeters, which is limited [2]. Alternative to this technique are 3D chemical dosimeters, commonly known as gel dosimeters. These dosimeters enable to acquire integrated dose distribution data in the volume. Working principle of chemical dosimeters is based on radiation induced chemical changes in the dosimetric material. Extent of these chemical changes is proportional to absorbed dose [1].

Two types of gel dosimeters are frequently used: Fricke and polymer gel. Fricke dosimeters consist of ferrous sulfate in gelatin solution. When such dosimeter is irradiated, ferrous ions are converted to ferric ions during oxidation process. Unfortunately, due to high ion diffusion these dosimeters demonstrate low spatial resolution [14]. Polymer gel dosimeters are used more frequently. Unlike Fricke gels, these dosimeters demonstrate high spatial resolution and chemical stability. Working principle of polymer gel dosimeters is based on radiation induced polymerization of monomers, dissolved in a gel. Dosimetric information from the dosimetric gels can be acquired using various methods: ultrasound, MRI, optical imaging, CT [14, 15].

Due to the nature of dosimetric gels, they are the only real 3D dosimeters that enable to acquire full dose distribution. High spatial resolution of these dosimeters is beneficial in investigating steep dose gradients. Another advantage – polymer gels mimic human tissues in terms of absorption of radiation, thus these dosimeters are tissue-equivalent [16]. Moreover, dosimetric gels can take the shape of the container they are in, consequently various phantoms (even individualized) can be made. These properties allow to apply polymer gel dosimeters in various fields of dose validation – external beam radiation therapy, brachytherapy (treatment technique, where radiation source is placed into the patients' body), evaluating new techniques [1, 4].



Fig. 3. Examples of various gel dosimeters: a) Fricke gel dosimeter irradiated with 12 MeV electron beams demonstrate color change; b) polymer gel dosimeter irradiated using intensity-modulated radiation therapy [1].

Advantages and disadvantages of the most common radiation dosimeters are summarized in table 1.

Table 1. Comparison of the most common radiation dosimeters [6, 14, 17-19].

Type of dosimeter	Advantages	Disadvantages
Ionization chamber	Instant, precise and accurate results.	Connecting cable, high voltage supply required, large size, corrections must be introduced, measurements in single point.
Semiconductor detector	High sensitivity, high voltage supply not required, instant results, inexpensive, small size.	Correction needed, angular dependence, connecting cable required, measurements in single point, non tissue-equivalent, radiation damage.
TLD/OSL	Small size, can be used in anatomic cavities, various forms can be used, no wires.	No instant results, separate reading procedure required, measurements in single point, calibration needed.
Detector array	2D dose information, instant results.	Limited spatial resolution, depends on density of detectors, angular dependence, radiation damage.
Film dosimeter	2D dose information, high spatial resolution, near tissue-equivalent.	No instant results, separate readout procedure required, non-reusable, relative results, energy dependent, calibration required.
EPID	2D dose information, instant results, 3D dose information can be reconstructed, can be used for in-vivo dosimetry during treatment.	Spatial resolution depends on density of detectors, complicated, lack of investigations, novel technique.
3D dosimetry phantom	3D dose information, instant results can be acquired (depending on technique).	Only sparse 3D dose distribution data, spatial resolution is limited and depends on density of detectors.
Polymer gel dosimeter	3D dose information, tissue-equivalent, various forms can be acquired, high spatial resolution.	Non-reusable, expensive, no instant results, complicated read-out procedure, toxic, cancerogenic materials, calibration required.

1.2. Basic principles of gel dosimetry

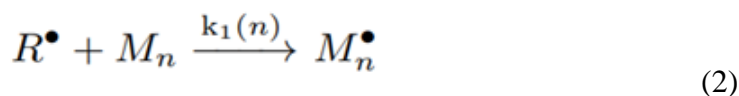
1.2.1. Processes in polymer gels

When polymer gel dosimeter is irradiated, water in the gel dissociates into radicals during a process called radiolysis. Radicals – atoms, molecules or ions that have unpaired electrons. Due to this configuration, radicals are highly reactive.

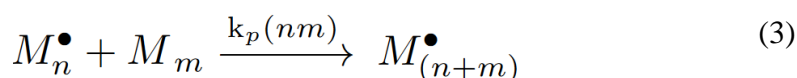
This process can be written in simplified manner where k_D is rate of dissociation [6]:



Created radicals react with monomers or previously created polymers and form polymer radical with reaction rate k_1 . This process is called initiation [4]:



Created polymer radicals grow by reacting with other monomers or polymer chains during process called propagation. General case, where polymer radical, containing n monomers, reacts with monomer or polymer chain consisting of m monomers, is written below [6]:



Type and ratio of monomers in a polymer gel formulation significantly affects structure of the polymer and properties of the formulation. If a linear monomer is used in the gel, for example, acrylamide, resulting polymers will be linear. If crosslinker, for example, *N,N'*-methylene-bis-acrylamide (Bis), is added to the formulation, branched polymer structure will be obtained. By changing the ratio of monomer and crosslinker it is possible to get differently branched polymers [6].

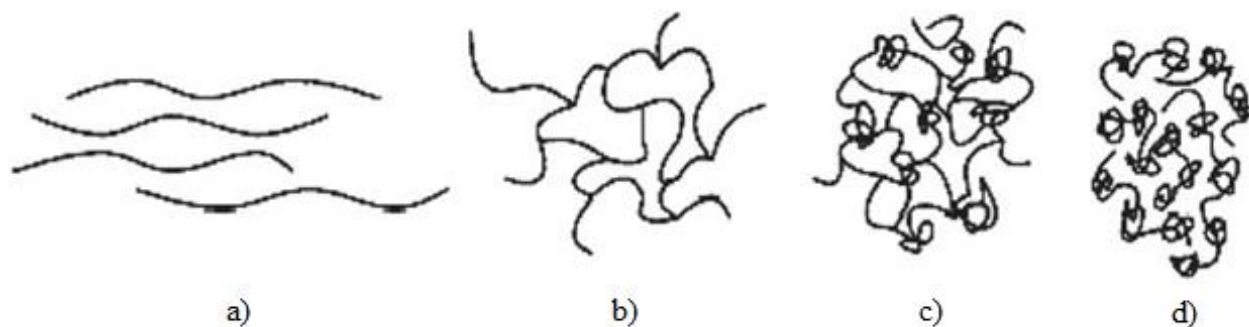
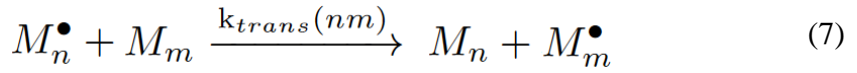
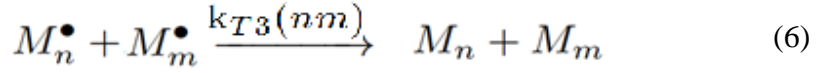
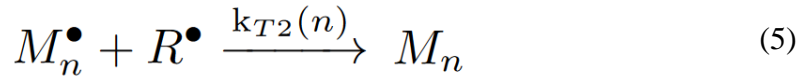
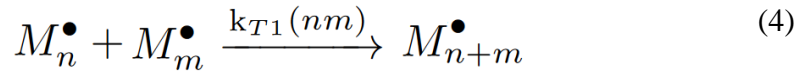


Fig. 4. Created polymer structures with different concentrations of crosslinker: a) only linear polymer is used; b) low fraction of crosslinker is used; c) high fraction of crosslinker is used; d) polymer gel consists only of crosslinker [4].

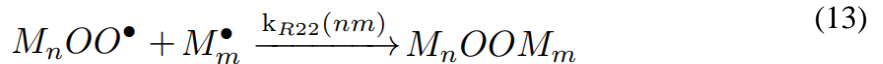
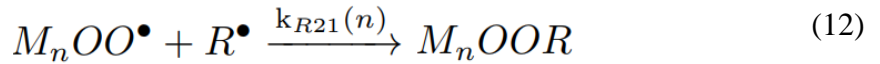
When two radicals react with each other, polymerization reaction is terminated during combination or disproportionation processes. These processes are very important because without termination reactions entire gel would polymerize when irradiated with even the smallest radiation dose. Combination reaction occurs when two radicals combine with each other (eq. 4-5). Disproportionation reaction occurs when hydrogen atom transfers from one polymer radical to another creating two non-radicals (eq. 6) [20]. Furthermore, termination of polymerization can be a consequence of radical group transfer to other molecules (eq. 7) [4].



Presence of oxygen in polymer gels can inhibit polymerization process. Highly reactive oxygen interacts with free radicals in the gel and peroxide radicals are created [21].



Created peroxide radicals react with other radicals in polymer gel causing termination of polymerization. These reactions progress in higher speed comparing to propagation reactions and can occur before irradiation of the gel [21].



This problem can be solved by preparing gel dosimeters in oxygen-free environment, for example, glovebox facility purged with nitrogen gas [4]. However, this technique is labor-intensive, specific equipment is required. There is an alternative for this approach – specialized antioxidants, such as ascorbic acid, tetrakis (hydroxymethyl) phosphonium chloride (THPC) can be added to polymer formulation intending to bind free oxygen and cancel termination effects [21].

In order to avoid diffusion of formed polymers and with this process associated spatial instability of the dosimeter, gelling agent is used. This agent fixes position of created polymer chains. Gelatin is most commonly used for this purpose [22]. Nevertheless, gelatin matrix is porous, thus small molecules and monomers are able to freely diffuse. If a polymer gel is irradiated with a half-blocked field, acquired dose profile oversteps expected profile. This is a consequence of diffusion of monomers from unirradiated area to irradiated area. Also, gelatin acts as a scavenger of water radicals, therefore sensitivity of the polymer gel depends on the gelatin fraction: with higher gelatin concentrations, sensitivity of the gel is lower due to smaller amount of available radicals for polymerization reactions. For sensitivity enhancement of polymer gel dosimeter catalyzers, which speed up chemical reactions, are frequently used [23].

All processes in polymer gel dosimeters are summarized in the figure below (Fig. 5). Firstly, free water radicals are created during radiation-induced radiolysis of water. Free radicals interact with monomers or polymers. Created polymer radicals react with other monomers or polymers forming polymer structures. Polymerization process can be inhibited due to radical interaction with other radicals, gelatin. Inhibitory effect of oxygen can be eliminated using antioxidants [22].

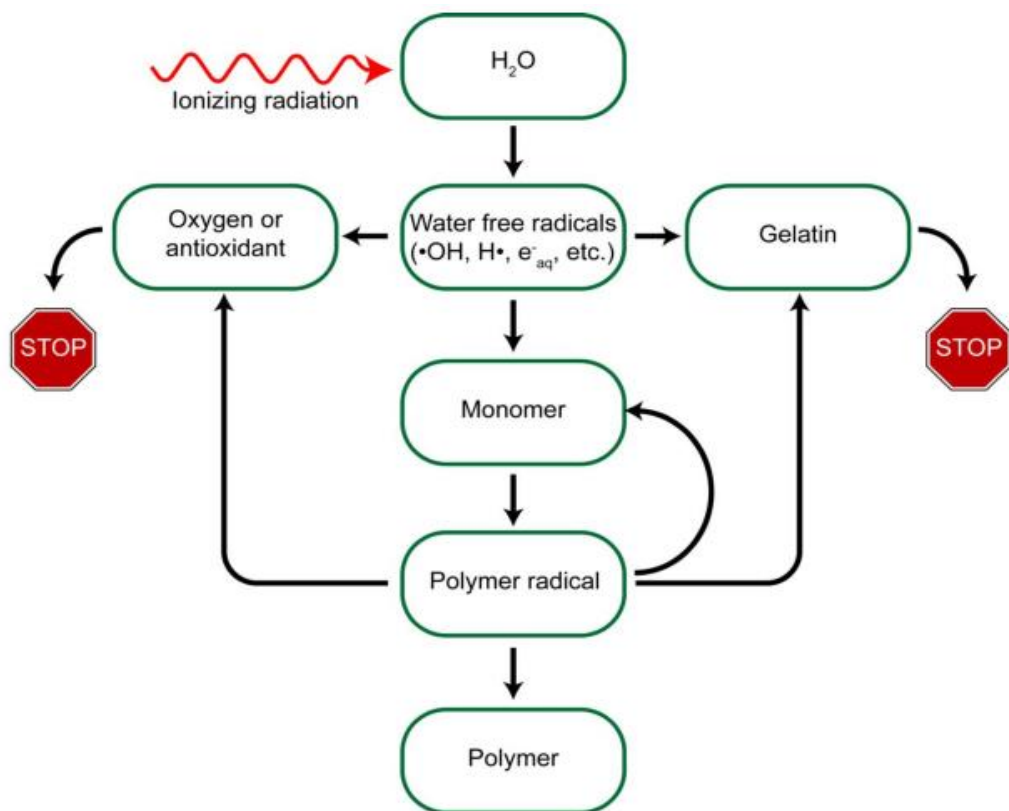


Fig. 5. Summary of processes in polymer gel dosimeters [23].

1.2.2. Development of gel dosimeters and their formulations

In order to better understand basic principles of gel dosimeters, development of gel dosimeter formulations must be reviewed, because it allows to ascertain why particular approaches are used. First formulations of radiation-sensitive gels were suggested in 1950 by Stein and Day. Irradiation of gels produced color changes [24]. Significant breakthrough was achieved in 1984 by Gore et al who investigated possibility to acquire dose information from Fricke ferrous sulphate chemical dosimeter using MRI. Unfortunately, due to diffusion of ions, it was unable to ensure stable dose distribution. Success solving this problem was limited [6].

First steps in polymer gel dosimetry were made in 1954, when Alexander et al investigated radiation effect on polymethylmethacrylate. In 1992, Maryanski et al proposed formulation where radiation-induced polymerization of acrylamide (AAM) and N,N'-methylene-bis-acrylamide (Bis) monomers occurs in agarose matrix. This gel had an acronym BANANA – Bis, AAM, nitrous oxide, agarose [25]. Important advantage of BANANA polymer gel dosimeter – this formulation does not have the diffusion problem, which was actual with Fricke gels, because created polymers are trapped in the gel matrix. Consequently, BANANA polymer gels were able to sustain dose distribution after the irradiation. Many different formulations of polymer gel dosimeters were investigated at that time [4].

Mentioned polymer gel dosimeters had a significant drawback – oxygen radicals, which were created during irradiation of the gel, diminished polymerization process. To avoid this problem gels had to be fabricated in oxygen-free environment, causing many inconveniences. This drawback was solved in 2001 by Fong et al who added antioxidants to gel formulation in order to bind atmospheric oxygen. Improvement enabled to fabricate polymer gel dosimeters in simple laboratory. Hence, new class of polymer gel dosimeters, named normoxic polymer gel dosimeters, was invented [25]. Various formulations of normoxic polymer gel dosimeters exist, for example, MAGIC gel, where methacrylic acid is used as a monomer and ascorbic acid acts as an antioxidant, or MAGAT gel, where methacrylic acid acts as a monomer and THPC is used as an antioxidant [6].

Therefore, typically polymer gel dosimeters consist of five major components [2]:

- Water
- Gelatin
- Monomer
- Catalyzer
- Oxygen scavenger (antioxidant)

Respect to type of monomer used all polymer gels can be grouped into two groups: polymer gel formulations where methacrylic acid is used are called MAG; formulations where acrylamide is used as a monomer are called PAG. Summary and composition of common polymer gel dosimeters are presented in the table below [20].

Table 2. Common formulations of polymer gel dosimeters [2].

Dosimeter designator	Base	Monomer	Crosslinker	Catalyzer/stabilizer	Scavenger/antioxidant
BANANA	Agarose	AAM	Bis		Nitrous oxide
BANG	Gelatin	AAM	Bis		Ammonium-persulphate, TEMED
BANG-2	Gelatin	MAA	Bis	Sodium Hydroxide	AA
BANG-3	Gelatin	MAA		CuSO ₄ -5H ₂ O	AA
MAGIC	Gelatin	MAA		CuSO ₄ -5H ₂ O, Hydroquinone	AA
MAGAT	Gelatin	MAA			THPC
nPAG	Gelatin	Acrylamide	Bis		THPS
nMAG	Gelatin	MAA			THPS
nMAG	Agarose, Gelatin	MAA			THPC
MAGIC-f	Gelatin	MAA	Formaldehyde	CuSO ₄ -5H ₂ O	AA
HEA	Gelatin	HEA	Bis		
VIPAR	Gelatin	VIPAR	Bis		
NIPAM	Gelatin	NIPAM	Bis		THPC
PAG	Gelatin	AAM	Bis	NaI	THPC

Bis: N,N'-methylene-bis-acrylamide; MAA: Methacrylic acid; AA: Ascorbic acid; THPC: Tetrakis (hydroxymethyl) phosphonium chloride; THPS: Tetrakis (hydroxymethyl) phosphonium sulfate; NIPAM: N-isopropylacrylamide; VIPAR: N-vinylpyrrolidone argon; HEA: 2-hydroxyethylacrylate; AAM: acrylamide;

1.2.3. Requirements for polymer gel dosimeters

Various polymer gel dosimeter formulations were investigated, but not all of them are applicable in clinical practice. Reliable polymer gel dosimeter should have these properties [20]:

- Dose response should be well-defined
- Dose response should not change over time (should be stable)
- Integrity of dose distribution should be stable over time
- Dose response should be not sensitive to environmental factors, energy, dose rate
- Dosimeter should be tissue-equivalent
- Dose range should be practical

In clinical practice, dosimeters are exposed to lower doses when compared to the actual patient exposure and then the dose distribution is scaled to the actual treatment dose. As a result, maximum dose of the dosimeter can be chosen freely [4]. In order to get best results dose range should be chosen considering linear dose range of the dosimeter because in case of non-linear response loss of dose resolution is present. Additionally, dosimeter should operate in dose range that is obtainable with the treatment unit [20].

To get reliable results with a polymer gel dosimeter it is important to ensure that dose response is not affected by the environmental factors, energy of the radiation and dose rate [26]. Temperature is one

of the most important environmental factors that affects speed of chemical polymerization reactions in gel dosimeter. In addition, viscosity of the gel changes with temperature. These factors can have a strong influence on the dose distribution. Moreover, fabricated polymer gel should be kept away from ambient light that can cause photopolymerization of the gel. Some dosimeters demonstrate response dependence on dose rate, consequently it can be complicated to determine actual dose. Energy dependence effects are not strong in external beam radiation therapy, but additional precautions should be made in brachytherapy [20].

Dose response should be stable in time. Response stability depends on polymer gel composition. Two parallelly occurring processes can affect dose information stability. One of them is associated with post-irradiation polymerization of comonomer (group of different type monomers) – polymer compositions. This process lasts up to 12 hours. Furthermore, dose response is affected by the gelation process of the gelatin. Gelation is a process when macromolecular chains form branched polymer structure leading to conversion of solution from liquid state to semi-liquid state. In polymer gels this process can last up to 30 days [27].

Integrity of dose distribution is mainly affected by the diffusion of monomers in the gel dosimeter. Monomers diffuse from unirradiated region to irradiated region, where they can react with polymer radicals changing dose distribution, particularly at steep dose gradients [4]. This effect appears as dose overshoots in transition region. Overshoot amplitude depends on many different factors. Dose overshoots are more pronounced with steep spatial gradients, at higher irradiation doses, lower gelatin, antioxidant (THPC) concentrations [28]. Also, it was notified that overshoot amplitude depends on post-irradiation time: overshoot increases till certain time and then starts to decrease [29].

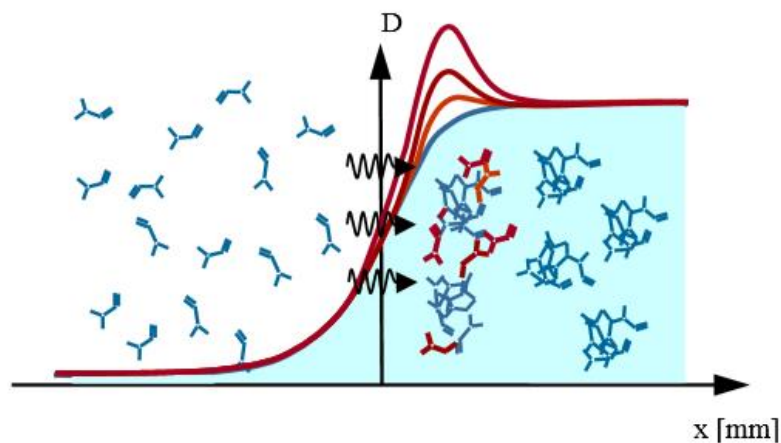


Fig. 6. Dose overshoots due to diffusion of monomers to irradiated area [27].

Spatial stability of polymer gel can be examined using dose profiles of a sample irradiated with half-blocked field. This allows to acquire information about extent of monomer diffusion in the polymer gel [27]. Width of penumbra region can be considered as a parameter of stability. Penumbra is defined as a region near the edge of the beam where dose falls. When conducting spatial stability measurements, it must be taken into account that beam divergence and scattering from shielding can have effect on the final result [30, 31].

Tissue-equivalency is also an important factor of the polymer gel dosimeters. In tissue-equivalent gel dosimeters, measured dose is equivalent to absorbed dose in the patient tissues. Electron density is

the leading factor determining tissue-equivalence [32]. Most polymer gel dosimeter formulations are tissue-equivalent, but there are some exceptions, especially at low energies [27].

As we can see, for primary evaluation of polymer gel formulation complex 3D imaging techniques are not obligatory. Polymer gels' performance - dose response, spatial, temporal stability - can be acquired using a 2D dose mapping system, which could significantly facilitate evaluation process.

1.3. Applications of polymer gel dosimetry

Polymer gel dosimetry has a unique set of properties when compared to other dosimetry methods: exclusively with polymer gels we can acquire a real 3D dose distribution with high spatial accuracy, polymer gels are tissue-equivalent in terms of absorption of radiation, they can be shaped to any form [33]. This allows to use polymer gel dosimetry in various medical and scientific fields – brachytherapy, external beam radiation therapy, diagnostic imaging, evaluating particle dose distributions [2].

1.3.1. External beam radiation therapy

Validation of external beam radiation therapy treatment plans is one the most promising application fields of polymer gel dosimetry. In this field gel dosimetry can be used to compare dose distribution, calculated by treatment planning system, with the actual measured dose distribution, determined using gel dosimeter. Precision of dose delivery is affected by many factors, for example, mechanical errors, scattering, patient positioning, anatomical variations [34]. There is a possibility that some of them will not be taken into account by the dose calculation algorithm leading to differences between calculated and delivered dose distributions. This aspect is extremely important with sophisticated treatment techniques, such as intensity-modulated radiation therapy or stereotactic radiosurgery, where steep dose gradients are present. When using these techniques even minor inaccuracies can lead to negative consequences to the patient. Only high spatial accuracy polymer gel dosimeters are able to provide reasonable data in this case. Other dosimetry techniques such as TLDs, ionization chambers, films, are inadequate to determine complex dose distributions [35].

1.3.2. Brachytherapy

Brachytherapy is a type of radiation therapy where radioactive source is placed inside the patients' body. Typical dosimeters, such as TLDs, ionization chambers, films do not demonstrate satisfactory performance with this type of procedure. These dosimeters are able visualize dose distributions only around single sources or simple arrangements. As polymer gel dosimeters are able to visualize complex dose distributions, these dosimeters are very attractive in brachytherapy. Nevertheless, use of polymer gel dosimeters in high dose rate brachytherapy faces some challenges. In some gel formulations shrinking of the gel was notified leading to inaccurate dose distributions, especially in high dose regions. This process is associated with polymerization-induced increase of polymer gel density and decrease of volume of the gel. Additionally, high dose rate near the source can induce temperature gradients which influence polymerization reactions. Problems also occur in low dose rate brachytherapy. As the time of exposure in low dose rate brachytherapy is long, diffusion of monomers becomes a problem and can lead to errors in dose distribution [36].

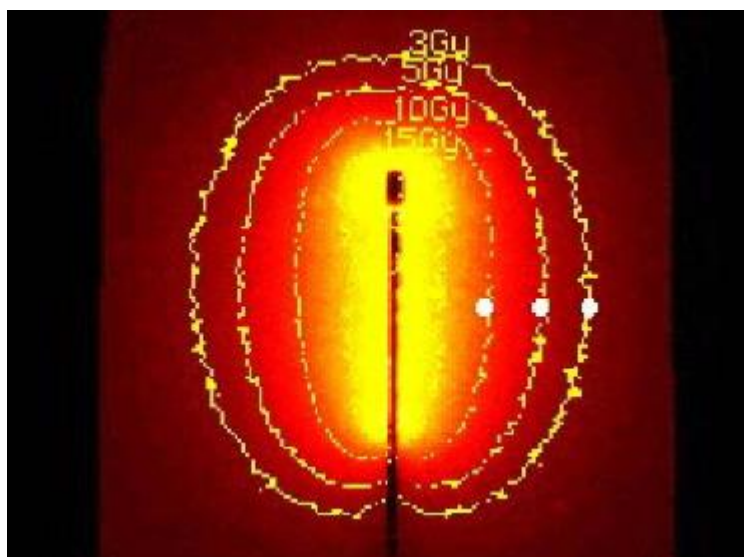


Fig. 7. Dose distribution around high dose rate brachytherapy source acquired by scanning polymer gel dosimeter with MRI [36].

1.3.3. Measurement of particle dose distributions

Using high linear energy transfer particles for radiotherapy it is possible to achieve very sharp dose delivery. Moreover, there is no dose to the patient from exiting beam due to Bragg peak phenomenon. Therefore, this is a type of radiation therapy that has a lot of potential. However, significant positioning uncertainty of sharp dose peak at particular depth exists. Polymer gel dosimeters, which can provide 3D dose distribution with high spatial accuracy, can help to validate dose deposition in the tissue [2].

1.3.4. Dosimetric investigations

As polymer gels allow to acquire dose distribution in multiple planes within single exposure, this technique enables simpler measurements of percent depth dose parameter (percentage of absorbed dose at any depth in relation to absorbed dose at reference depth), which is an essential characteristic of a linear accelerator. Polymer gels are also valuable in evaluating the effects of tissue heterogeneities because they are tissue-equivalent. For example, presence of lungs can be simulated by placing some plastic structures in the polymer gel, using air cavities, polystyrene or even lung-equivalent gel [36]. Polymer gel dosimetry can be potentially applied in quality assurance procedures of CT scanners. High sensitivity polymer gel is used for this purpose [37].

1.4. Read-out techniques of polymer gel dosimeters

In order to acquire dose distribution data from an irradiated polymer gel, various techniques can be used: MRI, CT, optical imaging and ultrasound. In this chapter, basic principles and features of each technique will be briefly described.

1.4.1. Magnetic resonance imaging

Magnetic resonance imaging is the most popular technique for acquisition of dose distribution data from polymer gels [38]. This technique allows to gather high contrast images in three dimensions, acquired results sufficiently agree with treatment planning systems' data [30].

When the object is placed in MRI machine, hydrogen nuclei in the object align with created strong external magnetic field because each hydrogen nuclei has magnetic dipole moment. Moreover, in presence of magnetic field nuclei precess in frequency called Lamour frequency [39].

$$f_{RF} = \frac{\gamma}{2\pi} B \quad (14)$$

where: f_{RF} – Lamour frequency, γ – constant, called gyromagnetic ratio, B – magnetic flux density.

Intending to gather images, radiofrequency (RF) pulse with frequency, equal to Lamour frequency, is sent to the object (Fig. 8a). The pulse makes net magnetic moment of hydrogen nuclei to change its orientation (Fig. 8b). When RF pulse is removed, net magnetic moment realigns with external magnetic field generating response signal in receiving coils during process called relaxation (Fig. 8c). From acquired data images are reconstructed using inverse Furje transform. Gathered images show proton density distribution. Density information mainly depends on measured T1 and T2 relaxation times, which are related to time needed in order to achieve initial value of net magnetization vector projections (Fig. 8d-e) [40].

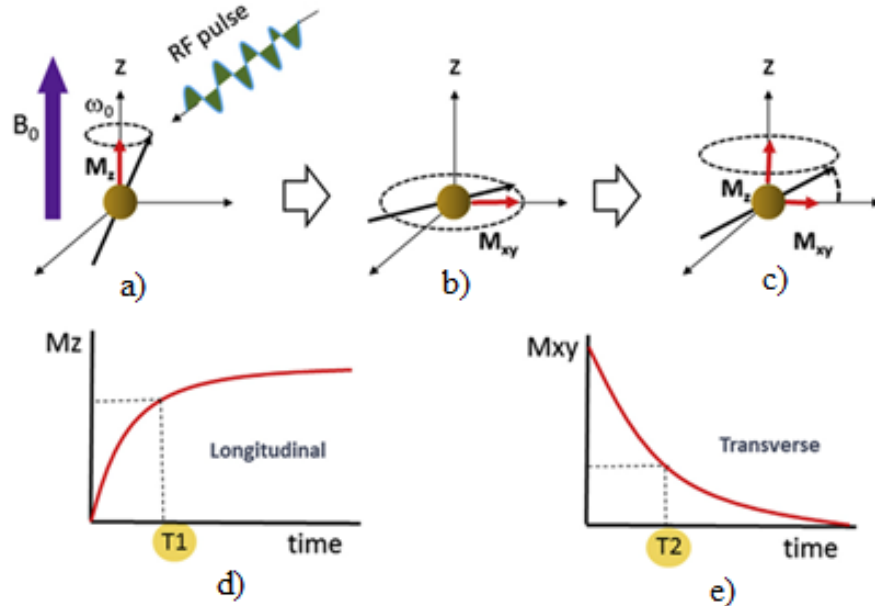


Fig. 8. Schematic of basic processes in MRI. a) alignment with external magnetic field; b) orientation change of net magnetization vector; c) realignment of net magnetization vector; d) longitudinal component recovery; e) transverse component recovery [40].

Main principle of dose distribution acquisition using MRI is based on the changes in mobility of water molecules in the gel after irradiation. Before irradiation, mobility of monomers is relatively high, also mobility of water molecules bound to monomers is high. When polymer gel is irradiated, mobility of water molecules, attached to polymer chains, becomes significantly lower, thus water proton relaxation times T1 and T2 are affected. Extent of polymerization depends on absorbed dose, thus it is possible to use dose-relaxation time calibration curve intending to acquire absolute dose information. T2 relaxation time is most frequently used for imaging of polymer gels because dose-relaxation time relationship is well-pronounced [41].

MRI imaging system has drawbacks. Firstly, sophisticated hardware, including superconductive magnet with liquid helium cooling, is needed. Moreover, clinical units are crowded with patients, system is expensive, consequently availability of this method for polymer gel imaging is low. Imaging artifacts are big problem also. Eddy currents, magnetic field inhomogeneities, temperature effects are common causes of distortion in acquired images [30]. Furthermore, according to some studies, source of uncertainty can be not optimal pulse sequences used for scanning. This effect especially pronounced at low doses: dose uncertainty at 1 Gy is 18.96%, but at 10 Gy decreases to 4.17 %. In order to get accurate results, optimized pulse sequences with particular repetition time, number of echoes and spacing between echoes must be used [38]. To sum up, imaging with MRI has drawbacks, therefore scientists turn their attention to less sophisticated, but sufficient imaging methods.

1.4.2. Ultrasound imaging

Ultrasound imaging is a perspective technique for polymer gel analysis. Ultrasound imaging is inexpensive, widely-available, relatively fast, demonstrates high sensitivity, acquired images have high resolution. Nevertheless, scientists are not giving much attention to this technique, more extensive studies are needed to explore perspectives of this method [42].

When polymer gel dosimeters are irradiated, polymerization processes affect ultrasonic parameters – ultrasound wave speed, attenuation (acoustic impedance). Typical ultrasound imaging device consists of translating or rotating table, where sample is placed, ultrasound transducer and detector. Transducer – detector system is placed on the opposite sides of the sample. In order to avoid attenuation effects, all components are immersed in the water. Amplitude difference between received and transmitted pulses or time of flight (TOF) of signal can be measured [43]. Each technique has its own advantages: TOF images have better image quality when compared to transmission images, however transmission images demonstrate better contrast between irradiated and unirradiated areas. Using translation or rotation of the sample during the imaging it is possible to acquire information from various sides of the sample and reconstruct tomographic images (cross-sectional 2D images) [4].

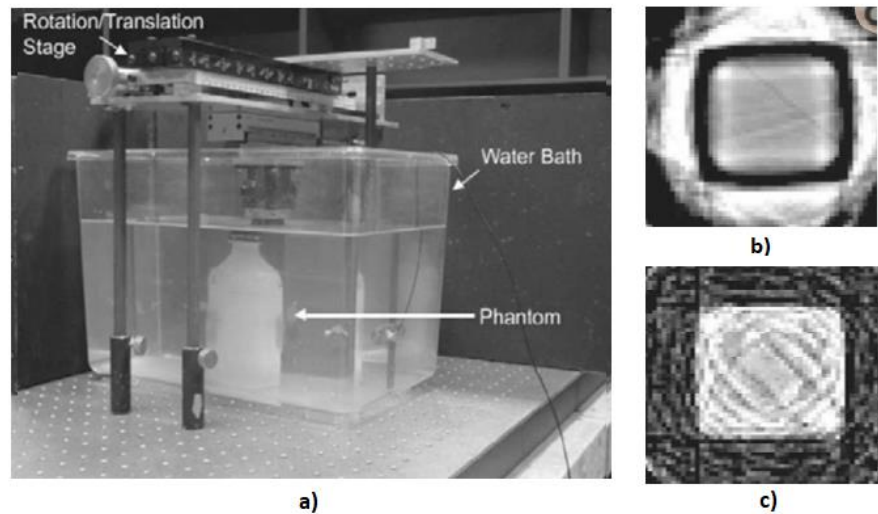


Fig. 9. Ultrasound scanner with translational mechanism (a); acquired transmission image (b); image, acquired using TOF method (c) [4].

Ultrasound imaging of polymer gels faces some challenges. Changes in ultrasonic properties are associated not only with physical density but also with elastic modulus, viscosity. Different polymer gel formulations have different elastic properties, as a result response of various gels can be considerably different. Furthermore, scattering, reflection effects are common, temperature effects on ultrasound parameters were observed. Influence of these parameters must be evaluated. Despite challenges, ultrasound imaging is a perspective technique, because it is simple, compact and low-cost. However, more investigations are needed to reveal its potential, since current research on the use of diagnostic ultrasound devices for polymer gel imaging is sparse [44].

1.4.3. Computed tomography imaging

CT imaging of polymer gels is based on polymerization – induced density changes in polymer gel. Due to density changes, x-rays are attenuated differently, thus it is possible gather dose distribution information. In CT imaging x-ray projection images are acquired from different angles around the object with table translation. It allows to reconstruct series of cross-sectional 2D images. CT imaging of polymer gels has practical advantages: CT scanners are more widely accessible than MRI, readout procedure is fast and simple, dose response acquired with a CT scanner is stable and not sensitive to environmental parameters, such as temperature [30].

In CT imaging it is very important to choose appropriate imaging parameters, because they can have a strong influence on the image noise level. Noise of the image can be reduced increasing tube voltage, current, slice thickness, pixel size, averaging, selecting appropriate reconstruction technique. Nevertheless, these modifications have significant impact on spatial resolution, dose level and imaging time, hence compromise between parameters should be found to get optimal results. Moreover, various post-processing algorithms can be used for image enhancement, for example, adaptive mean filtering which utilize local image characteristics [4, 45].

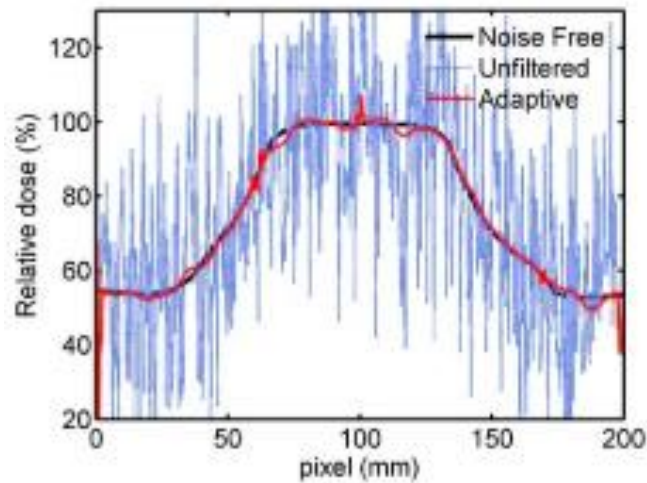


Fig. 10. Dose profile of unfiltered, filtered (adaptive mean filtering) and noise free images [45].

CT is not broadly used for polymer gel imaging because it has several significant drawbacks. Firstly, this method has low sensitivity at low doses. Dose sensitivity varies with gel composition, however even with the sensitive composition, lowest detectable dose is typically higher than 1 Gy. Another disadvantage – polymer gels are irradiated with additional dose during imaging. This effect is especially relevant when intense averaging is used (Fig. 11). Also, contamination problem becomes more significant with development of more sensitive polymer gel formulations for CT imaging in order to compensate low sensitivity of this technique [46].

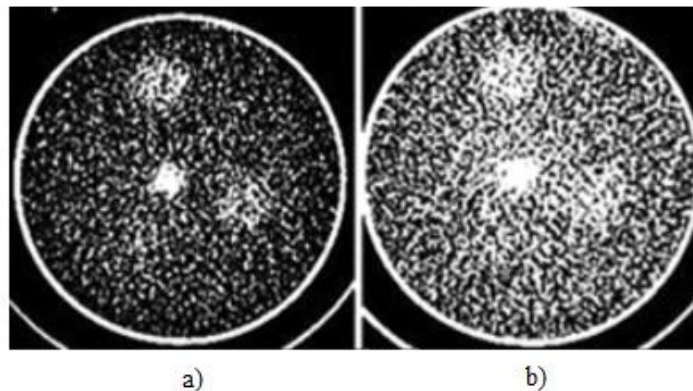


Fig. 11. Initial CT image (a); image after 360 iterations (b) - changes in the image becomes apparent due to the CT imaging dose [46].

1.4.4. Optical imaging

When polymer gel dosimeter is irradiated, polymer structures, that have light scattering properties, are formed. Consequently, optical attenuation in the gel depends on the absorbed dose. This property can be used to acquire dose distribution information. According to Beer's law, measured signal intensity I and intensity without sample I_0 are related in this manner (eq. 15) [30]:

$$I=I_0 \exp \left[- \int_{\text{ray-path}} \mu (s) ds \right] \quad (15)$$

Where μ is optical attenuation coefficient, s – optical path.

Basic principle of optical scanner for polymer gel dosimetry is very similar to x-ray imaging, but visible light instead of x-rays is used. Intensity of light, which passed through the sample, is measured with photoreceiver (typically, charge-coupled device (CCD) or similar semiconductor detector). Laser beam or incoherent light can be used as a light source [44].

Various configurations of such systems can be used to gather dose distribution information. In simple systems the sample is shifted to gather information from different points [47]. More complex systems use transmission information from various angles around the sample to reconstruct tomographic images similarly to x-ray CT. These scanners enable to acquire 3D dose distribution information and are called optical computed tomography (OCT) scanners [48].

There are several generations of optical tomography scanners. First generation optical tomography scanners typically use a laser and a single detector which are translated synchronously to acquire data from different points. Moreover, the sample is rotated to gather information at different angles around the object [45]. Frequently the sample is bathed into container with matching liquid intending to reduce the number of imaging artifacts, associated with refractive index differences. Significant drawback of first-generation systems – long scanning time. Full 3D scan of the sample can take hours to finish. To overcome this problem, systems with rotating mirrors or galvanometer-controlled mirrors were developed. These improvements allow to reduce scanning time to minutes rather than hours [4].

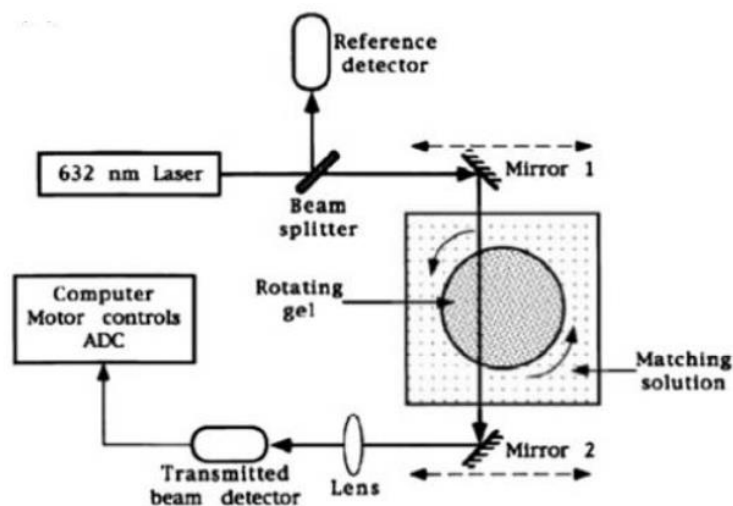


Fig. 12. Schematic of first generation optical tomography system [4].

Second generation optical tomography scanners are more advanced. In these scanners a cone shaped light beam and a CCD detector are used to acquire several slices simultaneously. It allows to considerably reduce imaging time when compared with the first generation systems. Third generation scanners use cone shaped light beam source also, but for detection a concentric array of detectors is used. Additionally, collimators for each detector are employed in order to reduce scattering effects. These systems have high scanning speed and scatter rejection capabilities, nevertheless they are only in development stage [49].

Optical imaging of polymer gel dosimeters has considerable advantages when compared to other imaging techniques. Optical imaging is simple, inexpensive, scanning device can be transported, 3D dose distribution can be acquired with high spatial resolution, noise level is lower comparing to MRI (Fig. 13). It is believed that optical imaging will substitute expensive and complicated MRI, which now is the most frequently used technique [44].

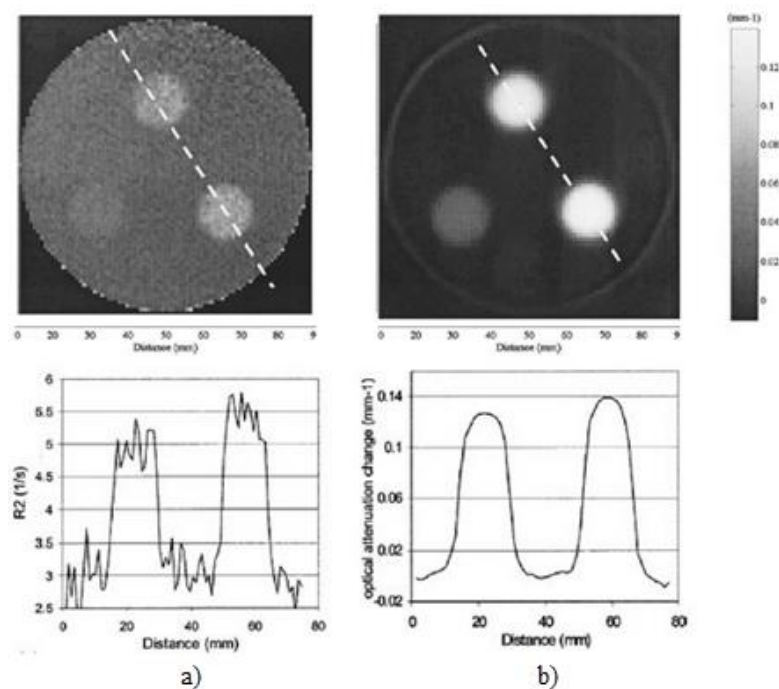


Fig. 13. Images and profiles along dotted lines of three means acquired with MRI (a) and OCT (b) [4].

Optical imaging of polymer gels has some disadvantages. Signal losses occur at the edges of the sample container. Furthermore, dose range is limited. Using optical imaging it is possible determine doses up to 10 Gy. At higher doses optical attenuation becomes so high, that it is impossible to acquire data. Conversely, if imaging is restricted only to low doses, it may lead to lower contrast. Additionally, size of the phantom (optical path length) is also limited because optical attenuation increases with size [30]. In various studies maximum diameter of cylindrical gel phantom for optical scanning varies up to 17 cm. Nonetheless, results depend on dose used, composition of the gel and scanning parameters [4, 50].

As an alternative for conventional optical imaging techniques, a standard document scanner could be used for integral dose distribution acquisition in 2D. Scanning principle of this device is based on capture of reflected light from the object using a photosensitive element. Typically, CCDs are used as sensors. Firstly, the document is illuminated with fluorescent lamp or a matrix of light-emitting diodes (LEDs). Then, the reflected light is captured from the sample while slowly translating the

scanning head across it. This technique allows to achieve unmatched spatial resolution, scanning speed is high, also reflection – based imaging could enable to use larger phantoms and higher irradiation doses. However, there are no studies regarding the application of a document scanners for polymer gel dosimetry.

Advantages and disadvantages of each polymer gel scanning technique are summarized in the table below.

Table 3. Comparison of polymer gel imaging techniques [4, 8, 30, 39, 41, 46, 49].

Technique	Advantages	Disadvantages
MRI	High contrast images, well-investigated technique, imaging is available in most clinics	MRI system is expensive and complicated, clinical units are busy, high noise level, artifacts are common, high uncertainty at low doses when not optimal parameters are used, sensitive to temperature changes.
Ultrasound	Inexpensive and widely available approach, high-resolution images, high dose sensitivity	Not well-investigated technique, scattering, reflection effects are common, temperature changes, elasticity, viscosity of the gel influence results.
Optical imaging	Relatively simple technique, good sensitivity, high spatial resolution can be achieved.	Poor signal at edges of the phantom, dose range and phantom size are limited, reflection – based imaging is not investigated.
CT	Stable dose response, cheaper and higher accessibility comparing to MRI, high spatial resolution, fast readout	Low sensitivity, polymer gel is irradiated with additional dose during imaging

MRI is considered as a gold standard of polymer gel imaging, however this technique is sophisticated and expensive. Computed tomography devices are more accessible, but this method has low sensitivity, the sample is irradiated with additional dose during the scanning. Perspective polymer gel imaging technique is ultrasound evaluation, nevertheless this method lacks of extensive studies. Optical imaging is promising alternative to expensive and cumbersome MRI. Optical imaging allows to achieve high spatial resolution, it has good sensitivity. This technique is particularly beneficial in situations with steep dose gradients where high spatial resolution data is required. However, existing in market optical tomography systems are quite expensive, sophisticated, inconvenient, they cannot be modified, it is not possible to acquire spectral information, select optimal acquisition wavelength. This limits applicability of the method. In addition, for primary analysis of polymer gels, acquisition of full 3D dose distribution with optical tomography is redundant, 2D dose mapping is sufficient. Therefore, current systems are not optimal for polymer gel analysis [2, 4, 5].

In this work simple, high spatial resolution, compact and open source photospectrometric 2D dose mapping system for primary analysis of dosimetric gels will be designed. Results will be compared with available conventional imaging method (CT) and alternative imaging techniques (ultrasound, flatbed scanner) in order to determine the most optimal method for polymer gel analysis.

2. Materials and methods

2.1. Design of dosimetric gel optical imaging system

In this work a simple high-resolution optical imaging system for polymer gel imaging was designed. Created measurement system is simple, compact, easily modifiable, has high spatial resolution – it is highly suitable for primary investigations of polymer gel formulations. System consists of Ocean optics USB650 UV-VIS optical spectrometer and cuvette positioning system. Ocean optics USB650 spectrometer is coupled to deuterium-tungsten halogen light source, with a wavelength range 350 – 1000 nm. Light reaches the sample through an optical fiber cable. Another optical fiber passes transmitted light to the spectrometer. Detector of the spectrometer is a 2048 element CCD detector with a 12 bit analog-to-digital converter and 25 μm slit size, allowing to achieve optical resolution of 2 nm FWHM (full width at half maximum).

Spectrometer itself can acquire information only in one point of the cuvette. In order to acquire data from various parts of the cuvette, positioning system was designed. Positioning system allows to shift cuvette in two directions – horizontally and vertically. Smallest possible step in the vertical direction is 0.15 mm, in horizontal direction – 0.125 mm. It means that spatial resolution, achieved with designed optical imaging system, is significantly higher when compared to most of existing optical tomography systems, which can achieve 0.33-0.5 mm spatial resolution at best [51, 52]. Additionally, spatial resolution of designed device is significantly higher compared to other, more complicated, imaging techniques, such as MRI and CT, that can achieve 0.5-1 mm spatial resolution [5]. Another advantage of the system – from gathered spectral data it is possible to choose optimal data acquisition wavelength that allows to achieve maximum sensitivity for any gel formulation. Created optical imaging system is especially valuable in situations where steep dose gradients are present, allowing to gather very precise dose distribution data. System is flexible and easily modifiable. High-resolution scanning can be set only in particular region of the sample, where detailed information is needed reducing imaging time. Designed optical imaging device is powered from the USB interface which is also can be used to acquire commands from computer. This permits for a high portability of the measurement system. Measurement results are saved in a .txt format using specialized spectrometer software. Further data processing is implemented using Matlab environment where final results are acquired.

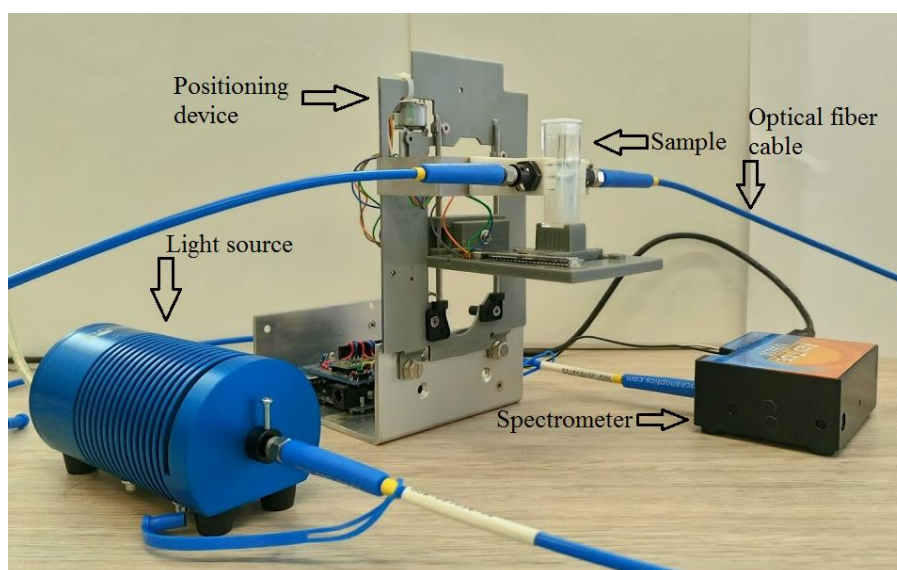


Fig. 14. Designed optical scanning system.

2.1.1. Design of scanning mechanism

All mechanical components of the system were designed using Solidworks or SketchUp CAD design software. Components were printed using Zortrax M300 3D printer using HIPS thermoplastic or laser cut from 300 series stainless steel.

As mentioned before, positioning mechanism transmits the cuvette in horizontal and vertical directions. Worm gear mechanism, powered by stepper motor, was selected to implement transitions of the sample. Selected solution provides good positioning accuracy, mechanism is compact. Another advantage - stepper motors have holding torque. It allows to maintain initial position of scanning mechanism. Worm gear mechanism for shifting in horizontal direction is mounted on specially designed plastic frame (Fig. 15). It is lightweight, thus reduces the load for vertical positioning mechanism. This mechanism consists of worm gear mounted on rigid metal frame. Vertical positioning part acts as a base and shifts entire horizontal structure.

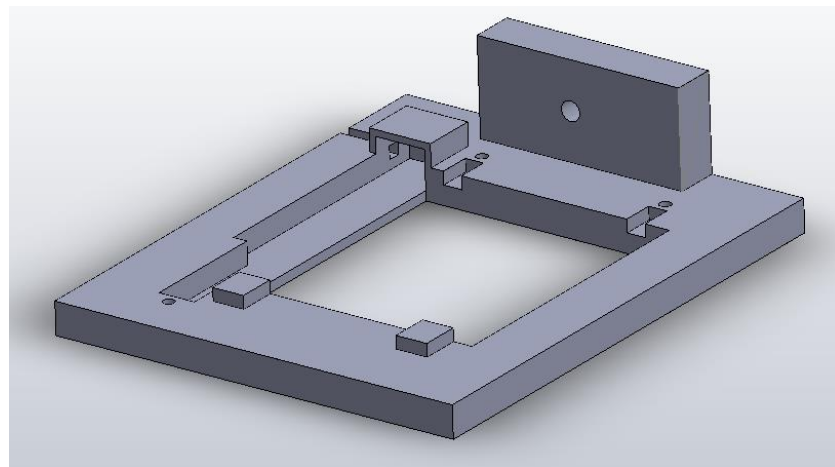


Fig. 15. Main frame of horizontal positioning mechanism.

In addition, with horizontal plastic frame two supplementary lightweight plastic parts were made: cuvette holding structure and horizontal frame mounting structure to vertical base frame.

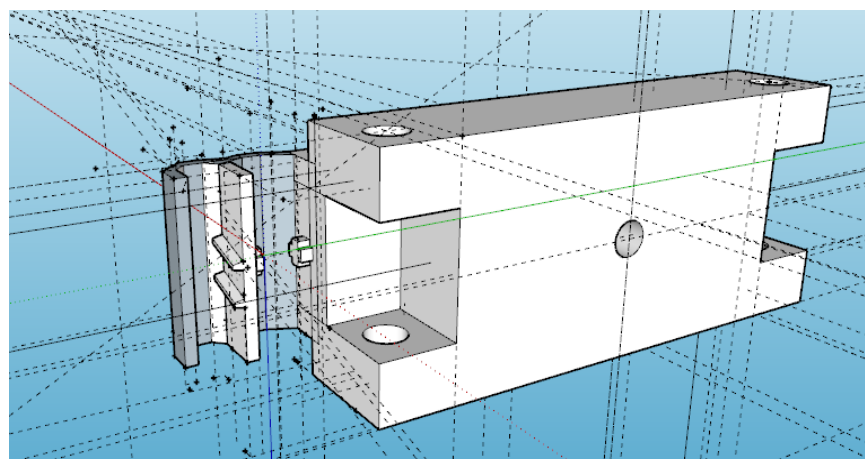


Fig. 16. Horizontal frame mounting structure to vertical frame.

Designed holding structure (Fig. 17) has two bulges that allow to steadily fix cuvette in the structure during the scanning. In addition, from the 3D model below it can be seen that mounting part of the cuvette is slightly extended. In absence of this extension it wouldn't be possible to scan full volume of the sample because optical fiber cable holders partially block movement of the sample.

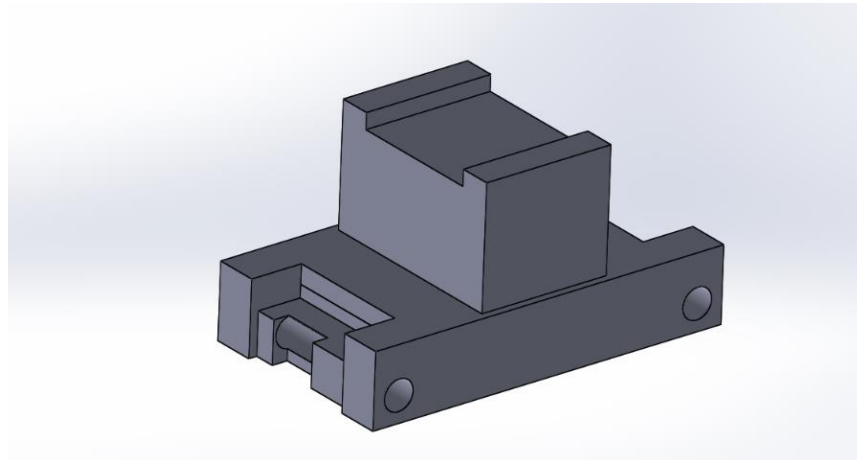


Fig. 17. Cuvette holding structure.

In the designed system two optical cables at opposite sides of the sample are used. One fiber is used to deliver light from the light source to the sample. A second fiber is used to transmit light from the opposite side of the sample to the spectrometer. In order to steadily fix optical cables, adjustable optical fiber holders were designed. The holder consists of two parts: stainless steel base, fabricated using laser cutting, and plastic holder for collimating lens block where optical fiber cable is screwed. Plastic component of the holder was fabricated with 3D printer. Moreover, adjusting screws were placed to enable the adjustment of the gap between holders where cuvette is placed.



Fig. 18. Fabricated parts of optical fiber holder.

2.1.2. Optical scanning system electronics

In order to control stepper motors, which were used in cuvette positioning device, specialized microprocessor-controlled system was designed. The system consists of microcontroller board, two different stepper motor driving circuits and voltage converter. Different stepper motor drivers were selected to reduce heating effects and optimize power consumption. Stepper motor drivers are controlled by the microcontroller board where all commands for transitioning system are defined. USB interface is used for control and power supply of the system.

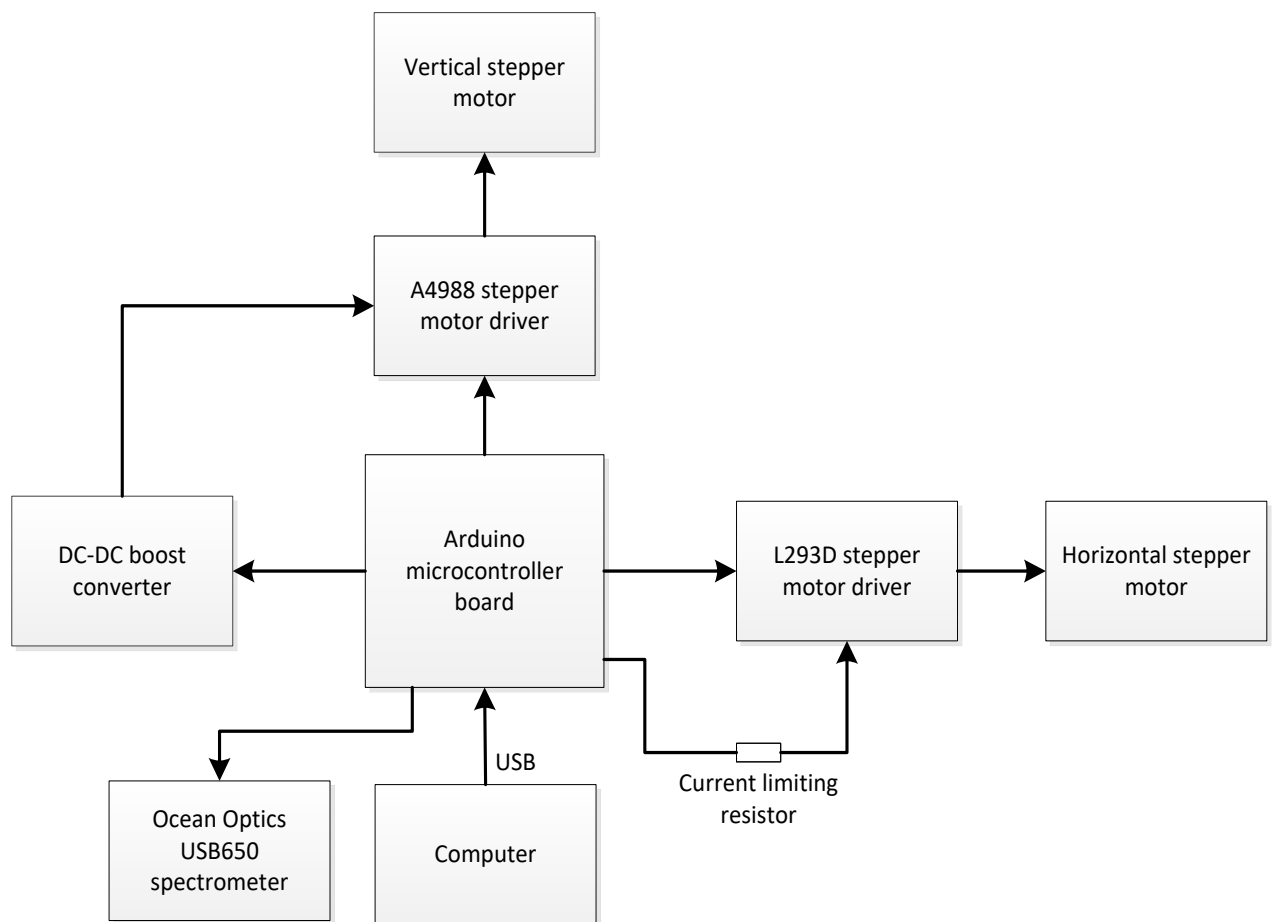


Fig. 19. Structural schematic of the electronics of the positioning system.

In the designed system low-power horizontal stepper motor is driven by L293D H-bridge chip. Vertical stepper motor shifts not only cuvette but also entire horizontal structure of positioning system, therefore in this case higher power stepper motor is used. This means that more powerful driving circuit is needed. A4988 stepper motor driver was chosen for this purpose. However, A4988 circuit has drawback – it must be powered with 8 V or higher voltage while USB interface provides only 5 V voltage [53]. To solve this problem additional DC-DC converter circuit XL6009E1 is used to boost the voltage to 10 V.

Arduino Uno microcontroller board for control of entire system was selected. Microcontroller board controls both transitioning mechanism and the spectrum acquisition with the spectrometer. Acquisition of spectrum occurs when the cuvette is shifted, and trigger pin of the spectrometer is set to high level. This feature allows to fully automatize scanning procedure, reducing possibility of errors and scanning time. In addition, there is possibility to control positioning mechanism manually using the created user interface.

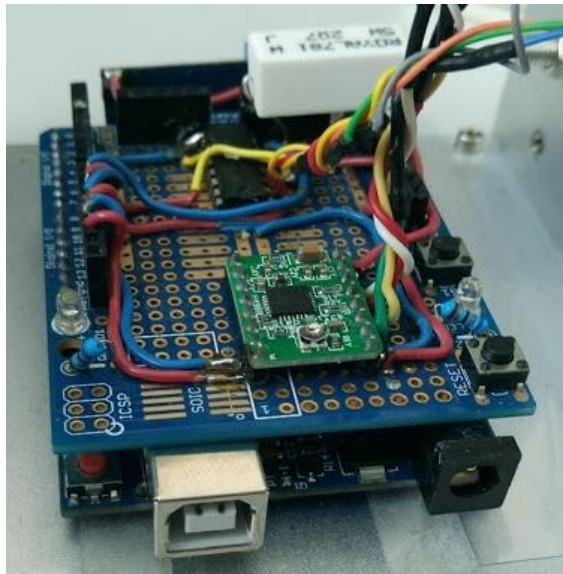


Fig. 20. General view of the control electronics.

2.1.3. Design of software

Software developing was implemented in three directions: creation of the firmware for the microcontroller, development of user interface in Windows environment and data processing automation using Matlab. Microcontroller firmware activates stepper motors according to predefined scanning order and controls spectrum acquisition. User interface in Windows environment was created for manual control of the positioning system. Matlab tools were designed to simplify analysis of results and will be described in separate data processing section.

Algorithm view of the microcontroller firmware is shown in figure 21. Firmware controls all variables, pin modes and interfaces for the A4988 and L293D stepper motor drivers. Additionally, at the end of motor activation functions, trigger signal is generated in order to initiate spectrum acquisition with Ocean Optics spectrometer when mechanical sample transition is complete.

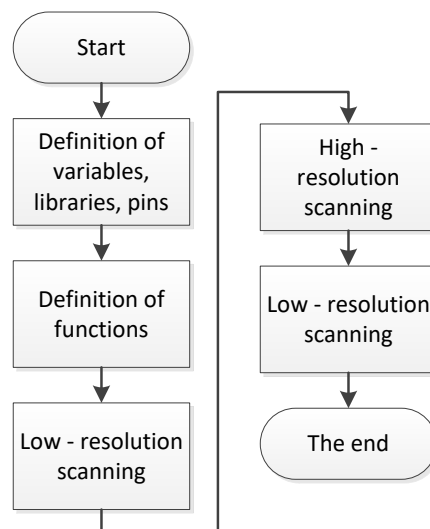


Fig. 21. Simplified structure of microcontroller program.

Designed software allows for two general modes of scanning – low and high resolution. Depending on the required experiment a custom scanning protocol can be devised. Areas of interest, for example, dose transition regions, were scanning with the following protocol. It consists of three parts: low-resolution lower part, high-resolution middle part and low-resolution over part. In low-resolution scanning region, 9 equally-distributed measurements are made by activating created transition–spectrum acquisition functions in predefined order. In high-resolution region scanning is implemented with highest possible resolution - 3762 equally spaced measurements are made. As mentioned before, distance between measurement points in horizontal direction – 0.15 mm, in vertical direction 0.125. After high–resolution scanning, remaining part of the sample is scanned in low resolution using procedure which is analogic to first part – 9 measurements are made. This scanning protocol is graphically depicted in figure 22.

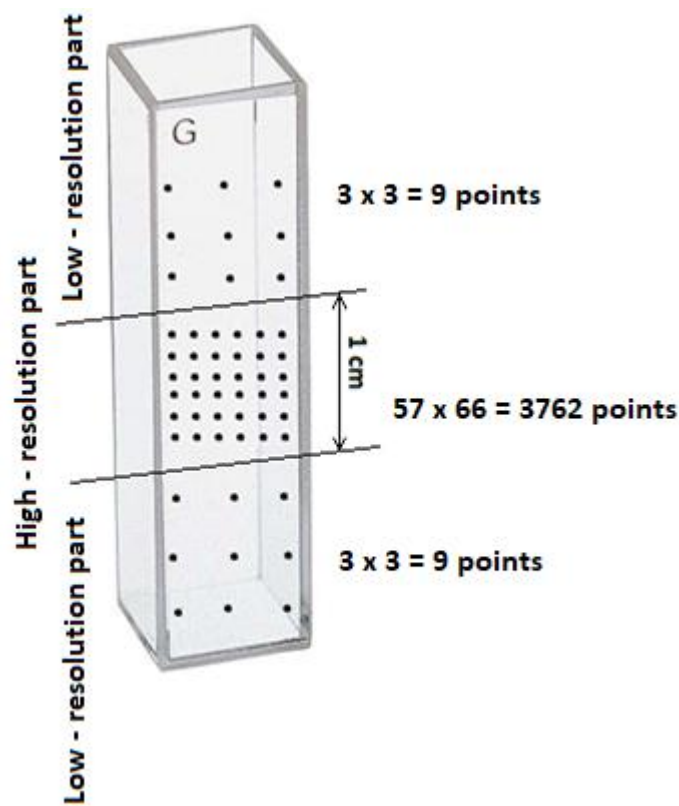


Fig. 22. Scanning protocol for dose transition regions.

Additionally, user interface for manual control of positioning table was created using Processing integrated development environment. This user interface sends specific code via serial interface to Arduino microcontroller when particular button is pressed. According to acquired code value microcontroller activate certain stepper motor. User interface of the position systems' control software is presented in Fig. 23.

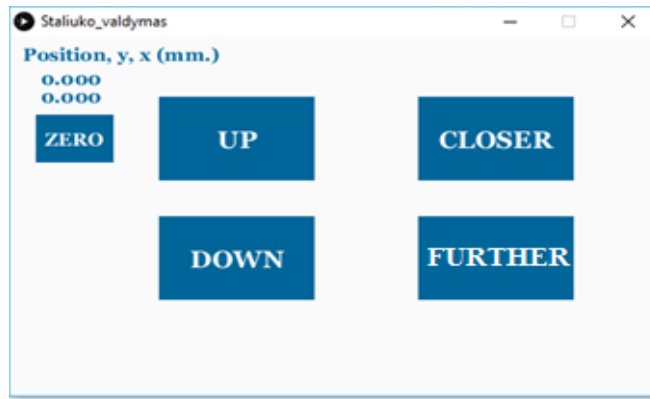


Fig. 23. User interface for manual control of the positioning system.

Separate Arduino microcontroller program was written to process code from user interface. In created program firstly code value is read from serial port. Gathered code value is checked with series of conditions. If the value satisfies particular condition, corresponding stepper motor is activated. For example, if acquired value is 3, then horizontal stepper motor is activated in clockwise direction. After activation of motor, process starts over again – new value from the serial interface is read. If the value does not satisfy any condition, process starts over again also. Structure of designed microcontroller program is depicted below:

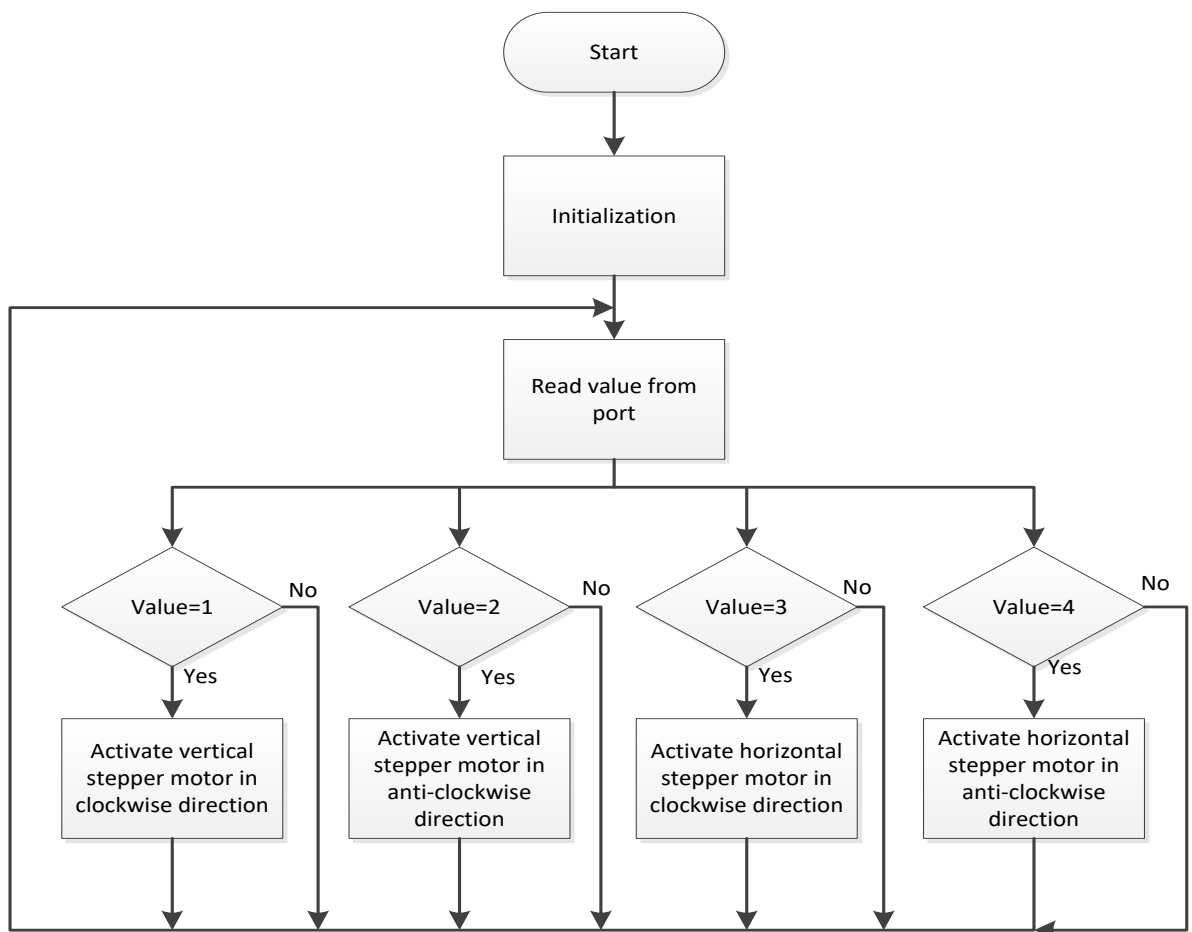


Fig. 24. Structural scheme of microcontroller program for manual table control.

2.2. Dosimetric Gel

nMAG normoxic polymer gel was used for comparative analysis of polymer gel imaging techniques. Used nMAG polymer gel formulation consists of:

- Gelatin
- Distilled water
- Methacrylic acid (MAA)
- Tetrakis (hydroxymethyl) phosphonium chloride (THPC).

Purpose of the gelatin in the polymer gel formulation is to prevent monomer diffusion, which greatly reduces the spatial integrity of the gel. Distilled water is used as a solvent and comprises the most of polymer gel mass. Methacrylic acid acts as a monomer. THPC is a very effective oxygen scavenger [54].

A total of 100 ml of the nMAG gel was prepared using the following procedure:

1. 5 g of gelatin (300 bloom, Sigma Aldrich) and 43 ml of distilled water were poured to the preparation container.
2. The mixture was left still for 15 min to swell. Then, additionally 43 ml of distilled water was added.
3. The solution was mixed in the mixer and at the same time heated to 40° C for 10 min until optical transparency was reached.
4. 4 g of MMA was added into the solution while mixing and heating to 42 °C for 5 min.
5. Solution at 41 °C temperature was poured to a separate container with 0.67 g of THPC and mixed with while sustaining temperature for 5 min.

Fabricated gel was poured to poly(methyl methacrylate) (PMMA) cuvettes (12 x 12 x 46 mm) with a sealing cup. When pouring polymer gel to cuvettes it is important to avoid any air bubbles in the gel because oxygen inhibits polymerization reactions, bubbles cause uniformities in acquired dose distribution [15]. In order to avoid photopolymerization effects, before irradiation, samples were held in a light-tight plastic box.

2.3. Irradiation of the dosimetric gel

Irradiation of polymer gel samples was conducted in the Hospital of Lithuanian University of Health Sciences Kaunas Clinics branch Oncology hospital. Varian Clinac DMX linear accelerator was used. Samples were irradiated with 6 MeV energy photon beam, field size: 10 cm x 10 cm, source-surface distance (SSD): 100 cm, dose rate: 300 cGy/min. During irradiation samples were placed behind tissue-equivalent PMMA slab phantom to ensure dose build-up. Different irradiation doses and field shape modification were applied during the irradiation of the samples. A set of gel samples were fully irradiated with 0.5 Gy, 1 Gy, 2 Gy, 3 Gy, 4 Gy doses in order to obtain calibration curve. Expected dose-response curve is linear, thus selected number of points is adequate [55, 56]. In addition, three gel samples for analysis were irradiated with a complex shape radiation field, by covering part of the sample with lead shielding. Irradiation was performed 72 hours after the preparation of the gel.

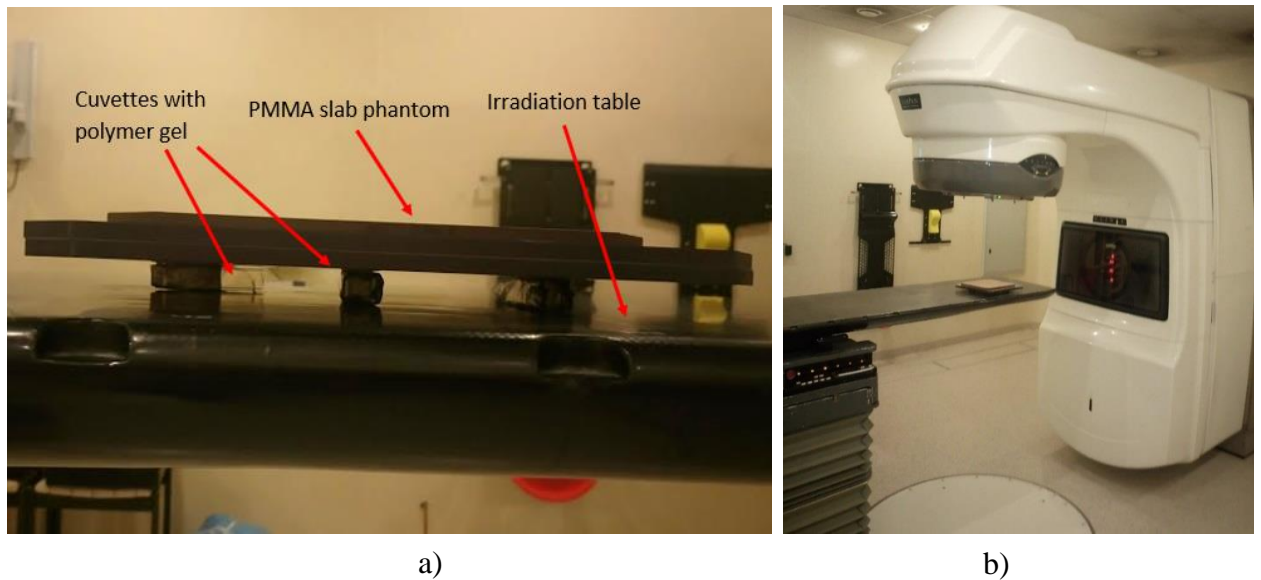


Fig. 25. Irradiation of samples arrangement: a) samples with polymer gel on the irradiation table; b) linear accelerator before irradiation.

2.4. Readout methods used for imaging comparison

Irradiated polymer gels were scanned using optical methods, computed tomography and ultrasound diagnostics equipment. All of the imaging methods provided a 2D matrices of data. Analysis of obtained results was predominantly implemented using created algorithms in Matlab, due to high amounts of data points.

2.4.1. Scanning using designed optical imaging system

When using the designed optical imaging system, different settings were applied for obtaining calibration curve data and acquiring the dose maps. Calibration curve was gathered by scanning the calibration samples in low resolution mode – 36 equally distributed measurements were taken in every sample. At each measurement point absorption spectrum was acquired. Using a specially designed Matlab code, calibration curves were generated from averaged spectral data at optimal wavelength which was determined.

Samples, irradiated with complex shape field, were scanned in high-resolution mode. Step size between data acquisition points was 0.15 mm in vertical direction and 0.125 mm in horizontal direction. In order to reduce scanning time, only 10 mm width dose gradient region was scanned. In the remaining part of the cuvette, where the sample was irradiated uniformly, scanning was implemented using low resolution mode: 9 equally distributed measurements were made in 5 mm width regions above and below high-resolution scanning region. Dose maps were generated by rearranging spectral data from 3780 points to absorbance map and applying calibration curve.

2.4.2. Scanning using diagnostic ultrasound imaging device

Esaote Biomedica medical ultrasound imaging device was used to evaluate viability of the method for gel imaging. Two polymer gel samples, irradiated with 0.5 Gy and 2 Gy doses, were scanned with three different ultrasound probes: 7.5 MHz linear probe, 2.5 MHz micro-convex probe and 6.5 MHz

endocavity probe. Samples were imaged in a container filled with water to ensure matching of acoustic impedances and avoid reflection of ultrasound waves before reaching the sample. During image processing, pixel values in images of differently irradiated samples were compared. Averaging functions were applied in areas of interest.

2.4.3. Scanning using a document scanner

Since there aren't any investigations about application of document scanner for polymer gel imaging, it is an interesting prospect and was included in this work. HP Scanjet G4050 document scanner was used in the experiments. Scanning was implemented using different resolutions: 300 dpi, 600 dpi, 1200 dpi, 2400 dpi and 4800 dpi. Selected color depth – 24 bits. Joint image of samples was saved in an uncompressed .bmp file format. Additional pre-processing step was used for conversion of images to grayscale, in order to match with the other used imaging techniques.

2.4.4. Scanning using computed tomography

GE BrightSpeed CT scanner, situated in the Hospital of Lithuanian University of Health Sciences Kaunas Clinics branch Oncology hospital, was used for dosimetric gel imaging. Scanning parameters were as follows: X-ray tube voltage - 120 kV, tube current – 340 mA, slice thickness – 1.25 mm, field of view – 500 x 500 mm, image size – 512 x 512. All samples were oriented parallelly to the scanning direction and scanned simultaneously. 89 cross-sectional images of samples were acquired in the helical scanning mode. From the obtained images digitally reconstructed radiograph was created using Plastimatch software.

2.5. Data processing

To optimize the analysis and reduce possibility of error, with the designed optical imaging system acquired data processing was automatized using created program in Matlab environment (see Appendix 2). For calibration curve generation program automatically calculates average spectrums from 36 measurement points in each differently irradiated calibration sample and converts spectrums to dose – absorbance calibration data at various wavelengths. After that, optimal acquisition wavelength is determined according to maximum differences between absorbance values in calibration data. Expected dose – absorbance relationship should be linear, therefore final calibration curve is generated when gathered calibration points at optimal wavelength are approximated with first order polynomial [55, 56].

For dose map of the sample acquisition, gathered 3780 spectrums at separate text files are converted to a single absorption data vector at optimal wavelength. After that, these values are automatically redistributed to absorbance matrix, where position of each element corresponds to measurement position. In order to acquire dose map, calculated calibration curve is applied to the absorbance matrix. Additionally, dose transition region between unirradiated and irradiated parts is depicted with 3D dose surface, where x, y coordinates correspond to position of points in 2D dose map and z coordinate describes dose level. For more detailed analysis of dose distribution at edge of irradiation field, in transverse direction averaged dose profile along the cuvette was generated. Average was calculated considering curved shape of dose distribution.

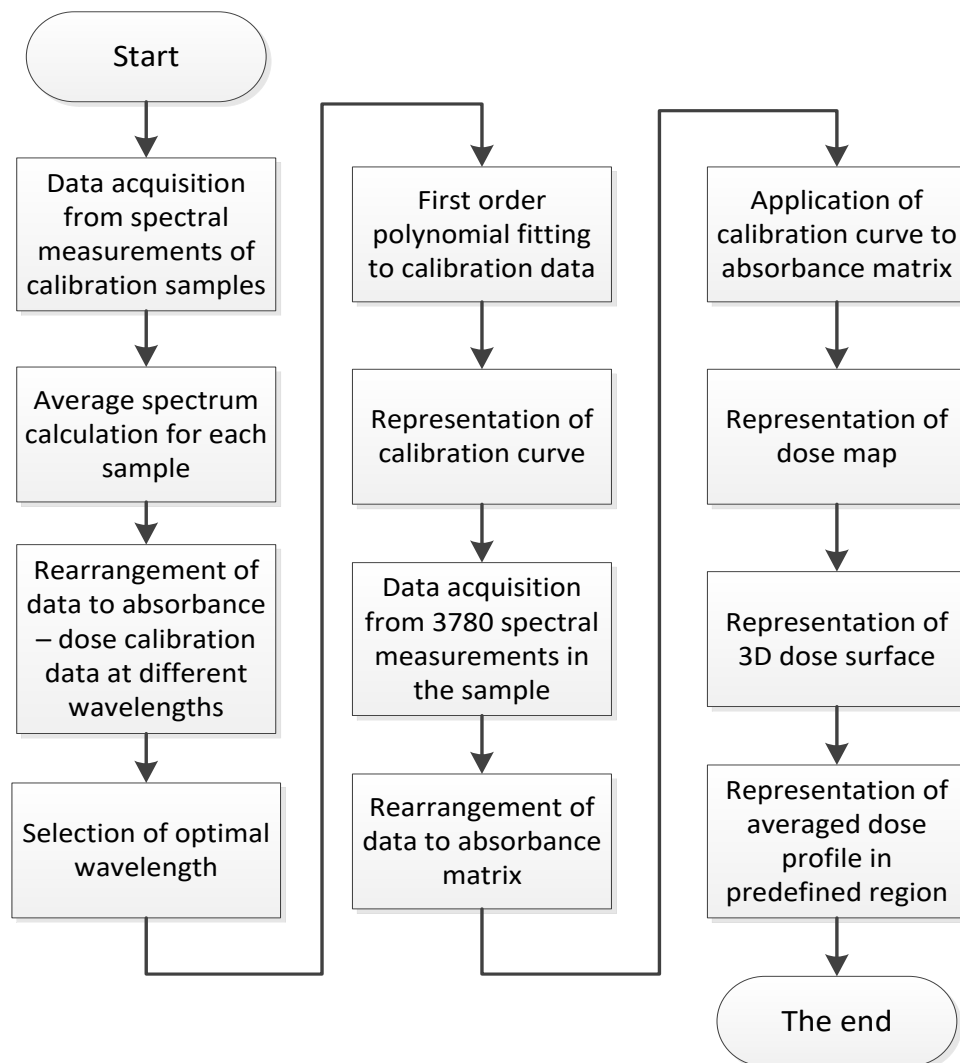


Fig. 26. Simplified structural scheme of data processing program for designed optical imaging system.

In addition, a separate Matlab program was created for automated analysis of polymer gel images acquired with CT and document scanner (see Appendix 3). Firstly, the image is read as a grayscale image for optimized analysis. After that, program asks user to mark regions in the photo, which will be used for acquisition of calibration data. In each marked region averaged calibration data is approximated with the first order polynomial. Acquired calibration curve is applied to the joint image of samples and dose map is generated. For more detailed analysis the program asks the user to mark transition region in sample which will be depicted as 3D dose distribution surface. The program also asks the user to mark curvature of dose distribution in sample to gather in transverse direction averaged dose profile of dose transition region along the cuvette.

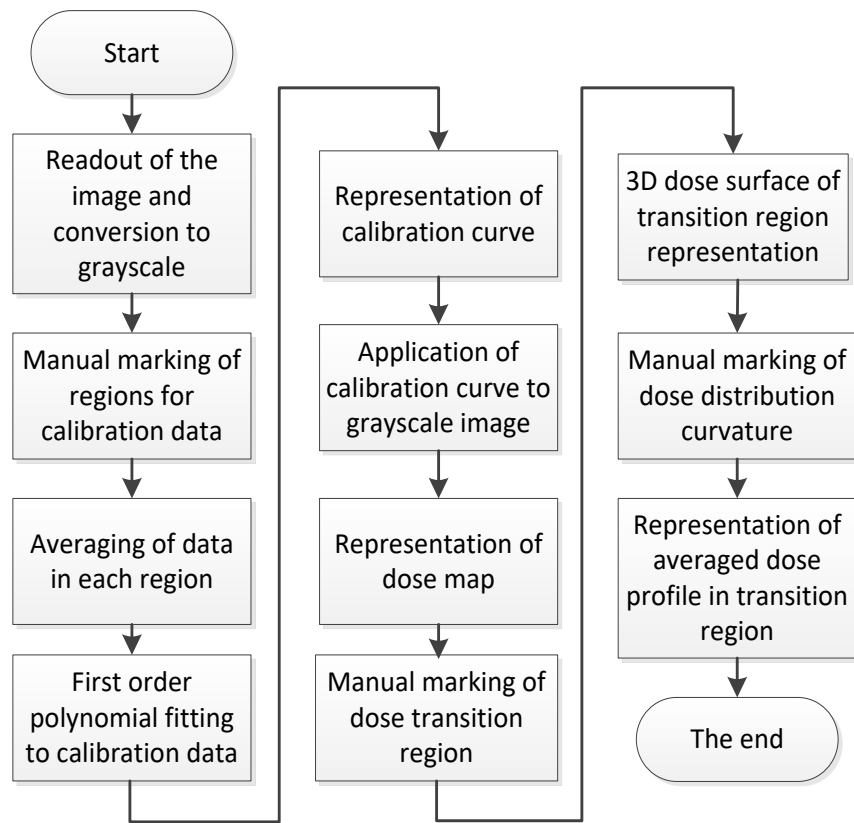


Fig. 27. Simplified structural scheme of polymer gel image analysis program.

3. Results and discussion

Different dosimetric gel imaging techniques will be evaluated in this section. Calibration curves and dose maps are analyzed, as these parameters are the most commonly used integral characteristics of the dose gels [4, 15]. A photo of the samples investigated and described next is shown in figure 28.

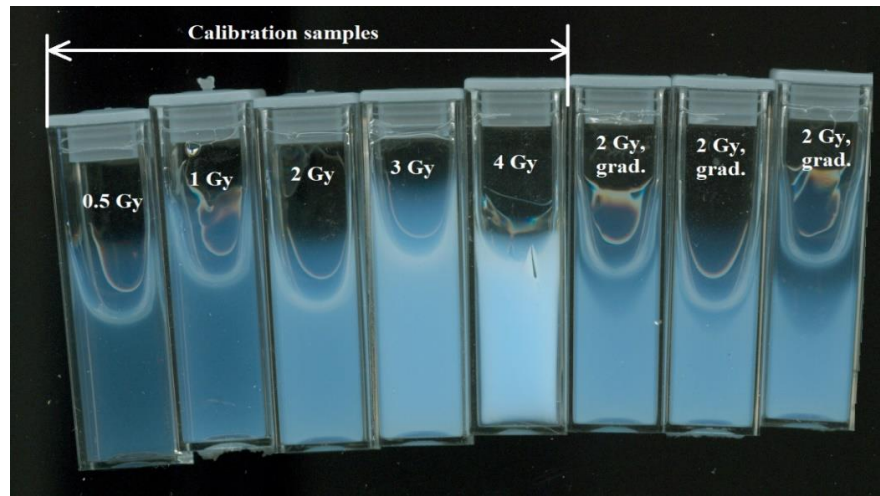


Fig. 28. A photo of irradiated nMAG gel samples: 1-5 cuvettes - calibration samples, 6-8 cuvettes - samples with steep dose gradients.

3.1. Determination of the optimal nMAG readout wavelength

Due to the nature of the designed optical imaging system, it generates a full spectral data file for each experimental point. Such quantities of data make data processing cumbersome, thus a pre-analysis of the obtained calibration data was performed, to obtain the most optimal single wavelength for further analysis. Criteria for optimal wavelength was the highest difference in response (sensitivity) between different doses.

From gathered data it was determined that the most optimal nMAG dosimetric gel readout wavelength is 509 nm. This result not only makes this research more efficient, but also allows for a simpler readout system, where a monochromatic light source could be employed with a simple light intensity sensor for readout.

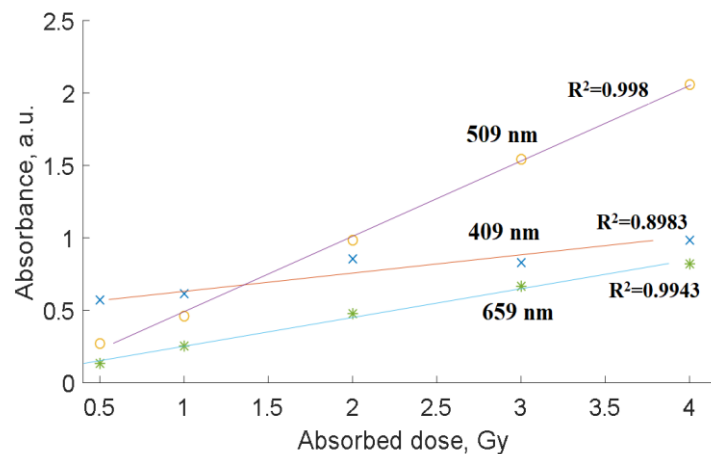


Fig. 29. Calibration curves at different wavelengths.

From the figure above it can be notified that at optimal wavelength maximum sensitivity (steepness of calibration curve) and linearity (R^2 value) can be achieved. When calibration curve was acquired at other wavelengths, results were worse. Hence, selection of optimal wavelength ensures the most optimal operating regime of the designed system.

3.2. Imaging of nMAG samples using designed optical imaging system

Firstly, a calibration curve was acquired at optimal wavelength using the designed optical imaging system. As it can be seen (Fig. 30), the calibration curve is close to ideally linear. Calibration data can be approximated by first order polynomial with $R^2 = 0.998$. Such linear dependency is of high practical value for nMAG dosimetric gel. To compare different readout methods, the derivative of calibration curve was used, as a measure of sensitivity. Determined derivative value, when normalized data was used – 0.253.

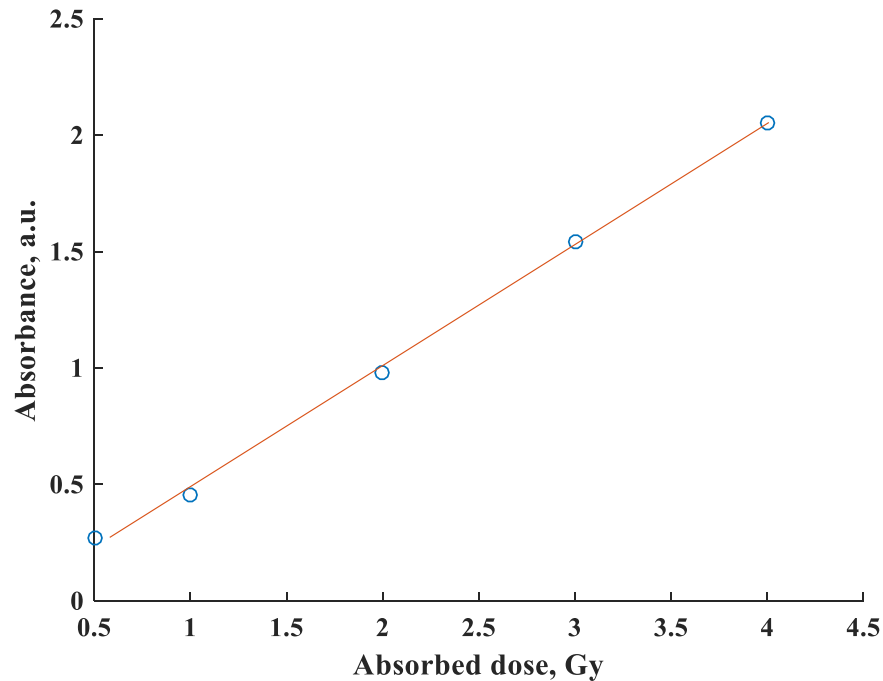


Fig. 30. Dose calibration curve at optimal wavelength (designed optical scanning system).

2D dose distribution maps of each complex irradiation field samples were measured, and the calibration curve was applied to indicate absolute dose values. Furthermore, for more visual representation and detailed analysis of dose distribution in transition region, 3D dose distribution surface and an average dose profile in longitudinal direction was generated. Distances in acquired figures are calculated considering top-left corner of 2D dose map as a zero point.

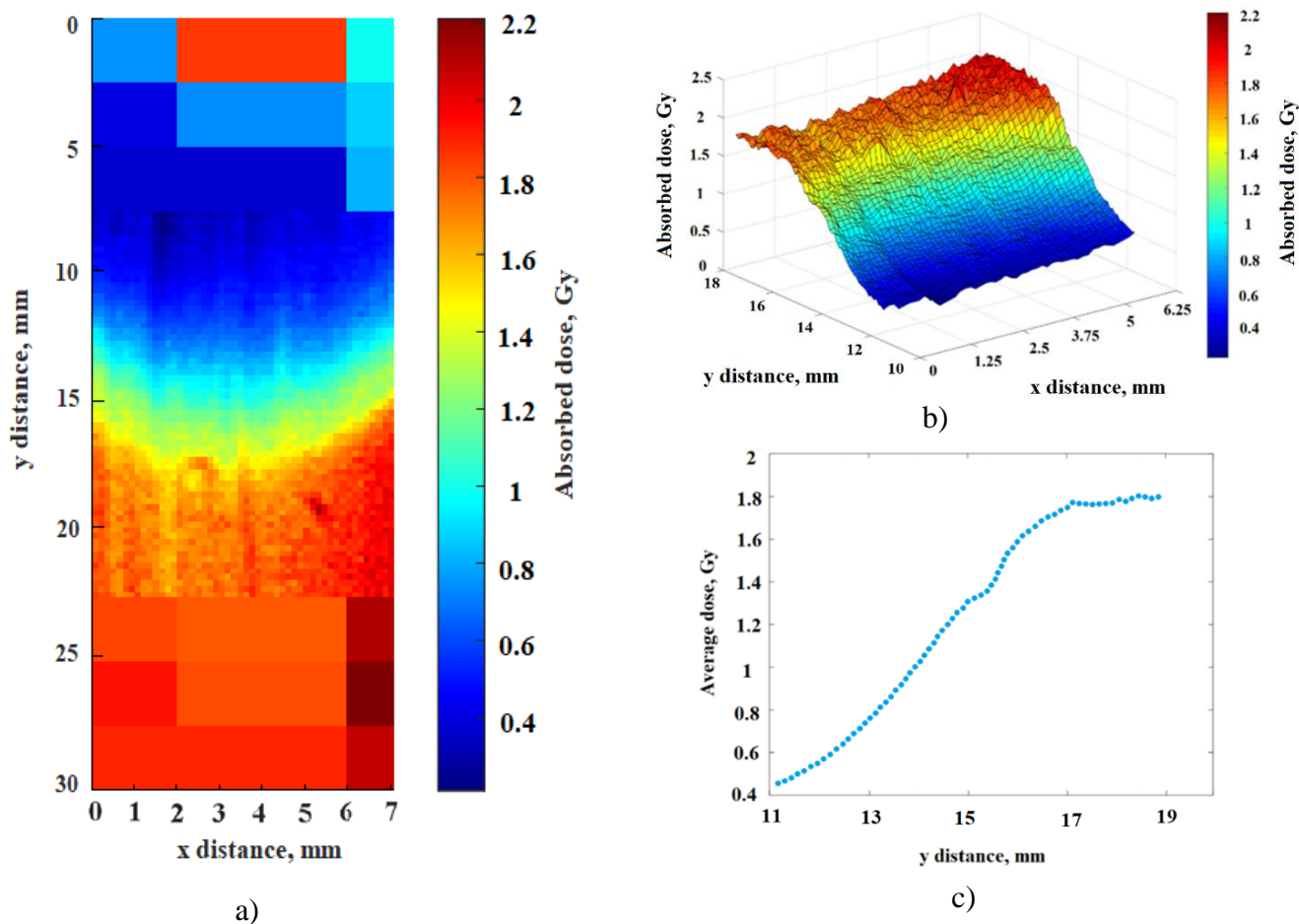


Fig. 31. Dose mapping results of the first complex irradiation field sample using designed optical imaging system: a) 2D dose map; b) 3D dose surface; c) averaged dose profile in longitudinal direction.

Designed optical imaging system demonstrates a respectable result. Shape of dose distribution does not differ from expected U-shaped distribution. Dose constantly increases when travelling from unirradiated region to uniformly irradiated part of the sample. This effect is mostly a consequence of monomer diffusion from unirradiated region to irradiated region. It is particularly visible in averaged dose profile along the cuvette. Therefore, imaging resolution is sufficient to investigate such polymerization and monomer diffusion processes in polymer gels. It can be noted that the number of measurement artifacts and obvious irregularities is small.

Slightly different results were obtained with the second complex irradiation field sample. Although dose distribution is U-shaped, in this case dose do not increase constantly from unirradiated region to irradiated region. It is well visible in the 3D dose representation or averaged dose profile along the cuvette. Possible cause of this irregularity can be associated with the fact, that dose transition region in this sample was close to the layered edge of polymer gel. In acquired dose map, bottom layer of the edge merged with the transition region, thus irregularities are observed.

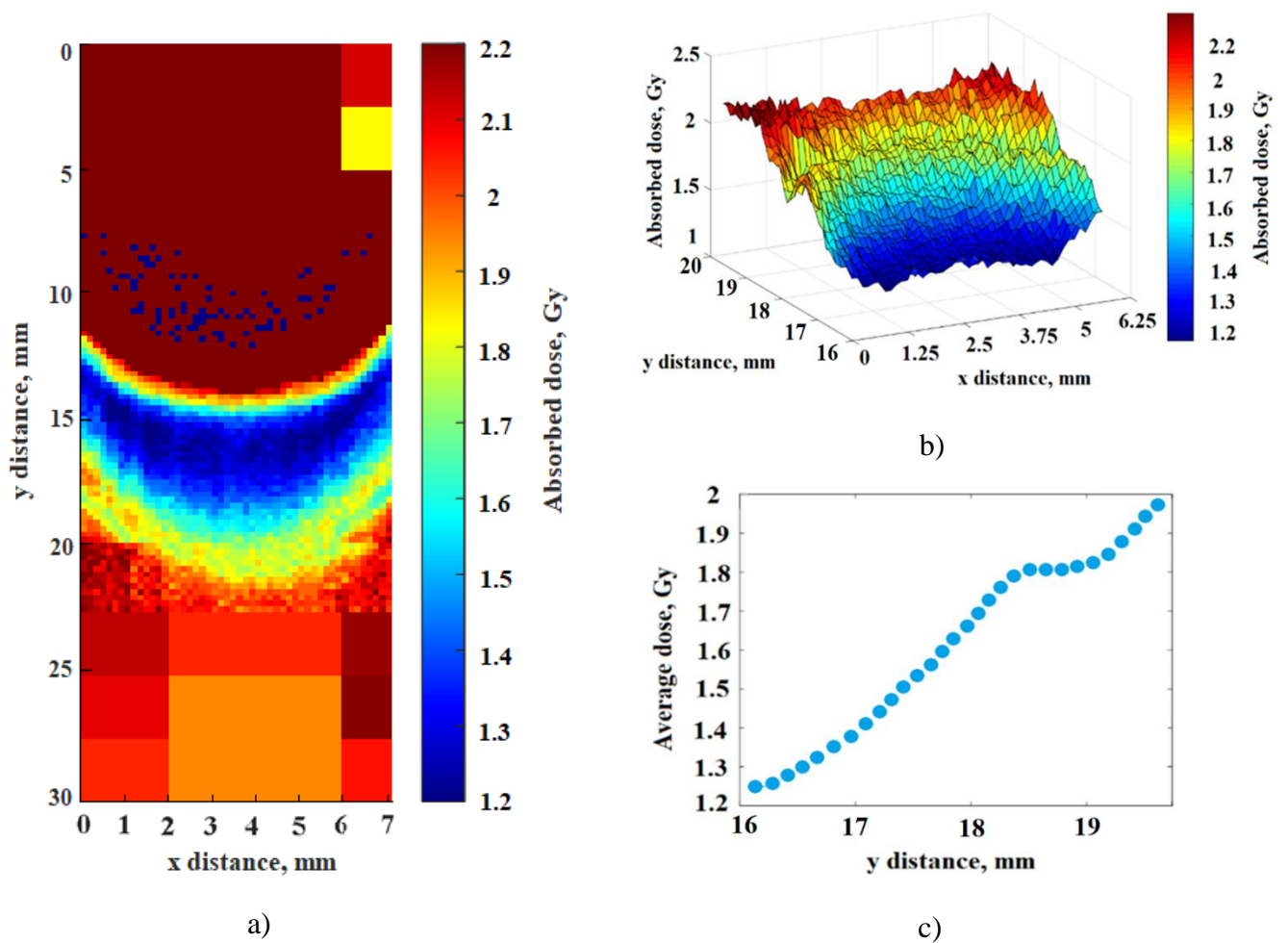


Fig. 32. Dose mapping results of the second complex irradiation field sample using designed optical imaging system: a) 2D dose map; b) 3D dose surface; c) averaged dose profile in longitudinal direction.

Results with the third complex irradiation field sample (Fig. 33) were very similar to results of the first sample. In this case dose distribution is also U-shaped as expected. Dose transition from unirradiated to irradiated part of the sample is continuous, clearly visible. However, in acquired dose profiles of all three samples, monomer diffusion induced dose overshoot, as reported in sources (Fig. 6), is not apparent [4, 27]. There are several explanations for this phenomenon. In current case irradiation dose (2 Gy) was relatively low. Dose overshoots are more pronounced at higher radiation doses. Overshoot amplitude depends on post-irradiation time: overshoot increases till certain time (12-54 h depending on composition) and then starts to decrease. As samples were scanned month after irradiation, this could have a significant influence on dose overshoot [29]. Additionally, overshoot amplitude depends on composition on polymer gel – different amounts of oxygen scavenger (THPC) and gelatin in formulation can influence results [28].

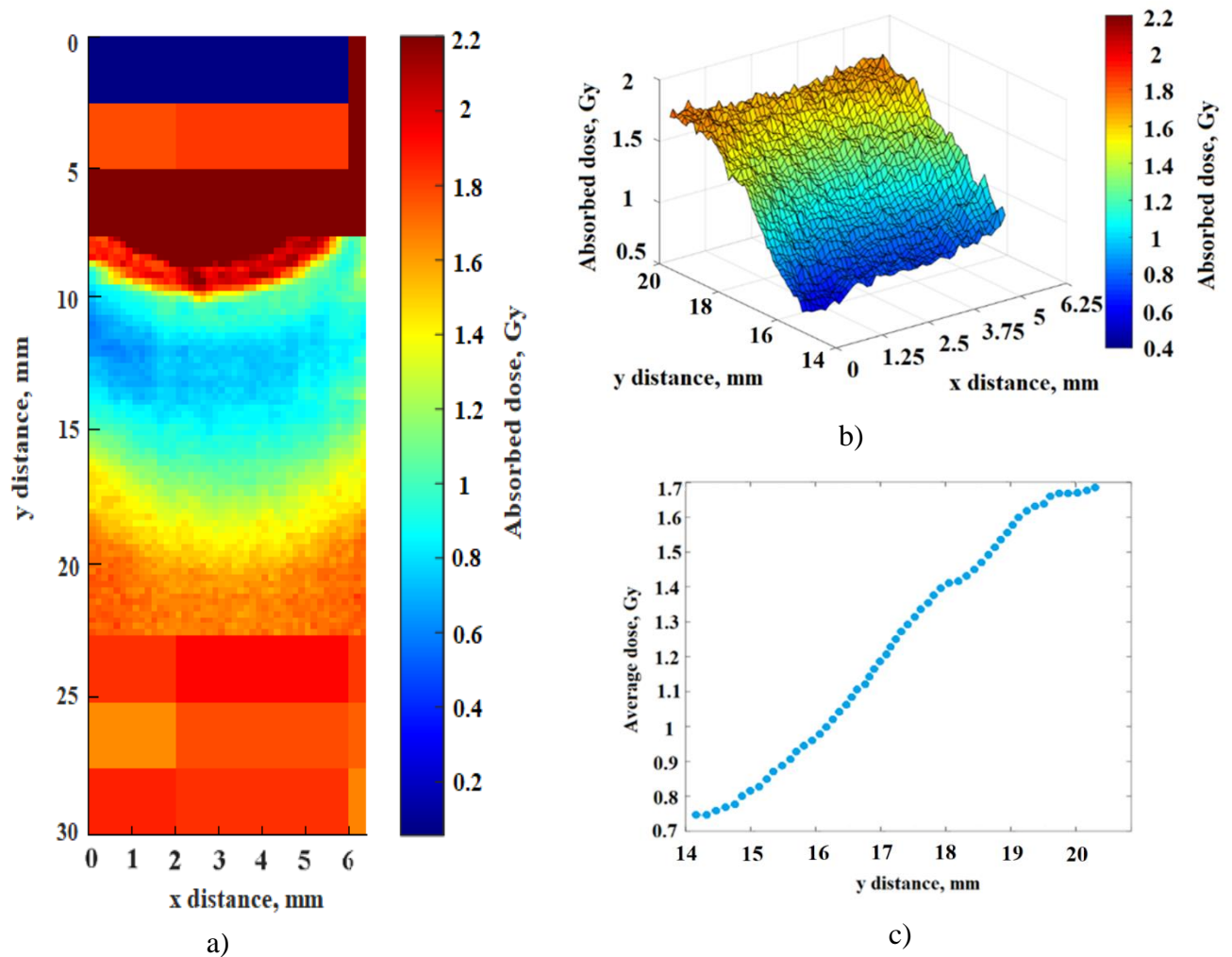


Fig. 33. Dose mapping results of the third complex irradiation field sample using designed optical imaging system: a) 2D dose map; b) 3D dose surface; c) averaged dose profile in longitudinal direction.

To sum up, results obtained using the designed optical imaging system are respectable. In all cases dose distribution is apparent. It is possible to track dose changes in boundary between unirradiated and irradiated regions of the sample indicating that imaging resolution and sensitivity are sufficient. Dose values correlates with the expected values (samples were irradiated with 2 Gy radiation dose). Number of artifacts and irregularities is small. Nevertheless, scanning time have room for improvement – in high-resolution scanning mode approximately 2.5 hours are needed to process one sample.

3.3. Imaging of nMAG samples using diagnostic ultrasound

Polymer gel samples were scanned with Esaote Biomedica ultrasound imaging device in order to examine possibility to use diagnostic ultrasound devices for polymer gel imaging. Firstly, with 0.5 Gy and 2 Gy doses uniformly irradiated samples were scanned using 7.5 MHz linear ultrasound transducer. This was done as a pilot experiment to determine whether diagnostic ultrasound imaging provides viable results.

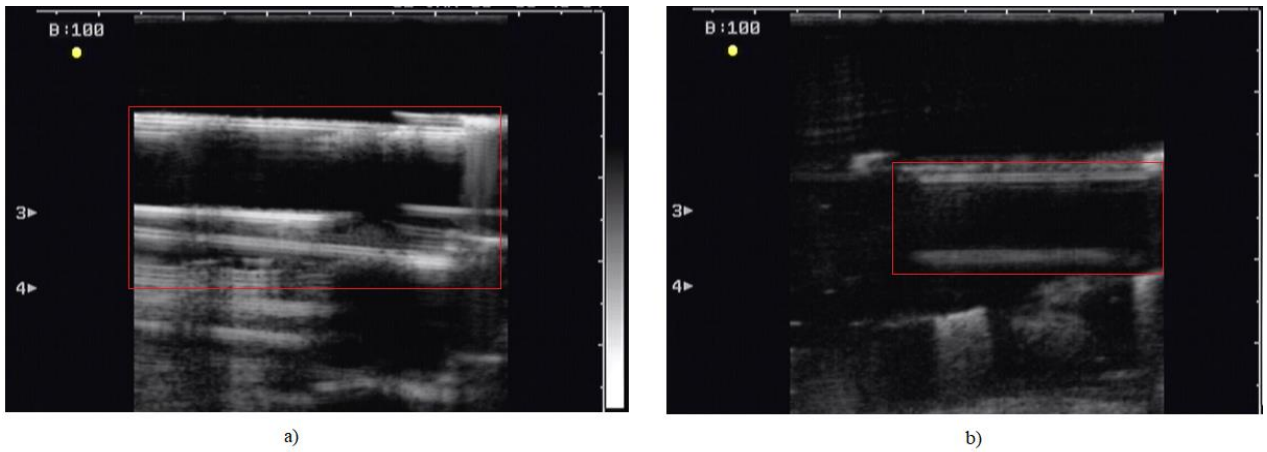


Fig. 34. With 7.5 MHz linear transducer acquired ultrasound images of samples irradiated with 0.5 Gy (a) and 2 Gy (b) dose.

As can be seen in Fig. 34, acquired results were not sufficient to perform any further analysis in terms of calibration curve or 2D dose maps. In the ultrasound images it is possible to discern edges of the cuvette, nonetheless there aren't any significant differences between samples irradiated with different doses. Average pixel value in the image of the sample irradiated with 0.5 Gy dose was 11.77. This value is very similar to average pixel value of the sample irradiated with 2 Gy dose – 11.71. Analogous imaging procedure was implemented with other ultrasound transducers expecting better results. When samples were scanned with 2.5 MHz micro-convex ultrasound transducer, better contrast images were acquired. Average pixel value in the image of the sample irradiated with 0.5 Gy dose was 89.09. Average pixel value in the image of the sample irradiated with 2 Gy dose – 88.61. Differences in the images of the investigated samples are negligible. They are mainly depending on selection of averaging region, not on different characteristics of the samples. Therefore, it is not possible to extract any reliable dose distribution information.

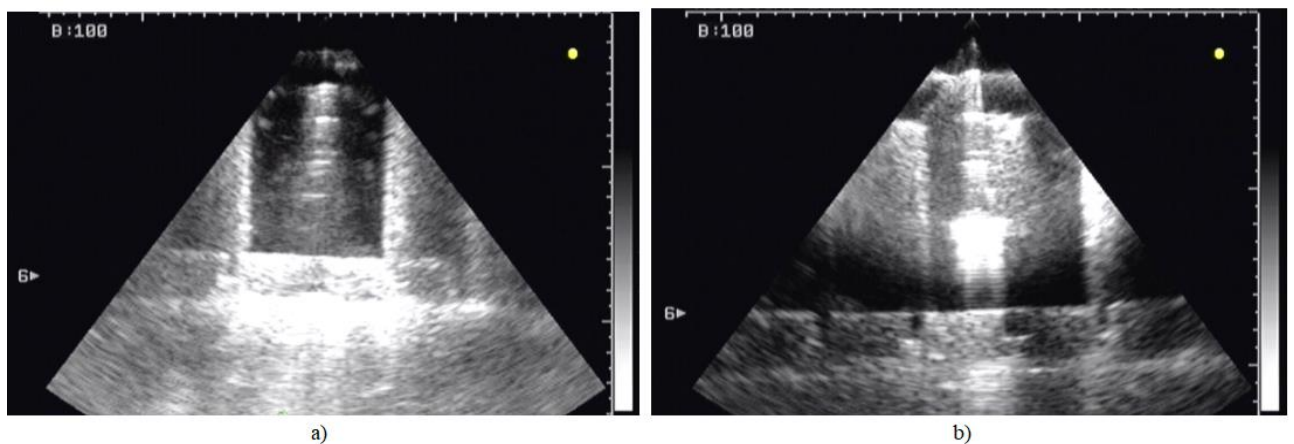


Fig. 35. With 2.5 MHz micro – convex transducer acquired ultrasound images of samples irradiated with 0.5 Gy (a) and 2 Gy (b) dose.

Similar results were acquired with 6.5 MHz endocavity ultrasound probe. From images it is not possible to determine dose, average pixel values are very similar between images of differently irradiated samples. Average pixel value in image of the sample irradiated with 0,5 Gy dose – 54.63. Average pixel value in image of the sample irradiated with 2 Gy dose – 53.72.

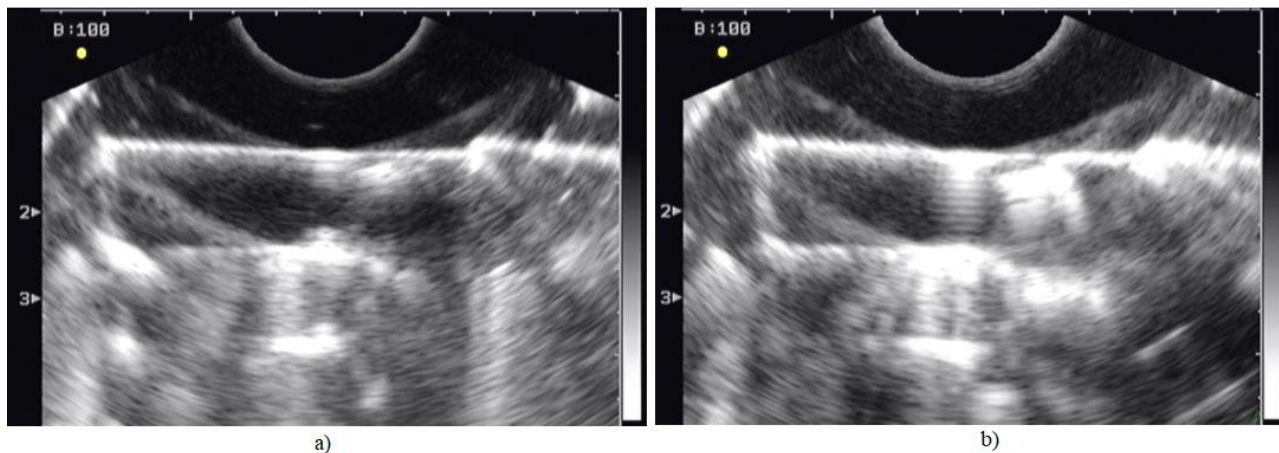


Fig. 36. With 6.5 MHz endocavity ultrasound probe acquired images of samples irradiated with 0.5 Gy (a) and 2 Gy (b) dose.

Using three different ultrasound imaging probes it was not possible to get any differences in the images of differently irradiated samples. Consequently, imaging of polymer gels with diagnostic ultrasound devices does not provide much interest. Possible cause, why imaging with diagnostic unit was unsuccessful, may be associated with the nature of this imaging technique. Diagnostic ultrasound imaging is based on reflection of ultrasound waves from density heterogeneities. In polymer gels density differences are miniscule, thus reflection-based imaging is complicated. As an alternative attenuation-based ultrasound imaging could be used. According to sources [4, 44], this technique demonstrates promising results, however more detailed studies are needed.

3.4. Imaging of nMAG samples using a document scanner

Possibility to use conventional document scanner for polymer gel imaging was also trialed. As mentioned previously, this technique would be a promising alternative to other methods due to simplicity and high availability. Images of the samples with resolution varying from 300 dpi to 4800 dpi were acquired for examination. Different resolutions yielded same calibration curve data, but the processing time increases superexponentially when resolution was increased. Because of this, further experiments were performed with a 300 dpi resolution, which is a de-facto standard for document scanners. Moreover, representation and storage are more practical with this lower resolution. Prior to any further processing, color images were converted to grayscale. From grayscale images of calibration samples, calibration curve was acquired and is depicted below.

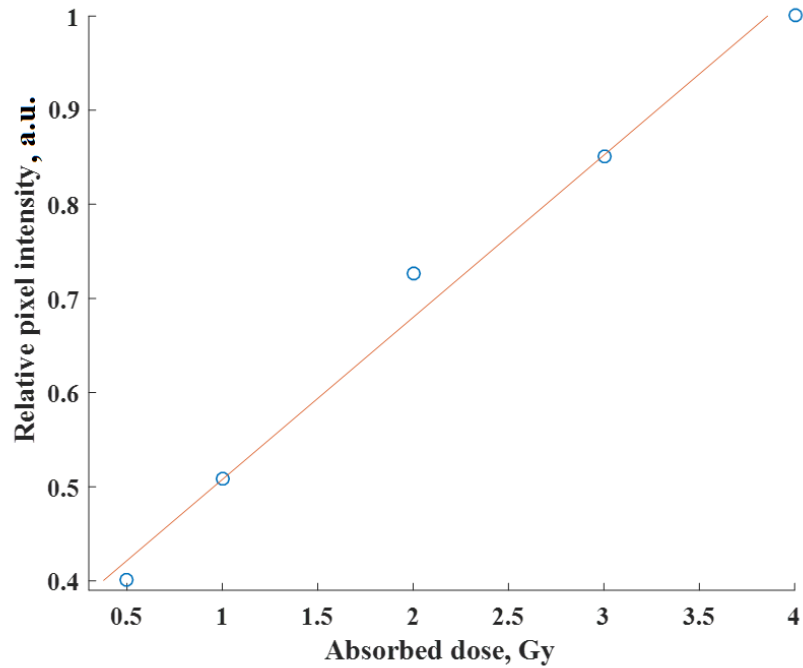


Fig. 37. Relative pixel intensity-dose calibration curve acquired with document scanner.

Calibration data can be approximated using first order polynomial with $R^2 = 0.987$. Therefore, R^2 value is lower when compared to the designed optical imaging system. Additionally, derivative of calibration curve with respect to dose was calculated. This value describes sensitivity of scanning method. Calculated derivative value when normalized data was used – 0.175. This means that sensitivity of this method is lower when compared to designed optical imaging system, where calculated derivative of calibration curve was 0.253. Calibration curve was applied to acquired image and dose map was generated.

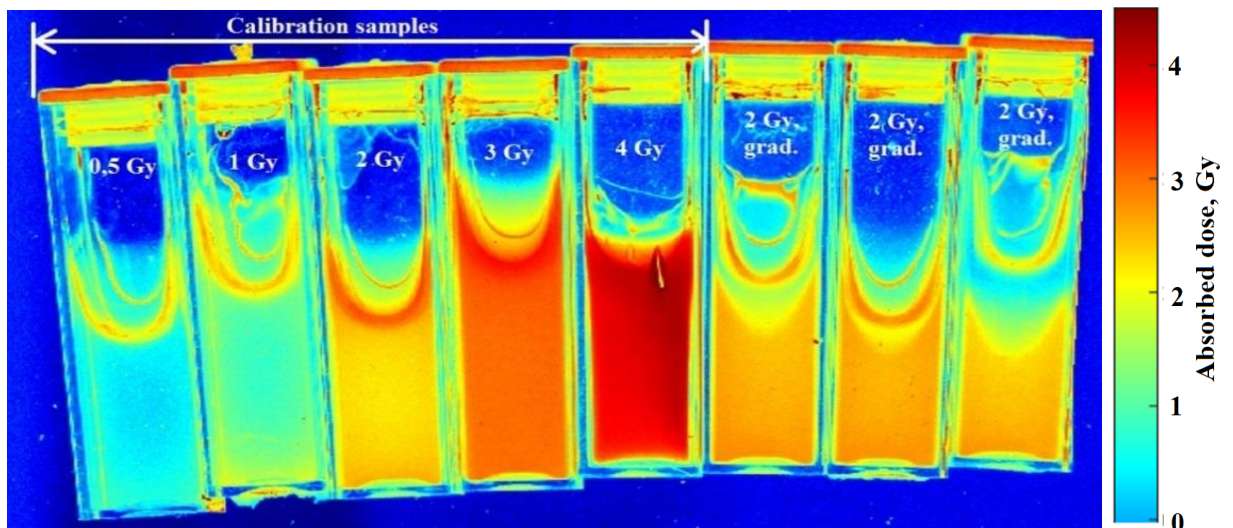


Fig. 38. Joint dose map of calibration vials (1 - 5 vials) and samples with steep dose gradients (6 - 8 vials).

From the image we can see that dose distribution in samples with steep dose gradients is clearly visible. For more detailed analysis of dose distribution in transition region between irradiated and unirradiated parts 3D dose surfaces were generated for each sample. Also, averaged dose profiles along the cuvettes were gathered. This was done using the sample principle technique as with the designed optical scanning system.

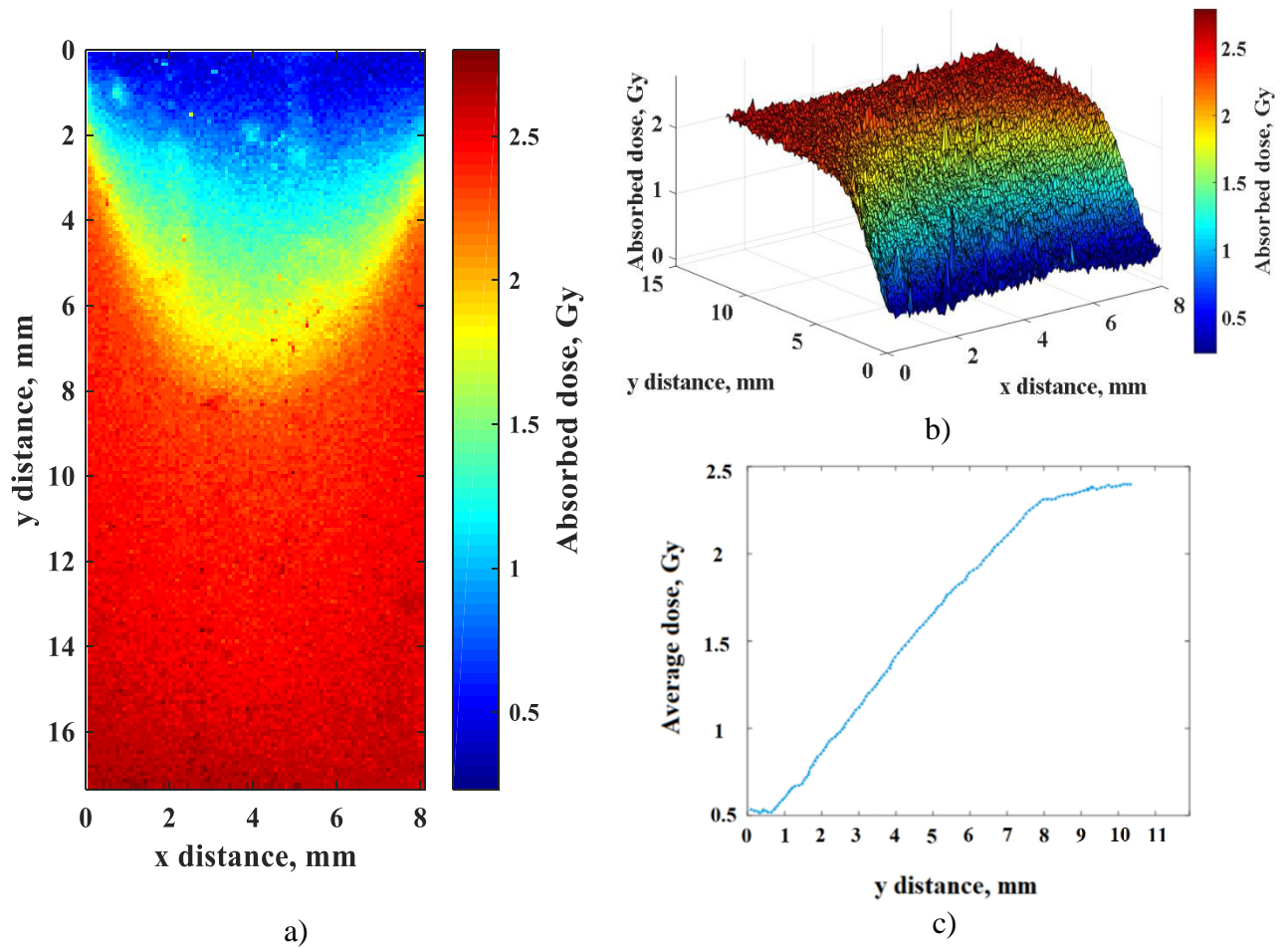


Fig. 39. Dose mapping results of the first complex irradiation field sample using flatbed document scanner: a) 2D dose map; b) 3D dose surface; c) averaged dose profile in longitudinal direction.

Dose constantly increases when analyzed in the direction from unirradiated region to irradiated region, until a uniformly irradiated region is reached. This is clearly visible in averaged dose profile along the cuvette in the gradient region. Acquired shape dose distribution do not differ from expected, it is very similar to dose distribution, gathered with designed optical imaging system.

Slightly different results were acquired with the second sample. In the transition region, irregular dose rise can be observed. Irregularities of dose transition between unirradiated and irradiated regions in the second sample were already notified with the designed optical imaging system. However, cause of this effect is more clearly visible when the sample was scanned in with the document scanner. Irradiation edge is close to the layered limit of polymer gel. These layers possess higher light reflection, consequently in dose map they appear as regions, irradiated with relatively high dose.

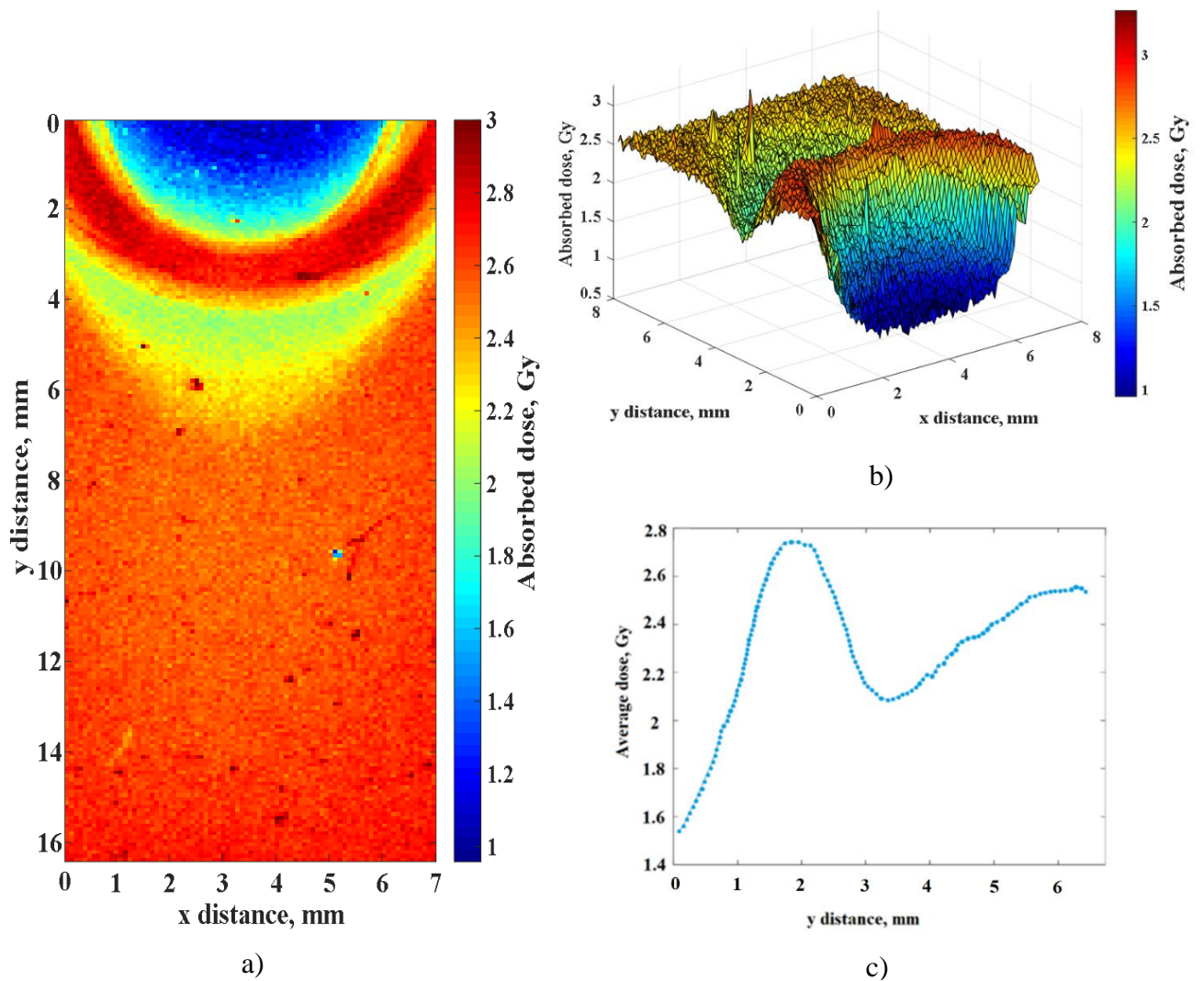


Fig. 40. Dose mapping results of the second complex irradiation field sample using flatbed document scanner: a) 2D dose map; b) 3D dose surface; c) averaged dose profile in longitudinal direction.

This case demonstrates advantage of document scanner – high spatial resolution can be achieved. Double dose rise is slightly better visible comparing to designed optical imaging system. Nevertheless, dose accuracy in this case is worse due to lower sensitivity of this technique.

Dose mapping results of the third sample were very similar to results of the first sample. Dose continuously increases from unirradiated part to irradiated region. Also, dose distribution maps are analogous to results acquired with designed optical imaging system. Nevertheless, in dose distribution maps of the third sample higher number of artifacts, irregularities can be notified. These effects can be associated with dust or other impurities on the surface of scanner or cuvette.

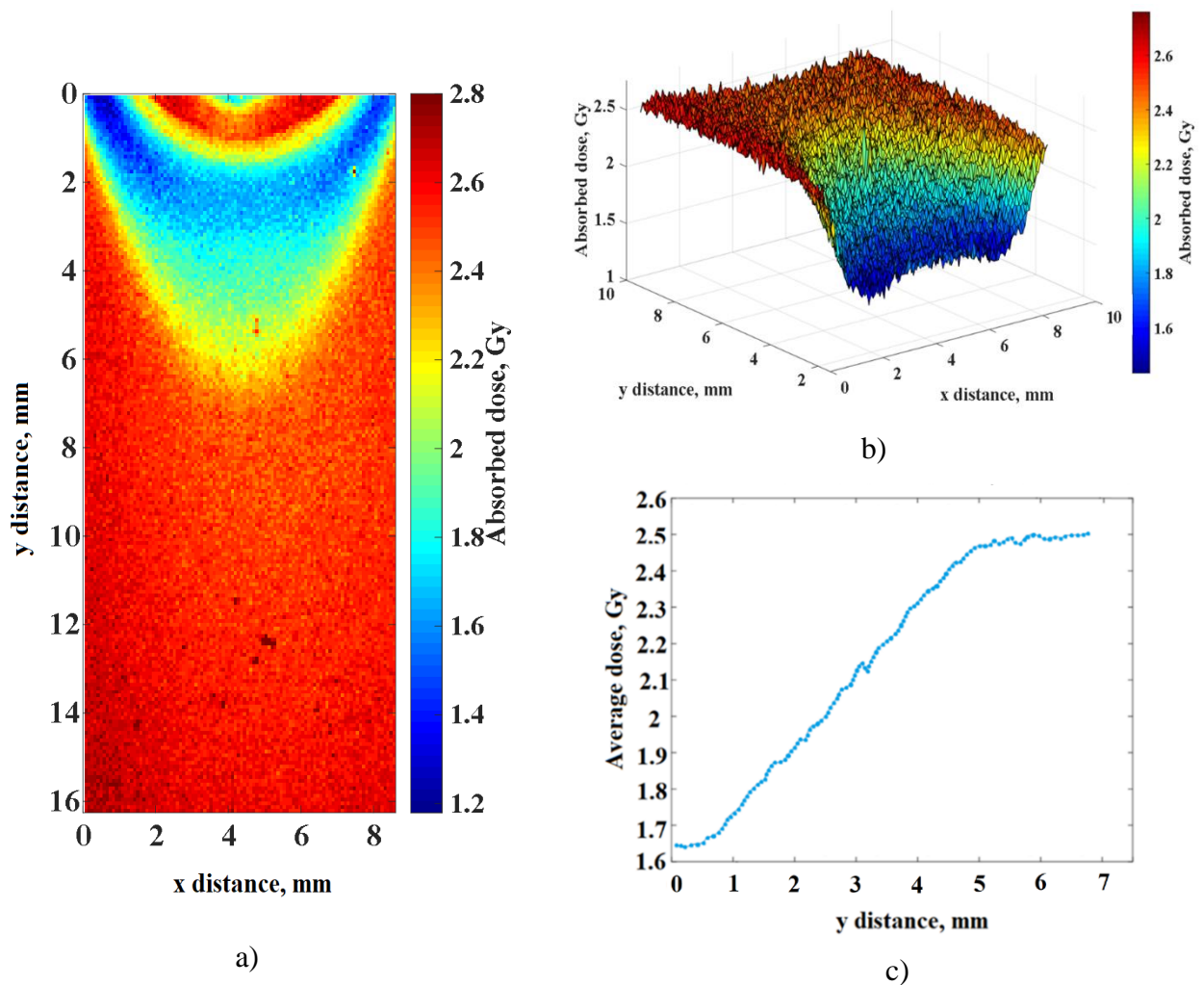


Fig. 41. Dose mapping results of the third complex irradiation field sample using flatbed document scanner: a) 2D dose map; b) 3D dose surface; c) averaged dose profile in longitudinal direction.

The main advantage of this technique - document scanner allows to acquire dose distribution images with unparalleled resolution ($84 \mu\text{m}$). Moreover, resolution can be significantly improved by adjusting scanning parameters. In addition, scanning speed is considerably higher comparing to other imaging methods. Simultaneous scan of all samples takes several minutes, while with other imaging methods procedure can take several hours.

However, higher scanning resolution means that influence of various artifacts (dust, impurities) is higher. It is clearly visible on 3D dose surfaces. Lower sensitivity comparing to absorbance – based spectrometric imaging is another disadvantage of document scanning method. In addition, it was notified that dose values acquired with document scanner are higher comparing to other imaging methods. Dose in uniform region reaches 2.5 Gy, while in the same region with designed optical imaging system determined dose 1.8 – 1.9 Gy. There are several possible explanations for this effect. Response of the scanner is non-linear to achieve better color accuracy when scanning color documents and photos. This color correction is intrinsic to the light sensor itself. Also, dose distribution can be affected by late polymerization effects. Moreover, dose inaccuracies could occur due to lower dose sensitivity of document scanner because the light source of the document scanner

is RGB LED white balanced for color accuracy (as mentioned previously). It is impossible to choose the optimal acquisition wavelength and achieve the highest sensitivity.

3.5. Imaging of nMAG samples using CT

Additionally, nMAG polymer gel samples were scanned using CT imaging technique. First of all, calibration data was acquired from digitally reconstructed radiograph (DRR) of samples. DRR instead of single slice data was used to achieve higher dose sensitivity. In single slice images, no differences were notified between differently irradiated samples. Acquired calibration points can be approximated using first order polynomial with $R^2 = 0.948$. Therefore, linearity of response is lower comparing to other investigated imaging techniques. Gathered calibration curve is depicted below.

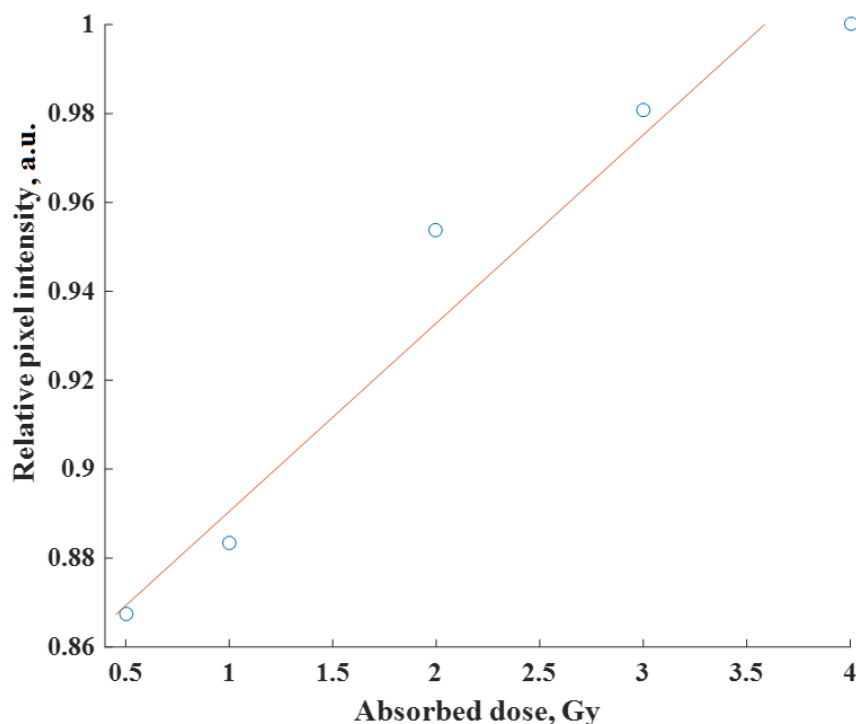


Fig. 42. Relative pixel intensity – dose calibration curve acquired with CT scanner.

Calculated derivative of the calibration curve after normalization of data – 0.043. Hence, sensitivity of this method is more than 4 times lower comparing to document scanner (0.175) and more than 5 times lower when compared to the designed optical imaging system (0.253). It coincides with studies of other researchers where low sensitivity of CT imaging technique was also reported [4, 46]. Although it is possible to calibrate the image in order to obtain a dose map, low imaging resolution (1.25 mm) and sensitivity determine low informativity of dose map (Fig. 43). Dose distribution is poorly visible in samples with steep dose gradients. For more detailed analysis of results in transition region, 3D dose surface and averaged dose profile along the cuvette were generated for each sample.

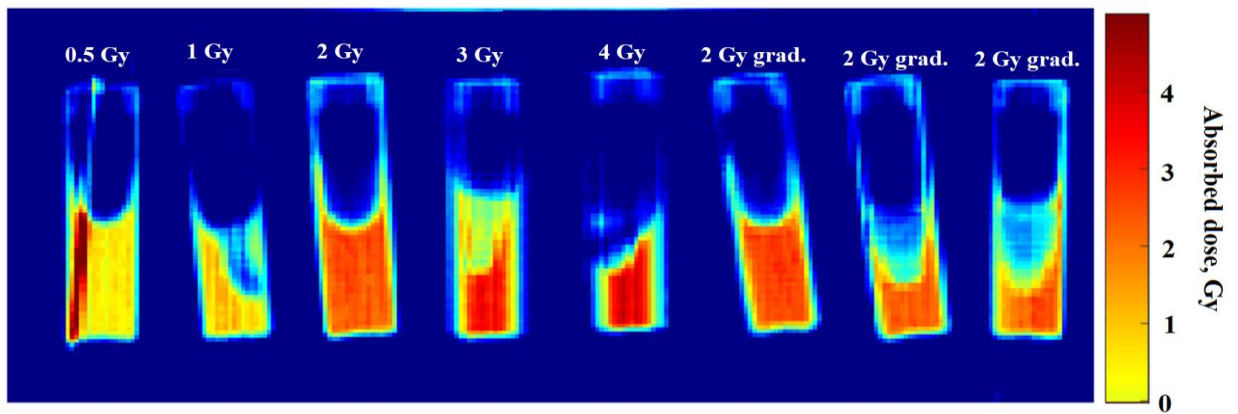


Fig. 43. Joint 2D dose map of irradiated nMAG samples (CT scan).

In dose maps of the first cuvette it is possible to discriminate curved dose distribution. Nonetheless, it is not uniform where the sample was irradiated uniformly. With other imaging methods uniform dose distribution was acquired in this case. Moreover, dose transition from unirradiated region to irradiated region is poorly discernable. Gathered dose distribution meaningfully differs from the results, acquired with other imaging methods. Lack of sensitivity and low spatial resolution are the main causes of these problems. Only several pixels depict dose rise in transition region. Also, changes in pixel intensity between different doses are small.

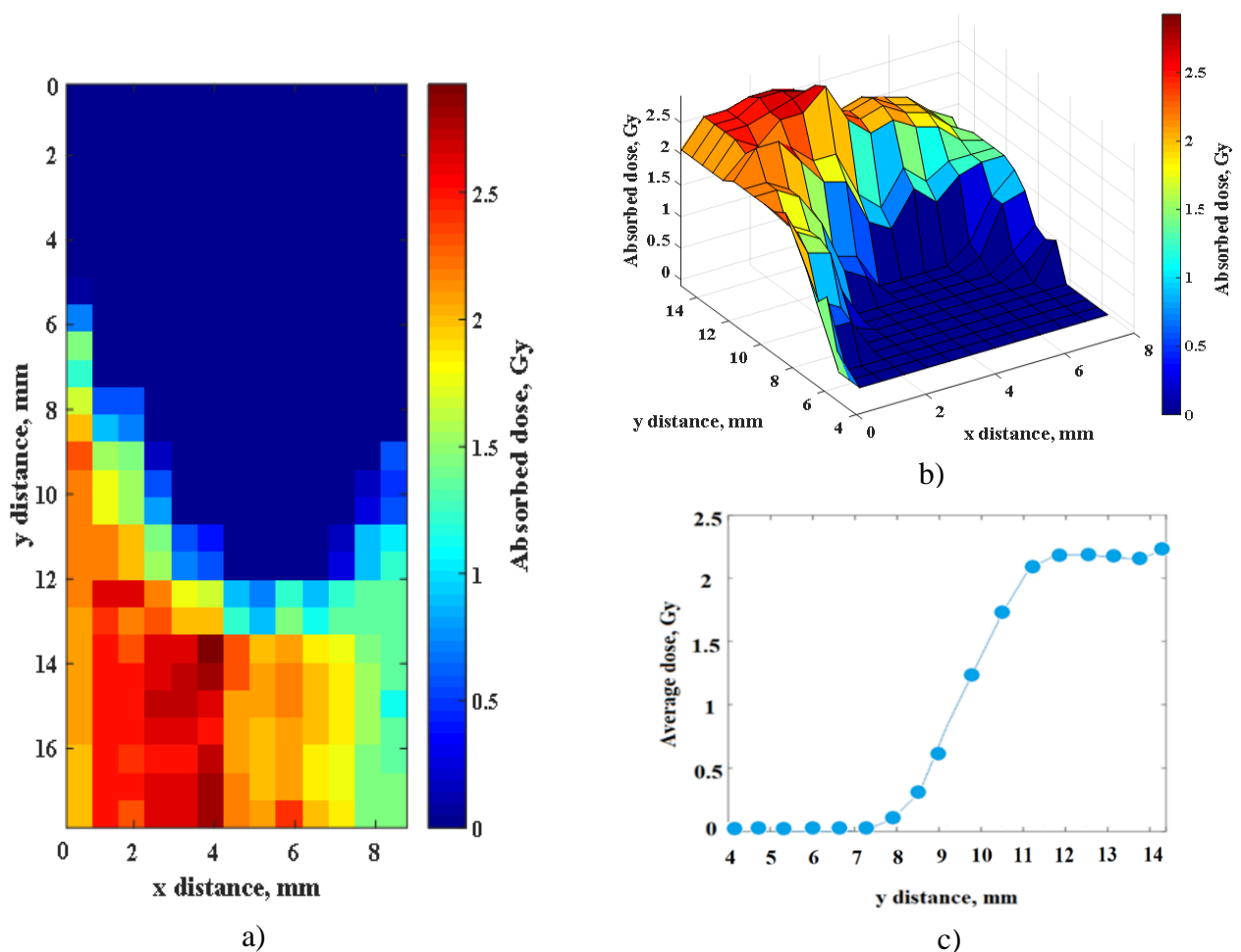


Fig. 44. Dose mapping results of the first complex irradiation field sample using CT scanning: a) 2D dose map; b) 3D dose surface; c) averaged dose profile in longitudinal direction.

Dose distribution of the second sample is rather constant in uniformly irradiated region. In dose profile mild dose rise can be notified. This phenomenon is possibly associated with irradiation edge convergence with layered edge of the polymer gel as notified with other imaging methods. Curved shape of distribution was not clearly reproduced. As in the first sample, dose transition from unirradiated region to irradiated region is barely visible.

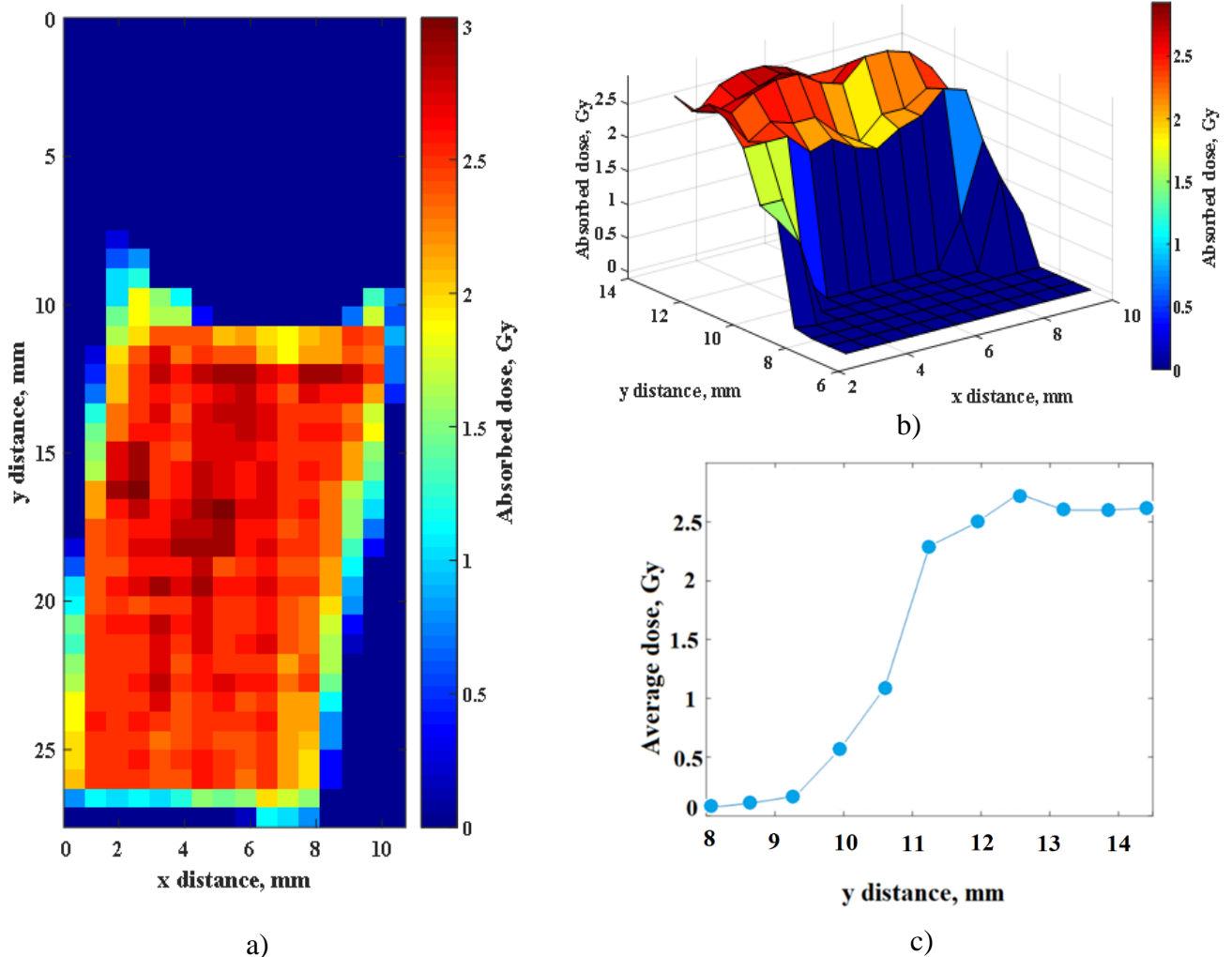


Fig. 45. Dose mapping results of the second complex irradiation field sample using CT scanning: a) 2D dose map; b) 3D dose surface; c) averaged dose profile in longitudinal direction.

Slightly better results were gathered with the third sample. In this case dose distribution is most similar to dose maps, acquired with other imaging methods. However, results are not promising as well. Dose transition between irradiated and unirradiated regions cannot be appropriately investigated due to low sensitivity and spatial resolution of this technique.

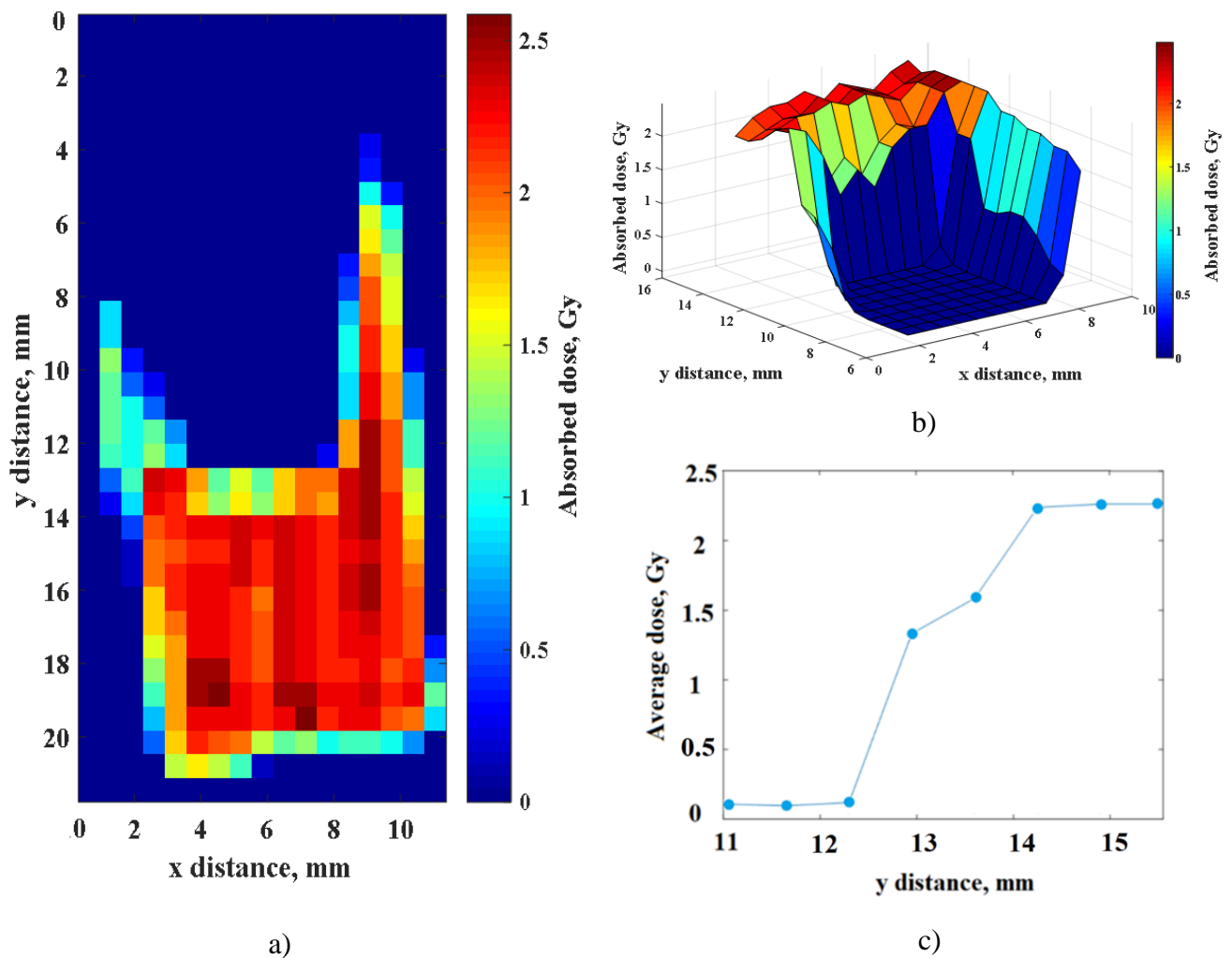
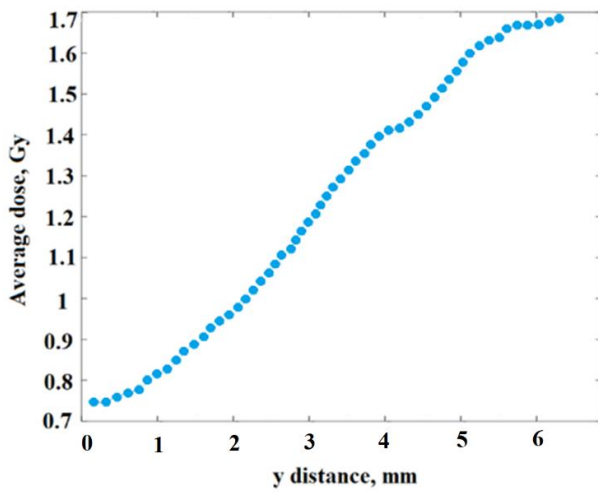


Fig. 46. Dose mapping results of the third complex irradiation field sample using CT scanning: a) 2D dose map; b) 3D dose surface; c) averaged dose profile in longitudinal direction.

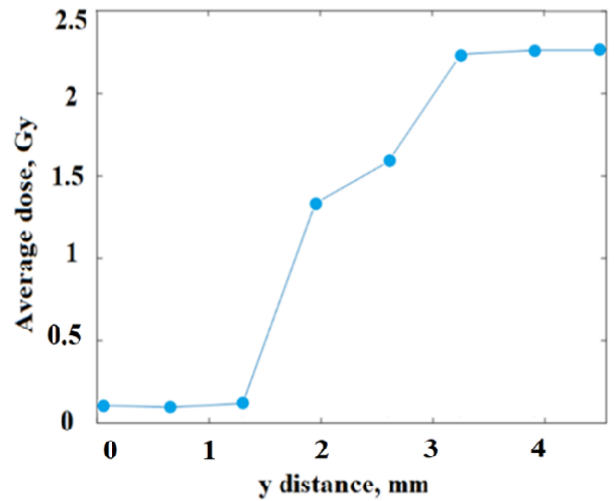
Advantages CT scanning – relatively short imaging time (5 minutes) and high accessibility in clinical environment. Nevertheless, for polymer gel imaging CT is not optimal. Although it is possible to calibrate images in order to acquire dose maps, spatial resolution and sensitivity of this technique are low. Furthermore, during imaging, samples are exposed to additional dose. Dose length product, which describes CT radiation output, was 856.29 mGy·cm. Nevertheless, this measure should not be considered as an additional absorbed dose to the samples because this parameter does not evaluate size of the object. In addition, since all samples, including calibration samples, were irradiated equally during the imaging, imaging dose does not have significant influence on measurement results. In acquired dose maps no dose increase was notified comparing to previously taken measurements with document scanner. Evaluated dose in uniformly irradiated region reaches 2.5 Gy in both cases. Also, this confirms previously stated assumption that higher than expected dose in samples is possibly due to late polymerization effects, not due to severe measurement inaccuracies

3.6. Comparison of imaging techniques

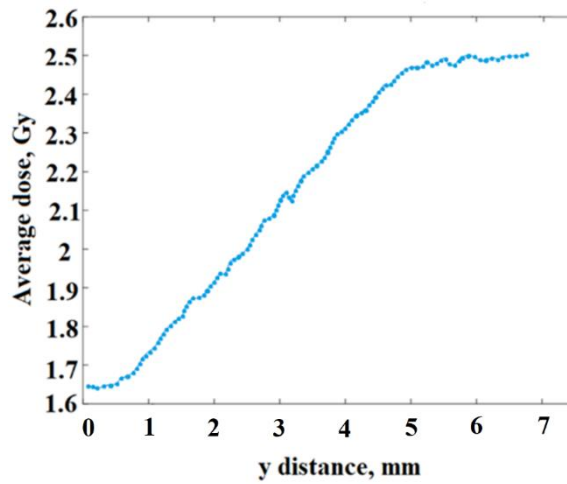
Each investigated technique has its own advantages and disadvantages. Averaged dose profiles in transition regions obtained using different methods are presented in the figure below.



a)



b)



c)

Fig. 47. Comparison of averaged dose profiles in the dose transition regions for the samples with complex irradiation field, using different imaging modes: a) designed optical imaging system; b) CT; c) document scanner.

Scanning of the samples with the document scanner and designed optical imaging system demonstrates reasonable dose profiles in transition regions. Acquired results in both cases are similar despite the fact that spatial resolution with the designed system (125-150 μm) is slightly lower comparing to the document scanner (84 μm). Results generally agree with investigations by other researchers if influencing factors on dose overshoot are taken into account [4, 28, 29].

CT imaging cannot provide results comparable to the optical imaging techniques. Only several pixels determine dose transition. This method lacks of spatial resolution (1.25 mm) and sensitivity to accurately depict dose distribution in transition region.

Further qualitative analysis of techniques can only be implemented by analyzing the calibration curves, due to late polymerization effects on dose distribution. Comparison of normalized calibration curves of different imaging techniques are presented below.

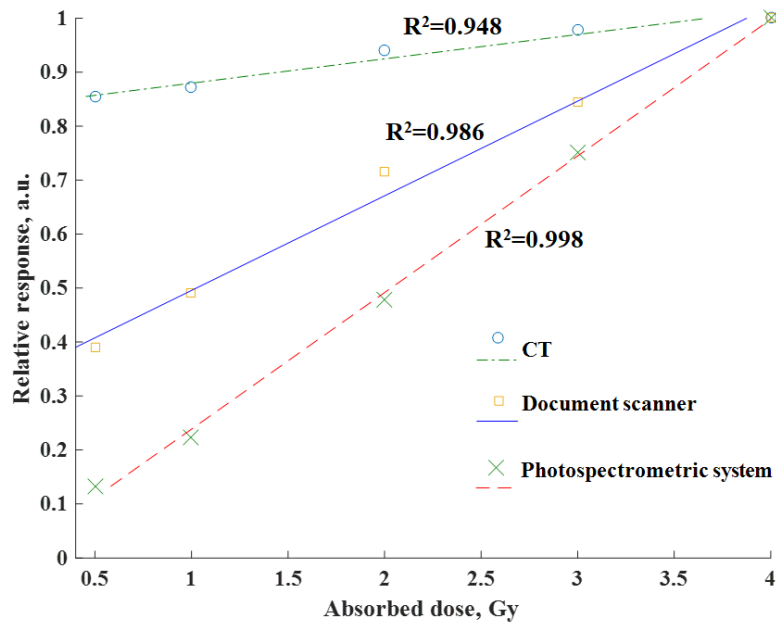


Fig. 48. Comparison of calibration curves obtained using different dosimetric gel imaging methods: CT, document scanner and created photospectrometric system.

As it was stated in the prior sections – designed optical scanning system has the best capabilities in terms of sensitivity (derivative of calibration curve) and dose response linearity (R^2 of calibration curve). These values were accordingly 0.253 and 0.998. Document scanner demonstrates slightly poorer results: calculated derivative of calibration curve - 0.175, $R^2=0.987$. Considerably worse performance comparing to optical methods was exhibited by CT imaging – sensitivity and response linearity were significantly lower. Calculated derivative of calibration curve - 0.043, $R^2=0.948$. With ultrasound imaging it was not able to get calibration curve.

Examined features of each polymer imaging technique are summarized in the table below.

Table 4. Comparison of investigated imaging techniques.

	CT	Designed optical imaging system	Document scanner	Diagnostic ultrasound
Spatial resolution	1.25 mm	125-150 μm	84 μm	n/a
Dose sensitivity	0.043	0.253	0.175	n/a
Linearity of response in calibration (R^2)	0.948	0.998	0.987	n/a
Noise level	medium	low	medium	high
Scanning speed	5 min	2.5 h	2-3 min	2-3 min
3D imaging	Available	Possible	Not available	Possible
Accessibility	High	n/a	Very high	High
Modification capability	Low	Very High	n/a	Low

From the table it can be concluded that the designed optical imaging system has many desirable properties: highest sensitivity among the investigated methods, sufficient spatial resolution, dose response is almost ideally linear. Acquisition of spectral data enables to choose optimal wavelength and achieve the highest sensitivity for any dosimetric gel formulation. Furthermore, 3D imaging is possible if designed positioning system would have more degrees of freedom. Disadvantage of this technique is relatively long scanning time.

Imaging of polymer gels with ordinary flatbed document scanner is also possible. The main advantage is this method - unmatched spatial resolution can be achieved. Moreover, accessibility of this technique is excellent, scanning time is short (depends on the resolution), dose sensitivity and response linearity do not substantially differ from the designed spectrometric imaging system. Nevertheless, implementation of 3D imaging and optimization in terms of wavelengths is impossible.

CT imaging of polymer gel samples demonstrated worse performance when compared to optical imaging techniques. Spatial resolution and dose sensitivity are comparatively low. In acquired dose maps it is not possible to track dose transition between unirradiated to irradiated regions. Hence, this method is not a viable option for polymer gel analysis and research. Advantages of this technique – 3D dose distribution images can be acquired, high scanning speed, technique is widely available in clinical environment.

Diagnostic ultrasound imaging did not provide any satisfactory results. No meaningful differences were notified between average grey levels in images of differently irradiated samples. In addition, noise level in acquired images was significantly higher when compared to other methods. Attenuation-based ultrasound imaging could be alternative technique which, according to sources [4, 44], demonstrates promising results.

Conclusions

1. A unique photospectrometric two-dimensional imaging system for investigations of polymer gel formulations was designed. Developed system is simple, compact, open-source and allows to achieve a higher spatial resolution (0.125 – 0.15 mm) when compared to existing conventional gel dosimeter research techniques (0.5 – 1 mm). Use of the spectrometer as the detector in the system, allows to optimize the readout procedure and achieve maximum sensitivity for any dosimetric gel formulation, by selecting the optimal acquisition wavelength (which for nMAG gel was determined to be 509 nm).
2. Performance of designed optical imaging system was compared with both conventional (computed tomography) and alternative (document scanning, ultrasound) imaging techniques. A set of nMAG dosimetric gel samples was prepared for the experiments. Calibration and complex irradiation field samples were irradiated using a linear accelerator.
3. Created photospectrometric system demonstrated superior results when compared to ultrasound, computed tomography and document scanner methods. Use of diagnostic ultrasound yielded unsatisfactory results, with no possibilities to distinguish different irradiation doses. Computed tomography provided spatial information, but at relatively low slice resolution of 1.25 mm. R^2 value of linearity of dose response was 0.948. Sensitivity of dose response was 83% lower when compared to the developed photospectrometric measuring system. Document scanner readout method proved time efficient but lacked the sensitivity, which was 69% that of the developed system. Also, dose response linearity ($R^2 = 0.987$) was lower. Developed photospectrometric system achieved the highest sensitivity and response linearity ($R^2 = 0.998$), therefore it can be considered as a preferred method for dosimetric gel analysis.

Acknowledgement

Author sincerely thanks to dr. Jurgita Laurikaitienė, who helped to irradiate samples and scan them with computed tomography device, and dr. Neringa Šeperienė, who cooperated in fabrication of polymer gel.

List of references

1. SCHREINER, L. J. True 3D chemical dosimetry (gels, plastics): Development and clinical role. of Physics: Conference Series. IOP Publishing, 2015. p. 012003.
2. WATANABE, Yoichi; WARMINGTON, Leighton; GOPISHANKAR, N. Three-dimensional radiation dosimetry using polymer gel and solid radiochromic polymer: From basics to clinical applications. World journal of radiology, 2017, 9.3: 112.
3. ALEXANDER, Kevin M., et al. 3D Slicer Gel Dosimetry Analysis: Validation of the Calibration Process. In: World Congress on Medical Physics and Biomedical Engineering, June 7-12, 2015, Toronto, Canada. Springer, Cham, 2015. p. 521-524.
4. BALDOCK, Clive, et al. Polymer gel dosimetry. Physics in Medicine & Biology, 2010, 55.5: R1.
5. BUZUG, Thorsten M., et al. Magnetic particle imaging: Introduction to imaging and hardware realization. Zeitschrift für Medizinische Physik, 2012, 22.4: 323-334.
6. VANDECASTEELE, Jan. Optimisation and validation of three-dimensional polymer gel dosimetry and radiochromic gel dosimetry for clinical applications. 2013. PhD Thesis. Ghent University.
7. FENOGLIETTO, Pascal, et al. Eight years of IMRT quality assurance with ionization chambers and film dosimetry: experience of the Montpellier Comprehensive Cancer Center. Radiation Oncology, 2011, 6.1: 85.
8. OLDHAM, Mark, et al. Optical-CT gel-dosimetry I: Basic investigations. Medical physics, 2003, 30.4: 623-634.
9. LOW, Daniel A., et al. Dosimetry tools and techniques for IMRT. Medical physics, 2011, 38.3: 1313-1338.
10. PARK, So-Yeon, et al. Validation of new transmission detector transmission factors for online dosimetry: an experimental study. Radiation Oncology, 2018, 13.1: 156.
11. HELD, Mareike, et al. Commissioning and Evaluation of an Electronic Portal Imaging Device-Based In-Vivo Dosimetry Software. Cureus, 2018, 10.2.
12. VAN ELMPT, Wouter, et al. A literature review of electronic portal imaging for radiotherapy dosimetry. Radiotherapy and oncology, 2008, 88.3: 289-309.
13. SARRUT, David; CLIPPE, Sébastien. Fast DRR generation for intensity-based 2D/3D image registration in radiotherapy. LIRIS UMR, 2003, 5205.
14. BALDOCK, C. Review of gel dosimetry: a personal reflection. In: Journal of Physics: Conference Series. IOP Publishing, 2017. p. 012029.
15. DIAS, Juliana Rosada, et al. Preliminary analysis of N-vinylpyrrolidone based polymer gel dosimeter. Polímeros, 2018, 28.5: 433-439.
16. FARHOOD, Bagher; GERAILY, Ghazale; ABTAHI, Seyed Mohammad Mahdi. A systematic review of clinical applications of polymer gel dosimeters in radiotherapy. Applied Radiation and Isotopes, 2019, 143: 47-59.
17. VAN ELMPT, Wouter; EZZELL, Gary A.; ORTON, Colin G. EPID dosimetry must soon become an essential component of IMRT quality assurance. Medical physics, 2009, 36.10: 4325-4327.

18. CHAIKH, Abdulhamid; GAUDU, Arnaud; BALOSSO, Jacques. Monitoring methods for skin dose in interventional radiology. 2014.
19. WONG, J. H. D., et al. Characterization of a novel two dimensional diode array the “magic plate” as a radiation detector for radiation therapy treatment. *Medical physics*, 2012, 39.5: 2544-2558
20. DE DEENE, Yves. Essential characteristics of polymer gel dosimeters. In: *Journal of Physics: Conference Series*. IOP Publishing, 2004. p. 34.
21. DE DEENE, Yves, et al. A basic study of some normoxic polymer gel dosimeters. *Physics in Medicine & Biology*, 2002, 47.19: 3441.
22. MCAULEY, K. B.; NASR, A. T. Fundamentals of gel dosimeters. In: *Journal of Physics: Conference Series*. IOP Publishing, 2013. p. 012001.
23. LEPAGE, M.; JORDAN, K. 3D dosimetry fundamentals: gels and plastics. In: *Journal of Physics: Conference Series*. IOP Publishing, 2010. p. 012055.
24. SANDWALL, Peter A., et al. Radio-fluorogenic gel dosimetry with coumarin. *Bioengineering*, 2018, 5.3: 53.
25. BALDOCK, Clive. Historical overview of the development of gel dosimetry: another personal perspective. In: *Journal of Physics: Conference Series*. IOP Publishing, 2009. p. 012002.
26. DE DEENE, Yves; JIRASEK, Andrew. Uncertainty in 3D gel dosimetry. In: *Journal of Physics: Conference Series*. IOP Publishing, 2015. p. 012008.
27. DE DEENE, Yves. On the accuracy and precision of gel dosimetry. In: *Journal of Physics: Conference Series*. IOP Publishing, 2006. p. 72.
28. SPĚVÁČEK, V., et al. The influence of antioxidant THPC on the properties of polymer gel dosimeter. *Physics in Medicine & Biology*, 2014, 59.17: 5141.
29. ABTAHI, Seyed Mohammad Mahdi. Response overshoot: a challenge for the application of polymer gel dosimeters. *Journal of Radioanalytical and Nuclear Chemistry*, 2019, 321.3: 885-893.
30. HURLEY, Christopher Anthony. The development of normoxic polymer gel dosimetry using high resolution MRI. 2006. PhD Thesis. Queensland University of Technology.
31. SMITH, S. T., et al. Characterisation of the half-field beam penumbra for a variety of blocking set-ups. In: *Journal of Physics: Conference Series*. IOP Publishing, 2015. p. 012073.
32. ABTAHI, Seyed Mohammad Mahdi; POURGHANBARI, Mohammad. A new less toxic polymer gel dosimeter: Radiological characteristics and dosimetry properties. *Physica Medica*, 2018, 53: 137-144.
33. MAYNARD, Evan, et al. Evaluation of accuracy and precision in polymer gel dosimetry. *Medical physics*, 2017, 44.2: 736-746.
34. KAPANEN, Mika, et al. Effects of remedies made in patient setup process on residual setup errors and margins in head and neck cancer radiotherapy based on 2D image guidance. *Reports of Practical Oncology & Radiotherapy*, 2015, 20.4: 292-298.
35. VEDELAGO, J., et al. Fricke and polymer gel 2D dosimetry validation using Monte Carlo simulation. *Radiation Measurements*, 2016, 91: 54-64.
36. IBBOTT, Geoffrey S. Clinical applications of gel dosimeters. In: *Journal of Physics: Conference Series*. IOP Publishing, 2006. p. 108.

37. CHUANG, Chun-Chao; WU, Jay. Dose and slice thickness evaluation with nMAG gel dosimeters in computed tomography. *Scientific reports*, 2018, 8.1: 1-7.
38. KESHTKAR, M., et al. Uncertainty Analysis in MRI-based Polymer Gel Dosimetry. *Journal of biomedical physics & engineering*, 2017, 7.3: 299.
39. DE DEENE, Yves. Review of quantitative MRI principles for gel dosimetry. In: *Journal of Physics: Conference Series*. IOP Publishing, 2009. p. 012033.
40. RIVAS, J.; KOLEN'KO, Y. V.; BANOBRE-LÓPEZ, M. Magnetic Nanocolloids. In: *Nanocolloids: A Meeting Point for Scientists and Technologists*. Elsevier, 2016. p. 75.
41. DE DEENE, Yves. How to scan polymer gels with MRI?. In: *Journal of Physics: Conference Series*. IOP Publishing, 2010. p. 012015.
42. MASOUMI, Hossein, et al. Determine the dose distribution using ultrasound parameters in MAGIC-f polymer gels. *Dose-Response*, 2016, 14.1: 1559325815625647.
43. KHOEI, Shadi; TRAPP, Jamie V.; LANGTON, Christian M. Ultrasound attenuation computed tomography assessment of PAGAT gel dose. *Physics in Medicine & Biology*, 2014, 59.15: N129.
44. MATHER, Melissa L.; WHITTAKER, Andrew K.; BALDOCK, Clive. Ultrasound evaluation of polymer gel dosimeters. *Physics in Medicine & Biology*, 2002, 47.9: 1449.
45. JIRASEK, A.; HILTS, M. An overview of polymer gel dosimetry using x-ray CT. In: *Journal of Physics: Conference Series*. IOP Publishing, 2009. p. 012038.
46. JIRASEK, A. Considerations for x-ray CT polymer gel dosimetry. In: *Journal of Physics: Conference Series*. IOP Publishing, 2013. p. 012005.
47. ABTAHI, S. M.; AGHAMIRI, S. M. R.; KHALAFI, H. Optical and MRI investigations of an optimized acrylamide-based polymer gel dosimeter. *Journal of Radioanalytical and Nuclear Chemistry*, 2014, 300.1: 287-301.
48. SHIH, Cheng-Ting, et al. Image reconstruction of optical computed tomography by using the algebraic reconstruction technique for dose readouts of polymer gel dosimeters. *Physica Medica*, 2015, 31.8: 942-947.
49. JIRASEK, A.; RUDKO, D.; WELLS, D. A prototype fan-beam optical CT scanner for polymer gel dosimetry. In: *Journal of Physics: Conference Series*. IOP Publishing, 2009. p. 012025.
50. XU, Andy Y.; WUU, C. S. Application of Optical CT Scanning in Three-Dimensional Radiation Dosimetry. In: *CT Scanning-Techniques and Applications*. InTech, 2011.
51. SRIPRISAN, S. I., et al. A Spatial Resolution Study of a New Optical Tomography-Based Polymer Gel Dosimetry System. *Technology in cancer research & treatment*, 2011, 10.6: 591-599.
52. DEKKER, Kurtis H.; BATTISTA, Jerry J.; JORDAN, Kevin J. Scanning laser optical computed tomography system for large volume 3D dosimetry. *Physics in Medicine & Biology*, 2017, 62.7: 2636.
53. ALLEGRO MICROSYSTEMS. A4988 DMOS Microstepping Driver with Translator And Overcurrent Protection. A4988 datasheet [Revised May 2014], 2012.
54. RESENDE, Thiago Dias, et al. Study of the formulation optimization and reusability of a MAGAT gel dosimeter. *Physica Medica*, 2019, 63: 105-111.

55. MUSTAQIM, A. S., et al. The dose enhancement of MAGAT gel dosimeter doped with zinc oxide at 6 MV photon beam. *Radiation Physics and Chemistry*, 2020, 172: 108739.
56. GOPISHANKAR, N., et al. Digital Filtering Techniques to Reduce Image Noise and Improve Dose Resolution in X-Ray CT Based Normoxic Gel Dosimetry. *Modern Practices in Radiation Therapy*, 2012, 327.

Appendices

Appendix 1. Conference “Multidisciplinary Research of Physical and Technological Sciences”

Application to present primary results of master`s final degree project in conference “Multidisciplinary Research of Physical and Technological Sciences” was accepted, however conference was postponed.

LIETUVOS MOKSLŲ AKADEMIJA
MATEMATIKOS, FIZIKOS IR CHEMIJOS MOKSLŲ SKYRIUS
TECHNIKOS MOKSLŲ SKYRIUS

10-OJI JAUNŪJŲ MOKSLININKŲ
KONFERENCIJA

**FIZINIŲ IR TECHNOLOGIJOS MOKSLŲ
TARPDALYKINIAI TYRIMAI**

2020 m.

Konferencijos globėjas

Lietuvos Respublikos Ministras Pirmininkas SAULIUS SKVERNELIS

RĖMĖJAI:

*Asociacija INFOBALT, VšĮ VISORIŲ INFORMACINIŲ TECHNOLOGIJŲ PARKAS, UAB VTEX,
UAB BIOTECHFARMA, UAB BALTIC AMADEUS, UAB BOD GROUP,
UAB VILTECHMEDA, UAB THERMO FISHER SCIENTIFIC*

Konferencijos organizacinio komiteto pirmininkas akad. Leonas Valkūnas

11.30–13.00 Pirmininkauja: **akad. Algirdas Vaclovas VALIULIS**
akad. Rimantas KAČIANAUSKAS
akad. Adolfas Laimutis TELKSNYS
akad. Gintautas DZEMYDA

11.30–11.42 **Giedrius JOČBALIS** (VGTU Antano Gustaičio aviacijos institutas). *Vario dalelės smūgio į varinį paviršių modelis esant dideliems greičiams ir plastinėms deformacijoms.*

11.42–11.54 **Mantvydas MERKIS**, Benas Gabrielis Urbonavičius (KTU). *Didelės erdvinės skyros vaizdinimo sistema polimerinių gelių dozimetrijai.*

11.54–12.06 **Mantas RUBEŽIUS** (Vytauto Didžiojo universiteto Žemės ūkio akademija, UAB „Addeco“). *Pirminio kraikinio vištų mėšlo apdoravimo biologiniais metodais įtaką biocheminio metano susidarymo potencialui ir amoniako emisijai.*

Appendix 2. Created tool for data, acquired with the designed system, processing in Matlab environment.

```
clc;
clear all;
close all;
Files=dir('*.txt'); %select all txt files
j=1; t=1; %counter
Csum=0; %sum of absorbance values at specific wavelength
for k=1:length(Files)
filename=Files(k).name; %acquire each name
Data = fileread(filename); %read data
Data = strrep(Data, ',', '.'); %string replace , to .
fileID = fopen(filename,'w');
fwrite(fileID, Data, 'char'); %save modified (replaced) data
fclose(fileID);
fileID = fopen(filename);
C = textscan(fileID, '%s%s', 'headerLines', 13); %scan text
fclose(fileID);
C1 =str2double(C{1,1});%column1 extract and convert from string to double
(wavelength)
C2 =str2double(C{1,2});%column2 extract and convert from string to double
(absorbance)
Csum=Csum+C2; % sum all absorbance values for mean calculation
end
C05=Csum/36; %average of absorbance values at each wavelength
filename='C:\gradientas\kalibraciniam.mat'; %saving spectrums at each dose
(manual) folder selection
save(filename, 'C1', 'C05', '-append'); % C05 - 0.5 Gy, C3 - 1 Gy, C4 -2 Gy, C5
- 3 Gy, C6 - 4 Gy, C45 - 4.5 Gy, C7 -5 Gy
%'-append' - use to add to existing .mat file
load(filename);
for i=1:length(C1)
Caldata(i,:)= [C05(i) C3(i) C4(i) C5(i) C7(i)]; %gather calibration curve data at
all wavelengths
Diffcaldata(i)=mean(diff(Caldata(i,:)));
end
%search for maximum differential in calibration curve
[value, position]=max(Diffcaldata);
wavelength=C1(position)
%Caldata(position,:)=Caldata(position,:)/max(Caldata(position,:));%
normalization step (inactivate)
P = polyfit(Caldata(position,:), [0.5 1:1:4],1); %fit first order polynomial
figure %draw calibration curve
hold on;
plot([0.5 1:1:4],Caldata(position,:), 'o'); %plot data points
plot(polyval(P, Caldata(position,:)), Caldata(position,:)); % plot approximation
hold off;
xlabel('Absorbed dose, Gy');
ylabel('Absorbance, a.u. ');
%R-squared calculation according to formula
B=[0.5 1:1:4]; % y values
f=polyval(P, Caldata(position,:)); %predicted y values
Bbar = mean(B);
SStot = sum((B - Bbar).^2);
SSres = sum((B - f).^2);
R2 = 1 - SSres/SStot
filename='C:\gradientas\linearcoef.mat'; %saving coefficients
save(filename, 'P');

%dose mapping (can be executed separately)
clc;
```

```

clear all;
close all;
Files=dir('*.txt'); %select all txt files
j=1; t=1; %counter
Csum=0; %sum of absorbance values at specific wavelength
for k=1:length(Files)
    filename=Files(k).name; %acquire each name
% filename = 'USB2G550821_00-00-05-798.txt'; %specify filename (optional)
Data = fileread(filename); %read data
Data = strrep(Data, ',', '.'); %string replace , to .
fileID = fopen(filename,'w');
fwrite(fileID, Data, 'char'); %save modified (replaced) data
fclose(fileID);
fileID = fopen(filename);
C = textscan(fileID, '%s%s', 'headerLines', 13); %scan text
fclose(fileID);
C1 =str2double(C{1,1});%column1 extract and convert from string to double
(wavelength)
C2 =str2double(C{1,2});%column2 extract and convert from string to double
(absorbance)
%extract measurement number from filename (comment for other data variant)
index0 = regexp(filename, '\d*', 'Match');
index=cell2mat(index0(1,1)); %convert from cell to single value
index=str2num(index); %convert string to number of measurements
index2(j)=index;
j=j+1;
%points acquisition
%lambda=509 nm, select absorbance values at this wavelength
for i=1:length(C1)
if C1(i)==509;
    values(index-1)=C2(i); %shifting index to left because counting starts from
2
    %values(j)=C2(i);
    %j=j+1; %other data variant
end
end
end
%% Data analysis part
clearvars -except values %clear variables
close all;
%high resolution part of the image
middle=vec2mat(values(10:3771), 57); %rearrange vector to matrix
for i=1:2:66
    middle(i,:)=flip(middle(i,:)); %flip 1,3.... rows according to motion of
scanning
%middle(i,:)=mean(middle(i,1:2)) middle(i,1:end-1)]; % correct for errors due
to changes of position of horizontal stepper motor
%middle(i+1,:)=middle(i+1,5:end) mean(middle(i,end-1:end)) mean(middle(i,end-
1:end)) mean(middle(i,end-1:end)) mean(middle(i,end-1:end))]; % correct for
errors due to changes of position of horizontal stepper motor
end
% structure of image
I=[repmat(values(1),11,14) repmat(values(2),11,28) repmat(values(3),11,15);
repmat(values(6),11,14) repmat(values(5),11,28) repmat(values(4),11,15);
repmat(values(7),11,14) repmat(values(8),11,28) repmat(values(9),11,15);
middle; % high resolution part of the image
repmat(values(3774),11,14) repmat(values(3773),11,28)
repmat(values(3772),11,15);
repmat(values(3775),11,14) repmat(values(3776),11,28)
repmat(values(3777),11,15);
repmat(values(3780),11,14) repmat(values(3779),11,28)
repmat(values(3778),11,15);
];
figure

```

```

imshow(I); % show absorbance map
load('linearcoef.mat'); %load coefficients
%apply model to data
I2=polyval(P,I);
%%%%%%%%%%%%%%%%%%%%%%%%%%%%%%%%%%%%%%%%%%%%%%%%%%%%%%%%%%%%%%%%%%%%%%%%
w=50; % specify number of columns in the image
%%%%%%%%%%%%%%%%%%%%%%%%%%%%%%%%%%%%%%%%%%%%%%%%%%%%%%%%%%%%%%%%%%%%%%%%
figure
imshow(I2(:, 1:w)); % show dose map
colormap jet
colorbar
caxis('auto');
c=colorbar;
c.Label.String = 'Absorbed dose, Gy';
%%%%%%%%%%%%%%%%%%%%%%%%%%%%%%%%%%%%%%%%%%%%%%%%%%%%%%%%%%%%%%%%%%%%%%%%
%supplementary part for graph analysis
i=1; % null counter
l=70; % length on acquisition column
k1=1; k2=l+k1; %counters of elements in dose array
a=26; % acquisition column starting point
for j=1:w
Dose(k1:k2)=I2(a:a+l,j); %acquire dose information in column
I2(a:a+l,j)=2; % mark used area
k1=k1+l+1;
k2=l+k1; %renew counters
end
[X, Y]=meshgrid(1:j, a:a+l); % rearrange x and y values to coordinates
Z=reshape(Dose, [l+1, j]); % reshape vector to matrix
figure
surf(X, Y, Z); %plot surface
xlabel('x, pixels')
ylabel('y, pixels')
zlabel('Absorbed dose, Gy')
figure
imshow(Z)
colormap;
%manually define starting points of strip where mean dose will be counted
%2 nd cuvette
a=[56 57 58 59 60 62 63 63 64 65 65 65 65 66 66 66 66 66 66 66 66 66 66 65
65 65 65 65 65 64 64 64 64 64 64 63 62 61 60 60 59 58 57 57 56 55]-20;
Dose=[];%clear array
%cycle rearranges curved shape averaging field to matrix
for i=1:l:w;
    Dose(:,i)=I2(a(i):a(i)+52, i); %specify width,
    I2(a(i):a(i)+52, i)=2;
end
figure
plot(mean(Dose, 2)); % mean of rows (dose profile)
xlabel('y, pixels')
ylabel('Average dose, Gy')
figure
imshow(I2(:, 1:w)); % show dose map
colormap jet
colorbar % show colorbar
caxis('auto');
c=colorbar;
c.Label.String = 'Absorbed dose, Gy';

```

Appendix 3. Created tool for data, acquired with computed tomography and document scanner, processing in Matlab environment.

```
%% calibration curve acquisition part
clc;
close all;
clear all;
I = rgb2gray(imread('300.bmp')); %read picture as an intensity image (scanner)
%I = imread('drrimage3.bmp'); %read picture as an intensity image (CT)
figure
imshow(I); %show picture
a05=mean(mean(imcrop())); %cut regions
a1=mean(mean(imcrop())); %cut regions
a2=mean(mean(imcrop())); %cut regions
a3=mean(mean(imcrop())); %cut regions
a4=mean(mean(imcrop())); %cut regions
%rearrange values to single vector
a=[a05 a1 a2 a3 a4];
a=a/max(a); %normalization
P = polyfit(a,[0.5 1:1:4],1); %fit first order polynomial
figure %draw calibration curve
hold on;
plot([0.5 1:1:4],a, 'o'); %plot data points (relative pixel intensity)
plot(polyval(P, a), a); % plot approximation
hold off;
xlabel('Absorbed dose, Gy');
ylabel('Relative pixel intensity');
%R-squared calculation according to formula
B=[0.5 1:1:4]; % y values
f=polyval(P, a); %predicted y values
Bbar = mean(B); % mean
SStot = sum((B - Bbar).^2);
SSres = sum((B - f).^2);
R2 = 1 - SSres/SStot
filename='D:\Scans\linearcoef2.mat'; %saving coefficients of
approximation, (manual) folder selection)
save(filename, 'P');
%% dose mapping part
clear all;
I = rgb2gray(imread('300.bmp')); %read picture as an intensity image (scanner)
%I = imread('drrimage3.bmp'); %read picture as an intensity image (CT)
filename='D:\Scans\linearcoef2.mat';
load(filename);
%convert data to double type
I=double(I);
%apply model to data
I2=polyval(P,I);
%show dose map
figure
imshow(I2); % show dose map
colormap jet
colorbar
caxis('auto');
c=colorbar;
c.Label.String = 'Absorbed dose, Gy';
I3=imcrop(); %cut image of gradient cuvettes
set(gca, 'XTickLabel', 0:2:12)
%show dose map
s=size(I3); %size vector
a=0.65; %scale factor
```



```

xVec=1:s(2); %x axis vector
yVec=1:s(1);%y axis vector
xVec1=xVec*a; %scaling
yVec1=yVec*a;
figure
imagesc(xVec1,yVec1,I3); % show dose map
colormap jet
colorbar
caxis('auto'); % colorbar axis set to auto
c=colorbar;
c.Label.String = 'Absorbed dose, Gy'; % colorbar label
axis on
xlabel('x distance, mm')
ylabel('y distance, mm')
%show dose map for marking
figure
imshow(I3);
colormap jet
colorbar
caxis('auto'); % colorbar axis set to auto
c=colorbar;
c.Label.String = 'Absorbed dose, Gy'; % colorbar label
axis on
xlabel('x distance, mm')
ylabel('y distance, mm')
%cut gradient region
[Ig, rect]=imcrop(); %cut gradient region, rect - position and size of cropping
rectangle
figure
imshow(Ig)
[X, Y]=meshgrid(round(rect(1))-1:round(rect(1))-1+round(rect(3))-1,
round(rect(2))-1:round(rect(2))-1+round(rect(4))-1); % rearrange x and y values
to coordinates
Ig(Ig < 0) = 0;% remove negative values
figure
surf(X*0.65, Y*0.65, Ig); %plot surface
zlim([-0.1 inf]); % set limits of z axis
xlabel('x distance, mm')
ylabel('y distance, mm')
zlabel('Absorbed dose, Gy')
colorbar % show colorbar
caxis('auto');
c=colorbar;
c.Label.String = 'Absorbed dose, Gy'; % colorbar label
%% averaged dose profile calculation
close all;
clc;
i=1;
figure
hold on
I4=I3; %copy array
imshow(I3); % show dose map
colormap jet
colorbar
caxis('auto');
c=colorbar;
c.Label.String = 'Absorbed dose, Gy';
h = imfreehand; % mark contour in the image
hold off
h2=round(h.getPosition); %get contour coordinates
clear a; %clear variable
araw=h2(1:end,2); %copy y coordinates to separate array
n=h2(end,1)-h2(1,1); %number of columns

```

```

a = round(resample(araw,n, length(araw))); %resample data to actual number of
columns
a = a(9:end-0)-9; % remove inaccurate edges in rows, specify offset
b=h2(9:end-0,1); % remove inaccurate edges in columns
%cycle rearranges curved shape averaging field to matrix
for i=1:1:length(a);
    Dose(:,i)=I4(a(i):a(i)+14, b(1)-1+i); %specify width,
    I4(a(i):a(i)+14, b(1)-1+i)=2;
end
figure
plot(flip(mean(Dose, 2))); % mean of rows (acquired dose profile)
xlabel('y, pixels')
ylabel('Average dose, Gy')
figure
imshow(I4); % show dose map
colormap jet
colorbar % show colorbar
caxis('auto');
c=colorbar;
c.Label.String = 'Absorbed dose, Gy'; % show colorbar title

```